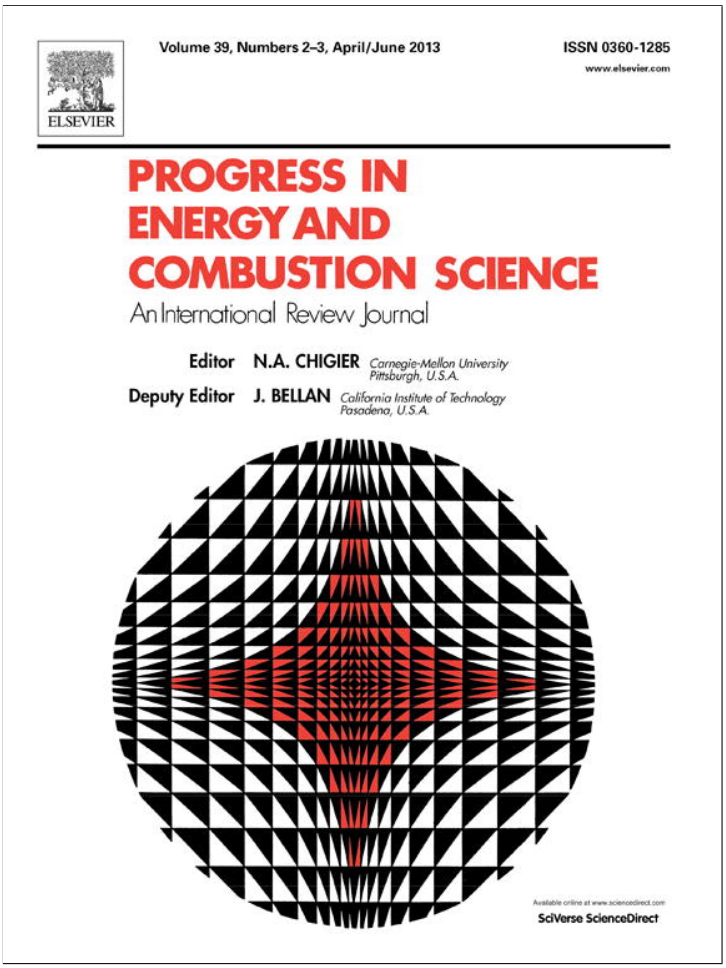

Progress in Energy and Combustion Science 39 (2013) 215–245

Contents lists available at SciVerse ScienceDirect

Progress in Energy and Combustion Science

journal homepage: www.elsevier.com/locate/pecs

Review

Lagrangian–Eulerian methods for multiphase flows

Shankar Subramaniam*

Department of Mechanical Engineering, Iowa State University, 2080 H.M. Black Engineering, Ames, IA 50011, United States

ARTICLE INFO

Article history:
Received 3 March 2012
Accepted 25 October 2012
Available online 29 December 2012

Keywords:
Particle-laden flow
Gas–solid flow
Multiphase flow theory
Spray
Droplet
Spray theory
Lagrangian–Eulerian
Spray modeling
Two-phase flow
Numerical convergence

ABSTRACT

This review article aims to provide a comprehensive and understandable account of the theoretical foundation, modeling issues, and numerical implementation of the Lagrangian–Eulerian (LE) approach for multiphase flows. The LE approach is based on a statistical description of the dispersed phase in terms of a stochastic point process that is coupled with a Eulerian statistical representation of the carrier fluid phase. A modeled transport equation for the particle distribution function — also known as Williams' spray equation in the case of sprays — is indirectly solved using a Lagrangian particle method. Interphase transfer of mass, momentum and energy are represented by coupling terms that appear in the Eulerian conservation equations for the fluid phase. This theoretical foundation is then used to develop LE sub-models for interphase interactions such as momentum transfer. Every LE model implies a corresponding closure in the Eulerian–Eulerian two-fluid theory, and these moment equations are derived. Approaches to incorporate multiscale interactions between particles (or spray droplets) and turbulent eddies in the carrier gas that result in better predictions of particle (or droplet) dispersion are described. Numerical convergence of LE implementations is shown to be crucial to the success of the LE modeling approach. It is shown how numerical convergence and accuracy of an LE implementation can be established using grid-free estimators and computational particle number density control algorithms. This review of recent advances establishes that LE methods can be used to solve multiphase flow problems of practical interest, provided sub-models are implemented using numerically convergent algorithms. These insights also provide the foundation for further development of Lagrangian methods for multiphase flows. Extensions to the LE method that can account for neighbor particle interactions and preferential concentration of particles in turbulence are outlined.

Contents

* Tel.: +1 515 294 3698; fax: +1 515 294 3261.
E-mail address: shankar@iastate.edu.

0360-1285/$ – see front matter © 2012 Elsevier Ltd. All rights reserved.
http://dx.doi.org/10.1016/j.pecs.2012.10.003

1. Introduction

1.1. Introduction and objectives

This paper describes the use of the Lagrangian–Eulerian (LE) approach to calculate the properties of multiphase flows such as sprays [4] or particle-laden flows that are encountered in many energy applications. The LE approach is used to denote a family of modeling and simulation techniques wherein droplets or particles are represented in a Lagrangian reference frame while the carrier-phase flow field is represented in a Eulerian frame. This paper primarily focuses on the use of the LE approach as a solution method for the transport equation of the droplet distribution function (ddf) or number density function (NDF), which is also known as Williams' spray equation. In a recent review article [1], Fox notes that the NDF representation of the particle phase constitutes a mesoscopic approach that offers a clear separation between physical and mathematical approximations. Since the LE approach is widely used to simulate multiphase flows, a comprehensive description of this approach can be of use to theoreticians, model developers and end-users of simulations.

In order for any simulation methodology such as the LE approach to be a predictive tool, it must be based on

(i) a mathematical representation that is capable of representing the physical phenomena of interest,
(ii) accurate and consistent models for the unclosed terms that need to be modeled, and
(iii) a numerically stable and convergent implementation.

There are challenges in each of these areas that must be surmounted in order to develop such a predictive LE simulation methodology for multiphase flows. Therefore, this paper addresses key issues related to the LE approach in the areas of: (i) mathematical representation, (ii) physics-based modeling, and (iii) numerical implementation. Considerable progress has been made

in addressing many of these challenges since the inception of the LE approach. This article attempts to summarize these advances and also outline opportunities for further development of the LE approach.

Multiphase flows in energy applications are often also turbulent, reactive flows. Since the field of turbulent reactive flows is a mature research area with many authoritative reviews [2–4], this work will focus mainly on the multiphase aspects of the flow with some reference to turbulence interactions. There is also a wide range of physico-chemical phenomena that are encountered in nonreacting multiphase flows alone, and these are highly dependent on the particular application area. For instance, in the area of sprays one can find many comprehensive reviews of single-droplet behavior and spray atomization and vaporization [5–7]. In light of the wide variety of physico-chemical phenomena in multiphase flows, this review will only consider those generic characteristics of a dispersed two-way coupled, two-phase flow that need to be incorporated in the LE formulation.

The nonlinear and multiscale interactions in multiphase flow result in a rich variety of flow phenomena spanning many flow regimes. One of the primary features of multiphase flow that distinguish it from advection and diffusion of chemical species in multicomponent flows is the inertia of dispersed-phase particles or droplets. Particle inertia results in a nonlinear dependence of particle acceleration on particle velocity outside the Stokes flow regime, and this nonlinearity is important in many applications where the particle Reynolds number is finite. Also in many multiphase flows one must consider the influence of the dispersed phase on the carrier-phase momentum balance, and this two-way coupling is a source of nonlinear behavior in the system.

Polydispersity of the dispersed-phase particles or droplets introduces a range of length and time scales. Interactions of these polydisperse particles with carrier-phase turbulence that is inherently multiscale in nature presents further modeling challenges. Furthermore, it is not uncommon to encounter a wide variation in dispersed-phase volume fraction in the same multiphase flow, ranging from dilute to dense. For example, in a fluidized bed the particle volume fraction can range from near close-packed at the base of the bed to less than 5% in the riser. The particle volume fraction in conjunction with the level of particle fluctuating velocity (that can be characterized by the particle Mach number) determines the relative importance of advective transport to collisional effects. Since unlike molecular gases not all multiphase flows are collision-dominated, it is possible for the probability density function (PDF) of velocity to depart significantly from the equilibrium Maxwellian distribution. These nonlinearities, multiscale interactions and nonequilibrium effects lead to the emergence of new phenomena such as preferential concentration and clustering that have a significant impact in multiphase flow applications.

Interpreting the LE simulation approach as a numerical solution to the ddf (or NDF) evolution equation reveals the specific advantages of this mesoscopic [1] mathematical representation underlying the LE approach for capturing these nonlinear, multiscale interactions and nonequilibrium effects in multiphase flow. Williams [8] introduced the ddf in his seminal 1958 paper, and its counterpart in the kinetic theory of gas–solid flow is the number density function or one-particle distribution function (see Koch, 1990 [9] for example). The ddf or NDF is an unnormalized joint probability density of droplet (or particle) size and velocity as a function of space and time. Since the ddf (or NDF) contains the distribution of droplet (or particle) sizes it naturally captures the size-dependence of drag and vaporization rate in closed form, whereas other approaches such as the Eulerian–Eulerian (EE) two-fluid theory [10–12] that only represent the average size and average velocity of droplets (or particles) must rely on approximate closure models. One of the major challenges in the two-fluid averaged equation approach that is based on average size is the incorporation of the range of droplet (or particle) sizes, and the nonlinear dependence of interphase transfer processes on droplet (or particle) size. The two-fluid EE approach referred to here is not to be confused with the Eulerian moment equations that can be derived from the ddf, although those moment equations also contain less information than the ddf. A complete discussion can be found in Pai and Subramaniam [13].

Similarly, because the ddf (or NDF) contains the velocity distribution of droplets (or particles), it also captures the nonlinear dependence of particle drag on particle velocity in closed form. Furthermore, particle velocity fluctuations, whose statistics are characterized by the covariance and higher moments of particle velocity, are also easily modeled in the LE framework [14,15]. As pointed out by Fox et al., the LE approach as well as the quadrature method of moments (QMOM) developed by Fox [16] lead to physically correct solutions to the problem of crossing particle jets [17–19], whereas the Eulerian two-fluid theory leads to anomalous results for this problem. Similar difficulties are encountered by the EE two-fluid approach to particle or droplet jets impinging on surfaces, and particle- or droplet-laden flows in regimes not dominated by collisions. This is because EE two-fluid formulations are not capable of representing the fluxes, and resulting physical phenomena, associated with two streams of particles (or droplets) moving with different velocities at the same physical location, whereas this is naturally incorporated in the LE approach.

In sprays and gas–solid flow in risers the particle Stokes[1] and Knudsen numbers[2] span a wide range resulting in velocity distributions that can be far from equilibrium and need not be close to a Maxwellian distribution. However, most EE two-fluid formulations are based on kinetic theory closures that are only valid in the limit of low Knudsen number for equilibrium velocity distributions that are Maxwellian, or nonequilibrium distributions that are slight departures from Maxwellian. Since nonequilibrium velocity distributions are admissible in the LE approach, it has a significant advantage when it comes to simulation of sprays or riser flows all the way from the dense to the dilute regime over a range of droplet or particle Stokes and Knudsen numbers.

Another advantage of the LE approach over the EE two-fluid theory is its ability to accurately represent collisions in the presence of flow. It is well known that interactions with the ambient flow can significantly alter the collision characteristics in particle-laden or droplet-laden flow (grazing collisions), and the effective restitution coefficient is a function of the particle or droplet Stokes number [20]. These effects are easily incorporated in the LE approach. Also from a numerical standpoint, the LE approach minimizes numerical diffusion in dispersed-phase fields such as volume fraction and mean velocity when compared to grid-based Eulerian approaches.

Along with the many advantages that the LE approach offers, there are some aspects of the LE approach that present opportunities for improvement as well. Since many early LE implementations are formulated only for dilute flow and invoke the point particle approximation, these have sometimes been misinterpreted as intrinsic features of the LE method. The formulation of LE models has also not always respected the requirement of being consistent with its corresponding Eulerian–Eulerian two-fluid counterpart,

[1] The particle or droplet Stokes number is the ratio of the particle momentum response time to a characteristic flow time scale.

[2] The particle or droplet Knudsen number is the ratio of the mean free path of a particle to a characteristic length scale associated with the variation of the average number density field.

and in some instances the models are not independent of numerical parameters. Straightforward numerical implementations of the LE method [21,22] without appropriate algorithms for computing particle-grid coupling terms has led to the conclusion that LE formulations may not be numerically convergent, or are at best conditionally convergent [23–26]. Finally, the computational work requirement of the LE method is higher than the EE averaged equation approach because it contains a more complete representation of the multiphase flow. Owing to these reasons, a cursory review of the literature on LE methods may leave the (incorrect) impression that while LE methods hold the promise of predictive simulation of multiphase, this has not been realized due to certain inherent limitations of the approach itself. In this context, the objectives of this review are to demonstrate that:

1. the LE formulation is general enough that it can be extended to dense multiphase flows with finite size particles, provided appropriate models are used and volume–displacement effects are accounted for
2. there are advantages to developing LE sub-models that are consistent with their EE counterparts, and multiscale interactions can be incorporated into LE sub-models to accurately model particle dispersion and energy transfer with the carrier fluid
3. comprehensive numerical tests reveal that the use of grid-free estimation methods and computational particle number density control result in numerically convergent and accurate LE simulations
4. understanding the mathematical formalism underlying the LE approach can give insight into how it might be extended to accurately represent new phenomena such as preferential concentration.

We begin with a brief history of the development of the LE method.

1.2. Lagrangian–Eulerian methods

Williams developed the fundamental spray equation based on a Lagrangian description of the spray droplets [8] using the droplet distribution function. Analytical approaches based on reduction of a Liouville-like equation to a one-particle distribution function have been developed for particle-laden suspensions [9] and bubbly flows [27]. O'Rourke developed the LE method for sprays by explicitly coupling Williams' ddf equation to an Eulerian description of the averaged gas-phase equations, and he derived the interphase exchange terms in terms of integrals over the ddf.

A landmark in the evolution of the LE method is the pioneering work of O'Rourke [28,29] and O'Rourke et al. [21], who developed a numerical implementation of the LE method for sprays in internal combustion engine applications that is now widely used as the KIVA family of codes [21,22]. These works laid the foundation of the modern LE approach and established the early sub-models to describe the physics of droplet acceleration, vaporization, collisions, coalescence and breakup. These two-way coupled calculations were a significant advancement over earlier one-way coupled computations, which are essentially Lagrangian tracking algorithms. Dukowicz [30] developed a two-way coupled particle-fluid numerical model for sprays that included momentum coupling and volume displacement effects.

The LE methods discussed thus far couple Lagrangian tracking of computational particles to a carrier flow description based on Reynolds-averaged Navier–Stokes (RANS) equations. However, it is possible to use the LE approach to couple a Lagrangian description of the dispersed phase with large eddy simulations (LES) or direct numerical simulation (DNS) of the carrier gas phase, resulting in the following principal categories of LE methods:

1. Fully-resolved DNS[3] of droplet or particle-laden flow where the exact Navier–Stokes equations are solved by fully resolving the droplet or particle by imposing boundary conditions at each particle or droplet's surface [31–40]: DNS in Table 1
2. Point particle DNS (PP-DNS) with physical droplets or particles [41–47]: PP-DNS$^{(p)}$ in Table 1
3. PP-DNS with stochastic particles [48]: PP-DNS$^{(s)}$ in Table 1
4. Point particle LES with physical droplets [49,50]: LES$^{(p)}$ in Table 1
5. Point particle LES with stochastic particles [51–53]: LES$^{(s)}$ in Table 1
6. Averaged equations: RANS CFD in Table 1.

The principal difference between DNS and PP-DNS is that while the former can be used to quantify the interphase models, PP-DNS requires assumed models for interphase transfer terms such as particle acceleration and droplet vaporization. Within PP-DNS a further distinction can be made whether computational particles or parcels are used to represent the physical system. In the LES studies this distinction is less significant, since the particles or droplets always obey modeled equations for interphase transfer due to drag or vaporization. The treatment of collisions can also be used to categorize LE methods as those that employ a statistical treatment of collisions [26,28,54] in contrast to direct calculation of collisions between particles using either hard-sphere collisions [55] for low volume fraction or soft-sphere discrete element method (DEM) collision models for high volume fraction [56–58]. Soft-sphere DEM collision models are used in LE simulation of fluidized beds [59].

1.3. Outline

With this brief background on LE methods, the rest of this paper is devoted to an exposition of the theoretical, modeling and numerical aspects of the LE approach as a solution to the ddf or NDF. The next section describes the two basic approaches used to formulate the theory of two-phase flows: (i) the Lagrangian–Eulerian based on a stochastic point process representation, and (ii) the Eulerian–Eulerian based on a random field representation. Section 3 describes the droplet distribution function and its regime of validity. The dilute flow approximation and the point particle approximation that are frequently invoked in the LE approach are reviewed. The mean mass and momentum conservation equations implied by the ddf evolution are derived. The EE closures implied by LE models at the level of the mean conservation equations are described. The velocity second moment equation implied by the ddf in the LE approach is also derived. The relationships between the LE and EE approaches are then briefly reviewed. The models that are used in the LE approach are discussed in Section 4. Numerical solution of the ddf equation is described in Section 5. Selected examples of state-of-the-art LE simulations are given in Section 6. Promising directions for extension of the LE approach are discussed in Section 7. Section 8 gives a summary and presents conclusions of the paper.

2. Multiphase flow representation

The principal mathematical representations of multiphase flows are described so that the LE approach can be understood in this wider context. This leads to the modeling principle of *consistency*: specifically, the development of LE sub-models that

[3] In the multiphase flow literature many studies use the acronym DNS for methods where the droplets or particles are not resolved. In this review such methods are referred to as PP-DNS, and the term DNS is used only for fully-resolved droplet or particle-laden flow simulations.

Table 1
Representation of carrier flow and dispersed phase in different LE simulations: DNS$^{(s)}$ and LES$^{(s)}$ are denoted hybrid simulations.

Simulation method	Carrier flow fields: velocity, pressure	Dispersed phase
DNS with fully-resolved physical particles/ droplets	Realization: $\mathbf{U}^{(f)}(\mathbf{x},t)$, $p(\mathbf{x},t)$	Realization: model as point field $\{\mathbf{X}^{(i)}(t), \mathbf{V}^{(i)}(t), i = 1,...,N_s(t)\}$
PP-DNS$^{(p)}$ with physical particles/droplets as point sources	Realization: $\mathbf{U}^{(f)}(\mathbf{x},t)$, $p(\mathbf{x},t)$	Realization: point field $\{\mathbf{X}^{(i)}(t), \mathbf{V}^{(i)}(t), i = 1,...,N_s(t)\}$
PP-DNS$^{(s)}$ with stochastic particles	Realization	Statistically averaged density $f(\mathbf{x},\mathbf{v},r,t)$
LES$^{(p)}$ with physical droplets as point sources	Filtered field of a realization	Spatially filtered point field
LES$^{(s)}$ with stochastic particles	Filtered field of a realization	Spatially filtered density
RANS	Mean fields $\langle \mathbf{U}^{(g)} \rangle, \langle p \rangle$	Statistically averaged density $f(\mathbf{x},\mathbf{v},r,t)$

are consistent with the EE two-fluid theory. It also gives insight into meaningful comparison of LE simulations with results from experiment and direct numerical simulation. Finally, it shows the extensions needed in the LE approach to accurately represent physical phenomena such as preferential concentration and clustering.

A statistical description of multiphase flows is useful to represent the statistical variability in configurations of the dispersed-phase particles or droplets. Also unlike single-phase flows, the velocity and pressure fields even in *laminar* multiphase flows exhibit statistical variability, and are meaningfully represented by random fields. In spite of the similarities between the statistical theory of multiphase flows and that of turbulent single-phase flow, there are in fact many important differences.

Statistical approaches to multiphase flow can be classified on the basis of three criteria: (i) whether each phase is represented using a *random field* or *stochastic point process*[4] description, (ii) whether each phase is represented in an Eulerian or Lagrangian reference frame, and (iii) the level of closure in the statistical theory.

As shown in Fig. 1, the two principal approaches are: (i) the *random field* approach in which both dispersed and carrier phases are represented as random fields in the Eulerian frame, and (ii) the *point process* approach in which the dispersed phase is represented as a stochastic point process in the Lagrangian frame and the carrier phase represented as a random field in the Eulerian frame. The random field approach at the closure level of moments leads to the EE two-fluid theory in its ensemble-averaged [10,11] and volume-averaged variants [60]. The LE approach corresponds to a closure of the point process approach at the level of the ddf or NDF, with the carrier phase being represented in a Eulerian frame through a RANS closure, LES or DNS. In the following subsections, the LE approach is developed in the context of this family of statistical theories of multiphase flow.

2.1. Realization of a multiphase flow

The foundation of any statistical theory rests on the definition of the ensemble Ω of realizations (or events) $\omega \in \Omega$ for which the probability measure is defined. Fig. 1 shows the description of a realization of a multiphase flow in the random field and point process descriptions. A brief description of these two principal statistical representations of multiphase flows follows.

2.2. Eulerian representation of both phases

2.2.1. Random field description

In statistical theories of turbulent single-phase flow, the Eulerian velocity field is represented as a random vector field [61]. A similar approach can be adopted for two-phase flows, but in addition to the velocity (and pressure) field it is also necessary to specify the location and shape of the dispersed-phase elements. The velocity field $\mathbf{U}(\mathbf{x},t;\omega)$, which is defined in both thermodynamic phases, is a vector field that is defined at each point $\mathbf{x}$ in the flow domain in physical space, on the ωth realization. The dispersed-phase elements in that same realization are similarly described by a dispersed-phase indicator *field* $I_d(\mathbf{x},t;\omega)$, which is unity for all points inside the dispersed-phase elements that are contained in the flow domain, and zero outside. Statistical theories based on random field representations require the consideration of multi-point joint probability density functions, and these have not resulted in tractable engineering models even for single-phase turbulent flow [61–63]. Edwards presents an attempt at formulating such a theory for multiphase flows [64], but no tractable models have emerged based on this theory.

The simplest multipoint theory based on the random field representation that is useful to modelers is a two-point representation. A comprehensive *two-point* statistical description of two-phase flows based on the random field representation can be found in Sundaram and Collins [65]. However, even this two-point theory needs to be extended to statistically inhomogeneous flows before it can be applied to realistic problems. Even in the homogeneous case the resulting two-point equations lead to many unclosed terms that need closure models. Finally, efficient computational implementations need to be devised before the practical application of the two-point theory can be realized. Therefore, most engineering models currently rely on a simpler single-point theory.

2.2.2. Two-fluid theory

If statistical information at only a single space–time location $(\mathbf{x},t)$ of the random field representation is considered, this results in a single-point Eulerian–Eulerian two-fluid theory. In this case the statistics of the velocity field $\mathbf{U}(\mathbf{x},t;\omega)$, and the dispersed-phase indicator field $I_d(\mathbf{x},t;\omega)$, are considered at a single space–time location, i.e., the indicator *field* reduces to an indicator *function*. The velocity and indicator function can be treated as random variables (or random vector in the case of velocity) *parametrized* by space and time variables. The averaged equations resulting from this approach are described in Drew [10], and Drew and Passman [11]. The single-point Eulerian–Eulerian theory can also be developed at the more fundamental level of probability density functions, and this theory is described in Pai and Subramaniam [13].

2.3. Lagrangian representation of the dispersed phase

An alternative approach is to describe the dispersed-phase consisting of N_s solid particles or spray droplets using Lagrangian coordinates $\{\mathbf{X}^{(i)}(t), \mathbf{V}^{(i)}(t), R^{(i)}(t), i = 1,...,N_s(t)\}$, where $\mathbf{X}^{(i)}(t)$ denotes the ith dispersed-phase element's position at time t, $\mathbf{V}^{(i)}(t)$ represents its velocity, and $R^{(i)}(t)$ its radius. Additional properties can be included in variants of this representation without loss of generality. The rigorous development of a statistical theory of multiphase flows [66] using the Lagrangian approach relies on the *theory of stochastic point processes* [67], which is considerably different from the *theory of random fields* [61,68,69] that forms the basis for the

[4] The term point process should not be confused with the 'point particle' assumption. Stochastic point processes are mathematical descriptors of non-contiguous objects in space that can be spheres of finite radius.

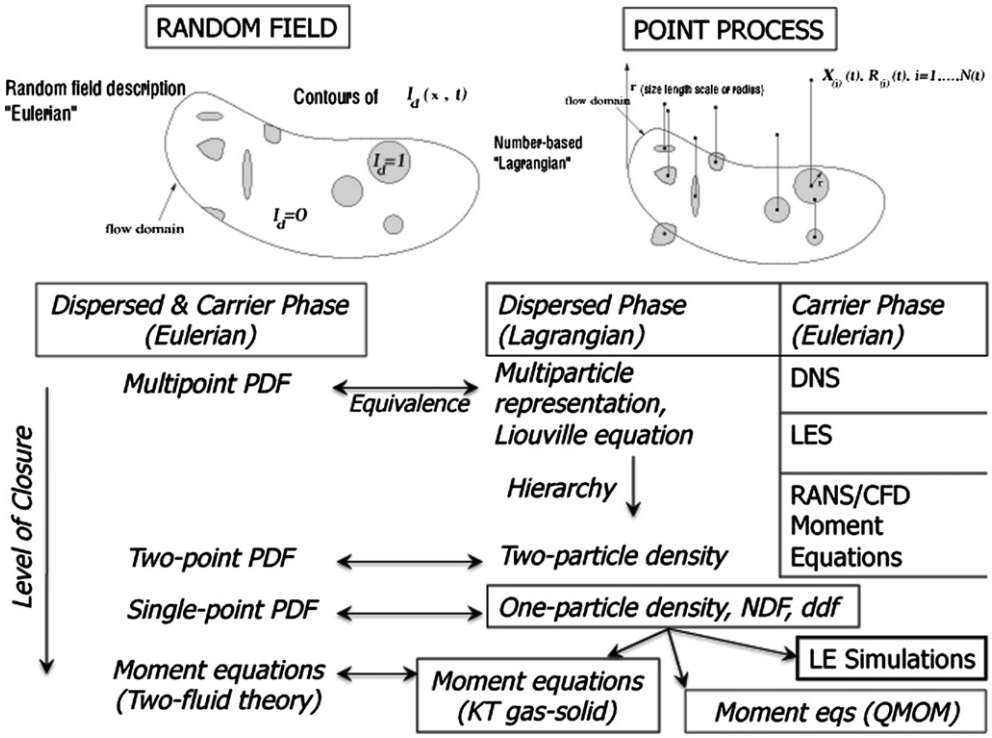

Fig. 1. Representations of multiphase flow as random fields or a point process embedded in a random field, leading to the EE and LE approaches, respectively. Both approaches can be used at different levels of closure, and their equivalence is indicated.

Eulerian–Eulerian approach. Such a theory of multiphase flows is not a trivial extension of the statistical theories for single-phase turbulent flows, but in fact bears a closer relation to the classical kinetic theory of gases and its extension to granular gases [70] and gas–solid flow [9].

2.4. Point process description

Stochastic point process theory [67,71,72] enables the statistical description of non-contiguous objects that are distributed in space, such as solid particles or spray droplets, as a *point process*. This provides the necessary mathematical foundation to describe the statistics of solid particles or spray droplets. The theory of marked point processes allows us to assign the size of the particle or droplet as a "mark" or tag to the particle or droplet location. From this it is clear that stochastic point process theory does not require that spray droplets be modeled as point particles that correspond to δ-function sources of mass and momentum. However, there is a widespread misconception in the spray literature that *point process* models imply 'point particle' models.

The simplest stochastic point process is the homogeneous Poisson process characterized by *complete independence* between the distribution of points, an example of which is shown in Fig. 2(a). This is not a good model for particles or droplets of finite size because the independence property allows neighboring particles or droplets to overlap (see Fig. 2(a)). A better analytical point process model for dilute multiphase flows is the Matérn hard-core process, which is obtained by thinning (or pruning) overlaps from the Poisson model. An example of the Matérn hard-core process obtained by thinning the Poisson process of Fig. 2(a) is shown in Fig. 2(b). The advantage of mathematical models such as the Matérn hard-core process is that their statistical properties, such as number density and pair correlation (see Fig. 3), are known analytically.

It is interesting to compare the spatial distribution of particles from simulation with these analytical point process models. Fig. 2(c) shows the equilibrium spatial distribution of particles obtained following elastic collisions using a soft-sphere DEM model, and its corresponding pair correlation function is shown in Fig. 3. There is a higher probability of finding neighbors within 2 particle diameters from the DEM simulation as compared with the Matérn model. Although these point process models are idealized representations of multiphase flows, they do provide a useful conceptual framework to analyze experimental and simulation data.

The statistical representation of a multiphase flow as a point process has been formulated by Subramaniam [66]. It is shown that the complete characterization of all multiparticle events requires consideration of the Liouville pdf (cf. Fig. 1), and a hierarchy similar to the BBGKY hierarchy [73] can be developed for multiphase flows as well [66].

2.4.1. Complete representation of the dispersed phase as a point process

A key result of the point process theory of multiphase flows [66] is the *complete* point process statistical description. This involves specifying the sequence of probabilities for the events $[N_s = k]$, $k \geq 1$, which are denoted

$$p_k = P[N_s = k], \quad k \geq 1, \tag{1}$$

and the corresponding sequence of symmetrized Liouville densities

$$f^{sym}_{N_s=k}(\mathbf{x}_1, \mathbf{v}_1, r_1, \ldots, \mathbf{x}_k, \mathbf{v}_k, r_k; t), \quad k \geq 1. \tag{2}$$

This complete point process statistical description of a multiphase flow is then related to Williams' droplet distribution function (ddf) through the single-particle surrogate pdf. The single-particle surrogate pdf is defined in terms of the symmetrized Liouville probability density, in a manner analogous to the single-particle probability density in the BBGKY hierarchy of kinetic theory. The single-particle surrogate density is defined as

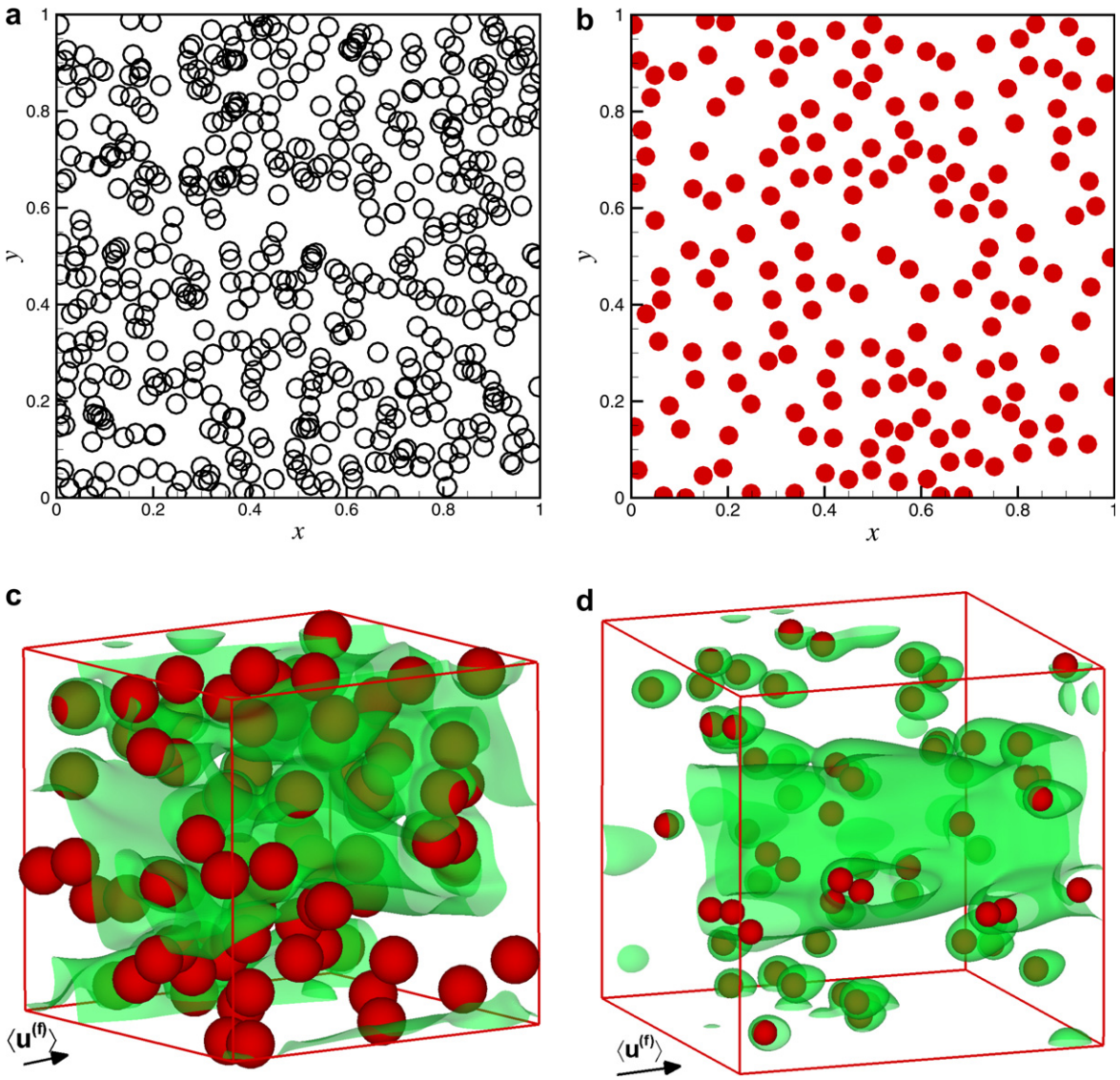

Fig. 2. Spatial distribution of the dispersed phase in multiphase flows. Point process models for representing multiphase flows at 10% dispersed-phase volume fraction: (a) the simple Poisson model results in overlapping particles or droplets. (b) The Matérn hard-core point process is obtained by removing overlapping spheres from a parent Poisson process through a procedure called dependent thinning. Particle configurations obtained from soft-sphere DEM with elastic collisions: (c) at 10% solid volume fraction, and (d) at 1% solid volume fraction. Contour levels in (c) and (d) are for a passive scalar value of 0.5 obtained from fully-resolved DNS at a Reynolds number of 20 ($Re_m = Wd_p/\nu$) in a homogeneous gas–solid flow with isothermal particles at zero scalar value, and the ambient fluid at scalar value of unity. Significant neighbor particle interactions are found even at 1% solid volume fraction!

$$f_{1s}^{[N_s=k]}(\mathbf{x}_1,\mathbf{v}_1,r_1;t) \equiv \int \mathrm{d}\mathbf{x}_2\mathrm{d}\mathbf{v}_2\mathrm{d}r_2\ldots\mathrm{d}\mathbf{x}_k\mathrm{d}\mathbf{v}_k\mathrm{d}r_k f_{[N_s=k]}^{sym}(\mathbf{x}_1,\mathbf{v}_1,r_1,\ldots,\mathbf{x}_k,\mathbf{v}_k,r_k;t), \tag{3}$$

where the superscript $[N_s = k]$ serves to indicate that this single-particle surrogate density is defined for the ensemble which has a total of $N_s = k$ particles or droplets. Therefore, the single-particle surrogate density $f_{1s}^{[N_s=k]}(\mathbf{x}_1,\mathbf{v}_1,r_1;t)$ is a density conditional on the total number of particles or droplets N_s being equal to k. For convenience of notation we use the simpler form $f_{1s}^{(k)}(\mathbf{x}_1,\mathbf{v}_1,r_1;t)$ to denote $f_{1s}^{[N_s=k]}(\mathbf{x}_1,\mathbf{v}_1,r_1;t)$.

2.4.2. The droplet distribution function

Williams' droplet distribution function is related to the single-particle surrogate pdf through the following relation:

$$f(\mathbf{x},\mathbf{v},r,t) = \sum_{k\geq 1} p_k f^{(k)}(\mathbf{x},\mathbf{v},r,t) = \sum_{k\geq 1} p_k k f_{1s}^{(k)}(\mathbf{x},\mathbf{v},r;t), \tag{4}$$

which reveals that the ddf is a superposition of each of the number densities of particles or droplets in phase space $f^{(k)}(\mathbf{x},\mathbf{v},r,t)$, where each number density $f^{(k)}(\mathbf{x},\mathbf{v},r,t)$ is weighted by the appropriate probability p_k.

If the multiphase flow is modeled as a marked point process [74], then the ddf can be expressed as the product of the intensity of the point process in physical space, and a joint probability density function (jpdf) of velocity and radius conditioned on physical

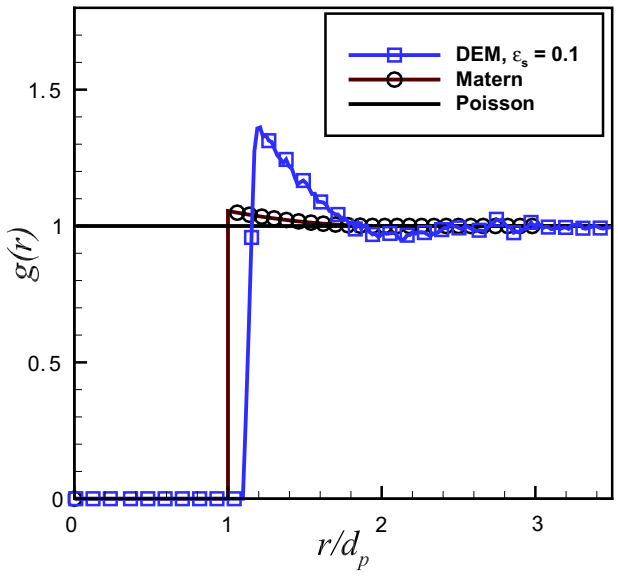

Fig. 3. Pair correlation function $g(r)$ as a function of separation distance between centers r for 2D disks distributed according to the Poisson and Matérn hard-core processes shown in Fig. 2 at 10% dispersed-phase volume fraction. The pair correlation function for 3D spheres from soft-sphere DEM is also shown at 10% solid volume fraction.

location. The jpdf of velocity and radius conditioned on physical location $f^c_{\mathbf{V}R}(\mathbf{v}, r|\mathbf{x}; t)$ is expressed in terms of the ddf as:

$$f^c_{\mathbf{V}R}(\mathbf{v}, r|\mathbf{x}; t) = \begin{cases} f(\mathbf{x}, \mathbf{v}, r, t)/n_s(\mathbf{x}; t) & \text{if } r > 0 \\ 0 & \text{if } r \le 0 \end{cases}, \tag{5}$$

where

$$n_s(\mathbf{x}; t) \equiv \int f(\mathbf{x}, \mathbf{v}, r, t)\mathrm{d}\mathbf{v}\,\mathrm{d}r \tag{6}$$

is the number density. This shows that the ddf is capable of representing polydispersity and capturing the nonlinear dependence of particle acceleration on velocity. However, the ddf does not contain two-particle information, nor does it account for the fluctuations in the number of particles about their mean value. These points are discussed in the following subsection.

2.4.3. Differences from classical kinetic theory

While this characterization is similar to the classical kinetic theory of molecular gases [73], some of the important differences are summarized below:

1. *Effect of neighbor particles can be significant even at low volume fraction* because these interactions are mediated by the carrier fluid. Fig. 2 shows that the scalar contours surrounding neighbor particles can interact even at 1% volume fraction, whereas the typical rule of thumb for neglecting such neighbor interactions in dilute sprays is for volume fraction up to 10%. Chiu et al. [75] have considered spray models that incorporate models for the pair correlation function that contains two-particle information.
2. *Scale separation may be absent in multiphase flows:* In molecular gases the macroscale variation of hydrodynamic variables such as bulk density occurs on scales much greater than the microscale (molecular size) or mesoscale (range of interaction of molecules such as mean free path). However, this is not guaranteed in multiphase flows. As the example in Fig. 4 shows, the mean fluid temperature may vary on scales comparable to the mesoscale spatial structure of particles as characterized by the pair correlation function. This is because of the strong coupling between phases whereby particles can heat up or cool down the fluid, thereby affecting the mean fluid temperature over relatively small length scales.
3. *Fluctuations in number of particles or droplets can be significant compared to the mean:* Fluctuations in number can be important near the edge of sprays or when clusters and streamers form in fluidized bed risers. Such fluctuations are typically neglected in classical kinetic theory of molecular and granular gases [76,77]. However, Subramaniam and Pai have recently shown that these fluctuations can be important in the kinetic theory of inelastic granular gases [78].
4. *Multiphase Liouville equation is not closed:* Another important difference is that while the Liouville equation in the classical kinetic theory of molecular gases is a *closed* equation, the same is not true for the multiphase Liouville equation. The multiphase Liouville equation depends on the statistics of the carrier phase because the acceleration of inertial droplets or particles depends on the slip velocity.

2.4.4. Equivalence and consistency

The schematic in Fig. 1 shows that a hierarchy of closures ranging from multipoint probability density functions (PDF) to moment equations is possible in both random field and point process descriptions. It can be shown that under certain conditions [13] there is an *equivalence* between the corresponding levels of closure in both descriptions. The hierarchy of closures implies that a closure at the NDF or ddf level in the LE approach implies a set of moment equations that correspond to the two-fluid theory in the random field description. This leads to the principle of developing *consistent* models in either approach. Recent work by Pai and Subramaniam establishes the relations between the point process (LE) and random field (EE) descriptions [13] at the single-point PDF level of closure.

2.5. Summary

This section described the principal statistical representations of multiphase flow. The classification of multiphase flow theories into point process (LE) and random field (EE) categories was explained. The foundations of the EE two-fluid theory were briefly described. The connection of the LE approach to kinetic theory was established. Important differences between the point process (LE) description of multiphase flows and the classical kinetic theory of molecular gases were noted. The relation of the ddf to a complete description of a multiphase in the Lagrangian stochastic point process approach was explained. This provides the necessary background to understand the LE formulation and its relation to the EE two-fluid theory.

3. Lagrangian–Eulerian formulation

A central concept in the LE formulation is the statistical equivalence of the evolution of the particle or droplet ensemble $\{\mathbf{X}^{(i)}(t), \mathbf{V}^{(i)}(t), R^{(i)}(t), i = 1,...,N_s(t)\}$ described in Section 2.3 to the evolution of the ddf. For generality here we consider droplets for which the radius may also change due to vaporization.

3.1. Droplet evolution equations

The droplet properties associated with the ith droplet evolve by the following equations:

$$\frac{\mathrm{d}\mathbf{X}^{(i)}}{\mathrm{d}t} = \mathbf{V}^{(i)}(t) \tag{7}$$

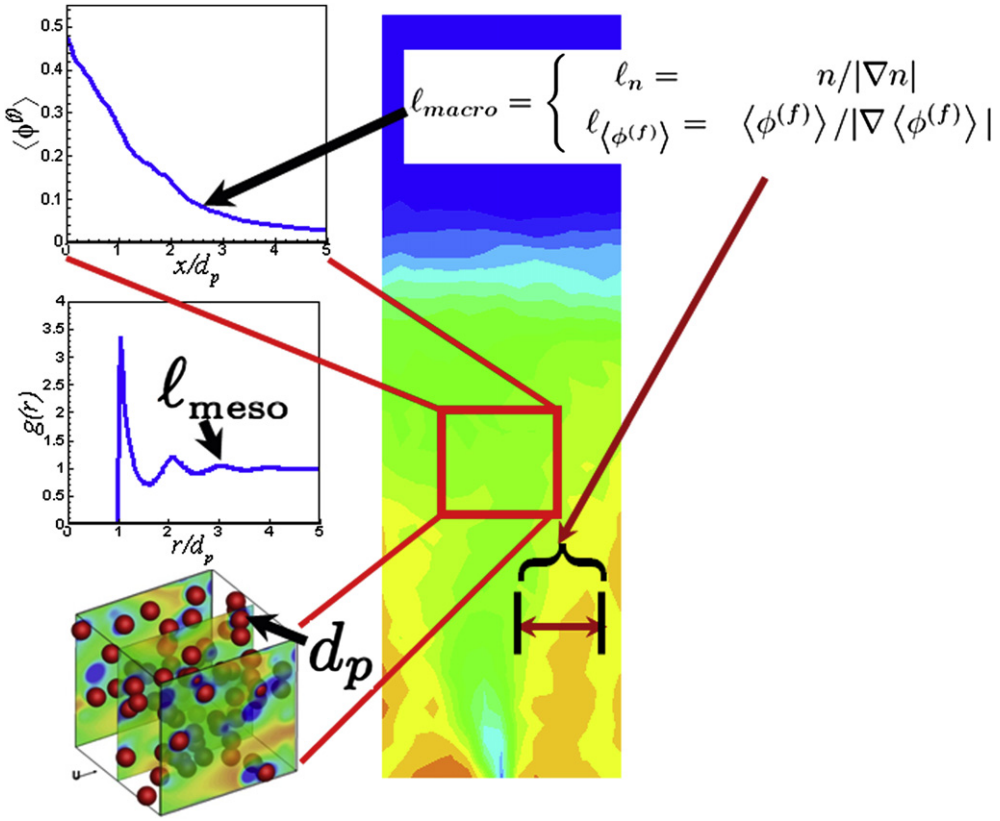

Fig. 4. Comparison of length scales in multiphase flows. The macroscale corresponds to the variation of average volume fraction or mean fluid temperature in a central jet fluidized bed (right panel), while the microscale corresponds to the diameter of particles show in the fully-resolved DNS (bottom left panel). The mesoscale corresponds to the spatial structure of the point process that is characterized by the pair correlation function (middle left panel). The DNS reveals that the normalized average fluid temperature $\langle\varphi^{(f)}\rangle$ (top left panel) varies on length scales comparable to the mesoscale, indicating lack of scale separation. Here $\langle\varphi^{(f)}\rangle \equiv (\langle T^{(f)}\rangle - T_s)/(T_{m,in} - T_s)$, where $\langle T^{(f)}\rangle$ is the mean fluid temperature, $T_{m,in}$ is the bulk fluid temperature at the inlet and T_s is the particle temperature.

$$\frac{d\mathbf{V}^{(i)}}{dt} = \mathbf{A}^{(i)}(t) \tag{8}$$

$$\frac{dR^{(i)}}{dt} = \Theta^{(i)}(t), \quad i = 1, \ldots, N_s(t), \tag{9}$$

where $\mathbf{A}^{(i)}$ is the acceleration experienced by the droplet, and $\Theta^{(i)}$ is the rate of radius change due to vaporization. The droplet acceleration $\mathbf{A}^{(i)}$ arises from the force exerted by the carrier gas on the droplet that can be calculated from the stress tensor at the droplet surface. Spray droplets also undergo collisions that modify their trajectory and velocity. Following collisions, droplets may coalesce or break up into smaller droplets. The evolution of the ddf corresponding to droplet evolution equations can be derived using standard methods [73,74].

3.2. Evolution equation for the ddf or NDF

Starting from the definition of the ddf in Eq. (4), one can derive [74] the following collisionless form of the ddf evolution equation (also referred to as the spray equation) that corresponds to the droplet evolution equations Eqs. (7)–(9):

$$\frac{\partial f}{\partial t} + \frac{\partial}{\partial x_k}[v_k f] + \frac{\partial}{\partial v_k}\left[\langle A_k|\mathbf{x},\mathbf{v},r;t\rangle f\right] + \frac{\partial}{\partial r}\left[\langle\Theta|\mathbf{x},\mathbf{v},r;t\rangle f\right] = 0. \tag{10}$$

Note that summation over Cartesian indices is implied by repeated Roman subscripts in this paper. In the above equation $\langle A_k|\mathbf{x},\mathbf{v},r;t\rangle$ represents the expected acceleration conditional on the location [**x**,**v**,*r*] in phase space. Similarly $\langle\Theta|\mathbf{x},\mathbf{v},r;t\rangle$ represents the expected rate of change of radius (hereafter referred to as the expected vaporization rate) conditional on the location [**x**,**v**,*r*] in phase space. The effects of collisions, coalescence and breakup can also be incorporated [8,21] to obtain

$$\frac{\partial f}{\partial t} + \frac{\partial}{\partial x_k}[v_k f] + \frac{\partial}{\partial v_k}\left[\langle A_k|\mathbf{x},\mathbf{v},r;t\rangle f\right] + \frac{\partial}{\partial r}\left[\langle\Theta|\mathbf{x},\mathbf{v},r;t\rangle f\right] = \dot{f}_{coll} + \dot{f}_{coal} + \dot{f}_{bu}. \tag{11}$$

3.2.1. Regime of validity of the spray equation

A detailed description of the mathematical basis of the ddf approach is given in Ref. [74]. The practical implications of the assumptions underlying the ddf approach are briefly summarized here.

The point process model underlying the ddf approach assumes that a characteristic size length scale can be associated with each droplet. From a purely representational standpoint this does not pose difficulties even for regions of the spray where the liquid phase is present as nonspherical elements, rather than as fully dispersed droplets. As long as the volume of such liquid elements can be defined, one can always associate with each liquid element a characteristic size length scale which is the radius of a spherical droplet of equal volume.[5] The point process model is strictly inapplicable only in the intact core region of a spray. Therefore, the

[5] The information concerning the shape of the nonspherical liquid element is lost in the process, and will have to be accounted for in the models.

LE approach does require a separate model for the primary breakup of a liquid jet resulting in an initial condition for the ddf.

It is noteworthy that two assumptions that are commonly perceived as necessary to establish the validity of the spray equation, have not been used in this derivation. They are: (i) the assumption of point particles, and (ii) the dilute spray assumption.

3.2.1.1. Point process vs. point particle assumption. The assumption of point particles is different from the stochastic point process model of a multiphase flow, and is considerably more restrictive. The point particle assumption requires that the size (radius) of the particles or droplets be infinitesimal, or at least smaller than the smallest scale of fluid motions, e.g., the Kolmogorov scale if the gas-phase flow is turbulent. Here it is shown that multiphase flows with particles or droplets of finite radius (which may be larger than the Kolmogorov scale of gas-phase turbulence) can be successfully modeled using the stochastic point process model. In summary, the point particle assumption is unnecessary for the representation and modeling of multiphase flows using the ddf or NDF approach, which admits particles or droplets of finite size.

3.2.1.2. Dilute assumption. Another commonly held view is that the ddf approach is valid only for dilute multiphase flows. This results in unnecessary restrictions being imposed on LE simulations that require the computed estimate for the average dispersed-phase volume fraction in a grid cell to be less than some user defined value (e.g., 0.1). This confuses a theoretical issue with numerics. The theoretical issue is clarified in this section revealing that this restriction has no basis, while Section 5.2 shows that numerically convergent estimation methods also do not impose any restrictions on the volume fraction.

The average dispersed-phase volume fraction is one measure of how dilute a spray is. The average dispersed-phase volume $\langle V_d(A;t)\rangle$ in a region A in physical space may be defined in terms of the ddf as:

$$\langle V_d(A;t)\rangle \equiv \int_A \theta(\mathbf{x};t)\mathrm{d}\mathbf{x} \equiv \int_A \int_{[\mathbf{v},r]} \frac{4}{3}\pi r^3 f(\mathbf{x},\mathbf{v},r,t)\ \mathrm{d}\mathbf{v}\mathrm{d}r\mathrm{d}\mathbf{x}, \quad r>0, \tag{12}$$

where

$$\theta(\mathbf{x};t) = \int_{[\mathbf{v},r]} \frac{4}{3}\pi r^3 f(\mathbf{x},\mathbf{v},r,t)\ \mathrm{d}\mathbf{v}\mathrm{d}r, \quad r>0, \tag{13}$$

is the density of average dispersed-phase volume in physical space. If V_A is the volume associated with region A, then the average dispersed-phase volume fraction in region A is given by

$$\frac{\langle V_d(A;t)\rangle}{V_A} = \frac{1}{V_A}\int_A \theta(\mathbf{x};t)\mathrm{d}\mathbf{x}, \tag{14}$$

which reveals that if the average dispersed-phase volume density $\theta(\mathbf{x};t)$ is uniform in the region A in physical space (i.e., the ddf $f(\mathbf{x},\mathbf{v},r,t)$ is statistically homogeneous in A), then θ is equal to the average dispersed-phase volume fraction. If f is statistically *in*homogeneous in A, then Eq. (14) states that the mean value of $\theta(\mathbf{x};t)$ over the volume A is the average dispersed-phase volume fraction.

The validity of the ddf evolution equation does not depend on the average dispersed-phase volume density. While some models for drag or heat transfer [21] may be limited to volume fraction $\theta(\mathbf{x};t) \ll 1$ because of limitations in the correlations on which they are based, these can be extended to include a dependence on volume fraction. In summary, restrictions on the volume fraction in LE simulations are unnecessary because there is no intrinsic theoretical limitation on the average dispersed-phase volume fraction in the LE approach, but rather they arise from non-convergent numerical implementations that compute the dispersed-phase volume fraction using Eulerian grid cell-based local averages. In Section 5.2 it is shown that kernel-based grid-free estimation methods result in numerically convergent values for the average dispersed-phase volume fraction and average interphase momentum transfer.

3.3. Eulerian representation of the carrier phase

The LE approach described thus far is very general, and applies to the entire range of simulations described earlier in Section 1.2, including coupling with Eulerian representation of the carrier phase using RANS, LES and DNS. Table 1 lists the representation of the carrier flow field and dispersed phase for different LE simulation methods.

The specific equations appropriate to each of these simulation methods can be recovered by appropriate interpretation (realization, filtered realization or statistical average) of the Eulerian fluid velocity field, stress tensor and interphase momentum transfer term. The specific form of the carrier-phase Eulerian equations naturally depends on the simulation approach: DNS, LES or RANS.

3.3.1. Instantaneous or filtered Eulerian carrier-phase equations

For DNS where every physical particle or droplet is fully resolved, these are simply the low Mach number variable-density Navier–Stokes equations with appropriate boundary conditions at each particle or droplet's surface. Details of such particle-resolved simulations can be found in many works [15,32–35,79–82]. If the droplets or particles are smaller than the Kolmogorov scale of gas-phase turbulence, then PP-DNS are useful. In this case the dispersed phase is coupled by kernel-averaging that particular realization of the point process [83]. However, Moses and Edwards [84] showed that coarse-graining DNS of force on a particle does not lead to a δ-function momentum source, as it is often treated in PP-DNS. The appropriate coarse-graining of momentum transfer from point particles, and its effect on the carrier-phase pressure field needs to be investigated more thoroughly.

In single-phase flows, the LES approach of filtering the Navier–Stokes equations offers an attractive alternative to DNS by capturing most of the turbulent kinetic energy at reduced computational cost. Similar considerations have led the development of LE methods for multiphase flow with LES of the filtered Eulerian gas-phase equations. The extension of the LES filtering approach to two-phase flows is neither straightforward, nor unique [49–53]. Since there are many approaches to LES of two-phase flows, the specific form of the coupling in LES$^{(p)}$ depends on the implementation: broadly speaking, in the LE context, this coupling results in local volume-averaging of the Lagrangian point process realization of the dispersed phase. The same comments on coarse-graining DNS to PP-DNS apply to LES$^{(p)}$ as well. PP-DNS$^{(s)}$ and LES$^{(s)}$ couple to a stochastic particle representation of the dispersed phase and are hybrid methods in the sense that they couple a realization of the carrier fluid phase with a statistical representation of the dispersed phase. The LE theoretical basis developed in this work is relevant for these simulations. For DNS$^{(s)}$ and LES$^{(s)}$ with stochastic particles, the fluid-phase Eulerian momentum equation in the dilute limit is often taken to be of the form

$$\rho_f\left(\frac{\partial \mathbf{U}^{(f)}}{\partial t} + \mathbf{U}^{(f)}\cdot\nabla\mathbf{U}^{(f)}\right) = \nabla\cdot\boldsymbol{\tau} - \left\langle \mathbf{F}^{fd}\right\rangle, \tag{15}$$

where $\mathbf{U}^{(f)}$ represents the instantaneous fluid-phase velocity in DNS$^{(s)}$ (and its filtered counterpart in LES$^{(s)}$). Note that this is simply

the single-phase momentum conservation equation augmented by the interphase momentum transfer term

$$\left\langle \mathbf{F}^{fd} \right\rangle = \int\limits_{[\mathbf{v},r]} m\langle \mathbf{A}|\mathbf{x},\mathbf{v},r;t\rangle f(\mathbf{x},\mathbf{v},r,t)\mathrm{d}\mathbf{v}\mathrm{d}r$$

that accounts for the coupling of the dispersed-phase momentum with the fluid phase.

Insofar as LE methods are concerned, the principal benefit of DNS is to quantify unclosed terms in the ddf evolution equation (or its moments), and to develop better models for these terms. Some details of how particle- or droplet-resolved DNS solutions can be used to develop LE and EE sub-models are given in Garg et al. [82]. If point particles are used, as in PP-DNS$^{(p)}$ and LES$^{(p)}$, then the foregoing LE theoretical development can be used to interpret the results. However, such simulations have less value for LE model development as compared to DNS. Simulations with stochastic particles such as DNS$^{(s)}$ and LES$^{(s)}$ are essentially LE models with better representation of the Eulerian carrier phase than RANS, and the preceding theoretical development is useful in interpreting the results of these models and comparing them with both fully-resolved DNS and LE coupled with RANS.

3.3.2. Averaged Eulerian carrier-phase equations

The averaged Eulerian carrier-phase equations are given by the two-fluid theory [10,11]. The specific form of these equations is taken from Pai and Subramaniam [13]. For CFD spray simulations using averaged carrier-phase equations that account for two-way coupling and do not assume a dilute spray, the Eulerian mean mass conservation equation is

$$\frac{\partial \alpha_f \left\langle \rho \middle| I_f = 1 \right\rangle}{\partial t} + \frac{\partial}{\partial x_i}\left(\alpha_f \left\langle \rho \middle| I_f = 1 \right\rangle \left\langle \tilde{U}_i^{(f)} \right\rangle \right) = \left\langle S_\rho^{(f)} \right\rangle, \tag{16}$$

where $\alpha_f = \langle I_f \rangle$ is the average fluid volume fraction, and the phase-averaged mean velocity in the gas-phase is given by

$$\left\langle \tilde{U}_i^{(f)} \right\rangle = \left\langle I_f \rho U_i \right\rangle \Big/ \left\langle I_f \rho \right\rangle. \tag{17}$$

In Eq. (16) the source term due to interphase mass transfer is

$$\left\langle S_\rho^{(f)} \right\rangle = \left\langle \rho \left(U_i - U_i^{(I)} \right) \frac{\partial I_f}{\partial x_i} \right\rangle. \tag{18}$$

The Eulerian mean momentum conservation equation is

$$\frac{\partial}{\partial t}\left[\alpha_f \left\langle \rho \middle| I_f = 1 \right\rangle \left\langle \tilde{U}_i^{(f)} \right\rangle \right] + \frac{\partial}{\partial x_j}\left[\alpha_f \left\langle \rho \middle| I_f = 1 \right\rangle \left\langle \widetilde{U_i^{(f)} U_j^{(f)}} \right\rangle \right] = \frac{\partial}{\partial x_j}\left\langle I_f \tau_{ji}^{(f)} \right\rangle + \left\langle I_f \rho b_i \right\rangle + \left\langle S_{Mi}^{(f)} \right\rangle, \tag{19}$$

where $\langle S_{Mi}^{(f)} \rangle$ is the interfacial momentum source term given by

$$\left\langle S_{Mi}^{(f)} \right\rangle = \left\langle \rho U_i \left(U_j - U_j^{(I)} \right) \frac{\partial I_f}{\partial x_j} - \tau_{ji} \frac{\partial I_f}{\partial x_j} \right\rangle. \tag{20}$$

The so-called "dilute approximation" to these equations that neglects the volume displaced by the presence of the dispersed-phase particles or spray droplets is often used [21]. It is obtained by setting $\alpha_f = 1$ in the above equations and neglecting the volume fraction of the dispersed phase. For example, in this notation the simplified mass conservation equation [21] reads

$$\frac{\partial \rho_f}{\partial t} + \nabla \cdot \left(\rho_f \left\langle \tilde{\mathbf{U}}^{(f)} \right\rangle \right) = \left\langle S_\rho^{(f)} \right\rangle, \tag{21}$$

where $\rho_f = \alpha_f \langle \rho | I_f = 1 \rangle$ (in implementations for dilute flows [21,22] α_f is set to unity, so the bulk or apparent gas density is simply the thermodynamic gas density).

However, there is another assumption implicit in this "dilute approximation" to the mass conservation equation that is worth noting. The proper simplification of the mean mass conservation equation in the dilute limit is not obtained by simply setting $\alpha_f = 1$ in Eq. (16), but by first expanding the terms and rearranging to obtain

$$\frac{\partial \rho_f}{\partial t} + \nabla \cdot \left(\rho_f \left\langle \tilde{\mathbf{U}}^{(f)} \right\rangle \right) = \frac{\left\langle S_\rho^{(f)} \right\rangle}{\alpha_f} - \rho_f \left[\frac{\tilde{D}}{\tilde{D}t} \ln \alpha_f \right], \tag{22}$$

where

$$\frac{\tilde{D}}{\tilde{D}t} \equiv \frac{\partial}{\partial t} + \left\langle \tilde{\mathbf{U}}^{(f)} \right\rangle \cdot \nabla.$$

Even in dilute sprays the effect of large *gradients* in the volume fraction at the edge of the spray can result in significant contributions from the term in $\ln \alpha_f$, and therefore this term needs to be quantified in spray calculations. Clearly, the assumption of $\alpha_f = 1$ only validates the simplification $\langle S_\rho^{(f)} \rangle / \alpha_f \approx \langle S_\rho^{(f)} \rangle$. Apte et al. [85] and Ferrante and Elghobashi [86,87] have developed LE simulations that account for volume displacement effects.

3.4. Interphase transfer terms

The source terms ($\langle S_\rho^{(f)} \rangle$ and $\langle S_{Mi}^{(f)} \rangle$) that appear in the Eulerian gas-phase-averaged equations (cf. Eqs. (16)–(20)) couple the dispersed-phase to the carrier phase, and are opposite in sign to their counterparts in the dispersed phase:

$$\left\langle S_\rho^{(f)} \right\rangle = -\left\langle S_\rho^{(d)} \right\rangle \tag{23}$$

$$\left\langle S_{Mi}^{(f)} \right\rangle = -\left\langle S_{Mi}^{(d)} \right\rangle. \tag{24}$$

Their counterparts in the dispersed phase can be expressed as integrals with respect to the ddf, and the relations are [13]

$$\left\langle S_\rho^{(d)} \right\rangle = \alpha_d \rho_d \left\{ 3\left\langle \tilde{\Omega} \middle| \mathbf{x};t \right\rangle + \left\langle \tilde{\Theta} \middle| \mathbf{x}, r = 0_+; t \right\rangle f_R^c(r = 0_+ | \mathbf{x};t) \right\}, \tag{25}$$

where $\Omega = \Theta/R$ and the volume-weighted average of any smooth function $Q(\mathbf{v},r)$ is defined as:

$$\left\langle \tilde{Q} \right\rangle \equiv \frac{\langle R^3 Q \rangle}{\langle R^3 \rangle}, \tag{26}$$

with

$$\langle Q \rangle \equiv \int\limits_{[\mathbf{v},r]} Q(\mathbf{v},r) f_{\mathbf{V}R}^c(\mathbf{v},r|\mathbf{x};t)\, \mathrm{d}\mathbf{v}\, \mathrm{d}r, \quad r > 0. \tag{27}$$

Details can be found in Ref. [13].

It is convenient to decompose the interfacial momentum source term $\langle \mathbf{S}_M^{(d)} \rangle$ into two parts, one attributable to interphase mass

transfer arising from phase change $\langle \mathbf{S}_M^{(d)(PC)} \rangle$, and the other to the interfacial stress $\langle \mathbf{S}_M^{(d)(IS)} \rangle$, which is nonzero even in the absence of interphase mass transfer. These are defined as:

$$\left\langle S_{Mi}^{(d)(PC)} \right\rangle \equiv \left\langle \rho U_i \left(U_j - U_j^{(I)} \right) \frac{\partial I_d}{\partial x_j} \right\rangle \tag{28}$$

$$\left\langle S_{Mi}^{(d)(IS)} \right\rangle \equiv - \left\langle \tau_{ji} \frac{\partial I_d}{\partial x_j} \right\rangle. \tag{29}$$

The momentum source due to interfacial stress can be expressed in terms of the dispersed-phase Lagrangian description as

$$\left\langle S_{Mi}^{(d)(IS)} \right\rangle = \alpha_d \, \rho_d \left\langle \tilde{A}_i \right\rangle, \tag{30}$$

while the momentum source due to phase change can be written as:

$$\left\langle S_{Mj}^{(d)(PC)} \right\rangle = \alpha_d \, \rho_d \left\{ 3 \left\langle \widetilde{V_j \Omega} \middle| \mathbf{x}; t \right\rangle + \left\langle \widetilde{V_j \Theta} \middle| \mathbf{x}, r = 0_+; t \right\rangle f_R^c (r = 0_+ | \mathbf{x}; t) \right\}. \tag{31}$$

Detailed derivation and discussion of these terms can be found in Ref. [13].

3.5. Dispersed-phase mean equations: mass and momentum conservation

The ddf evolution equation implies an evolution of mean mass and momentum in the dispersed phase. If a constant thermodynamic density of the dispersed phase ρ_d is assumed, then the mean mass conservation equation implied by the ddf evolution equation is obtained by multiplying Eq. (10) by $(4/3)\pi r^3 \rho_d$ and integrating over all $[\mathbf{v}, r_+]$ (r_+ is simply the region of radius space corresponding to $r > 0$), to obtain:

$$\begin{aligned} \frac{\partial}{\partial t} \left[\frac{4}{3} \pi \left\langle R^3 \right\rangle \rho_d \, n \right] + \frac{\partial}{\partial x_k} \left[\frac{4}{3} \pi \left\langle R^3 \right\rangle \left\langle \tilde{V}_k \right\rangle \rho_d \, n \right] \\ = n \frac{4}{3} \pi \rho_d \left\langle R^3 \right\rangle \left\{ 3 \left\langle \tilde{\Omega} \middle| \mathbf{x}; t \right\rangle + \left\langle \tilde{\Theta} \middle| \mathbf{x}, r = 0_+; t \right\rangle f_R^c (r = 0_+ | \mathbf{x}; t) \right\}. \end{aligned} \tag{32}$$

The source term on the right hand side of Eq. (32) contains two parts. One part corresponds to a loss of mean mass due to vaporization. The other part represents the depletion of number density due to a flux of droplets across the $r = 0_+$ boundary, which corresponds to the smallest radius below which a drop is considered evaporated.

The mean momentum conservation equation implied by the ddf evolution equation Eq. (10) is obtained by multiplying Eq. (10) by $(4/3)\pi r^3 \rho_d v_j$ and integrating over all $[\mathbf{v}, r_+]$:

$$\begin{aligned} \frac{\partial}{\partial t} \left[n \frac{4}{3} \pi \rho_d \left\langle R^3 \right\rangle \left\langle \tilde{V}_j \right\rangle \right] + \frac{\partial}{\partial x_k} \left[n \frac{4}{3} \pi \rho_d \left\langle R^3 \right\rangle \left\langle \widetilde{V_j V_k} \right\rangle \right] \\ = n \frac{4}{3} \pi \rho_d \left\langle R^3 \right\rangle \left\langle \tilde{A}_j \middle| \mathbf{x}; t \right\rangle + n \frac{4}{3} \pi \rho_d \left\langle R^3 \right\rangle \left\{ 3 \left\langle \widetilde{V_j \Omega} \middle| \mathbf{x}; t \right\rangle \right. \\ \left. + \left\langle \widetilde{V_j \Theta} \middle| \mathbf{x}, r = 0_+; t \right\rangle f_R^c (r = 0_+ | \mathbf{x}; t) \right\}. \end{aligned} \tag{33}$$

where mass-weighted averages have been used as in Eq. (32). The last term on the right hand side of the above equation corresponds to a loss of mean momentum due to vaporization, and the depletion of mean momentum due to a flux of droplets across the $r = 0_+$ boundary.

Substituting Eq. (32) into Eq. (33) results in:

$$\begin{aligned} n \frac{4}{3} \pi \rho_d \left\langle R^3 \right\rangle \left\{ \frac{\partial \left\langle \tilde{V}_j \right\rangle}{\partial t} + \tilde{V}_k \frac{\partial \left\langle \tilde{V}_j \right\rangle}{\partial x_k} \right\} \\ = n \frac{4}{3} \pi \rho_d \left\langle R^3 \right\rangle \left\langle \tilde{A}_j \middle| \mathbf{x}; t \right\rangle - \frac{\partial}{\partial x_k} \left[n \frac{4}{3} \pi \rho_d \left\langle R^3 \right\rangle \left\langle v_j''^{(d)} \widetilde{v_k''^{(d)}} \right\rangle \right] \\ + n \frac{4}{3} \pi \rho_d \left\langle R^3 \right\rangle \left\{ 3 \left\langle \widetilde{V_j \Omega} \middle| \mathbf{x}; t \right\rangle \right. \\ \left. + \left\langle \widetilde{V_j \Theta} \middle| \mathbf{x}, r = 0_+; t \right\rangle f_R^c (r = 0_+ | \mathbf{x}; t) \right\} \\ - n \frac{4}{3} \pi \rho_d \left\langle R^3 \right\rangle \left\{ 3 \left\langle \tilde{V}_j \right\rangle \left\langle \tilde{\Omega} \middle| \mathbf{x}; t \right\rangle \right. \\ \left. + \left\langle \tilde{V}_j \right\rangle \left\langle \tilde{\Theta} \middle| \mathbf{x}, r = 0_+; t \right\rangle f_R^c (r = 0_+ | \mathbf{x}; t) \right\}. \end{aligned} \tag{34}$$

where

$$\left\langle v_j''^{(d)} \widetilde{v_k''^{(d)}} \right\rangle \equiv \int\limits_{[\mathbf{v}, r_+]} \left(v_j - \left\langle \tilde{V}_j^{(d)} \right\rangle \right) \left(v_k - \left\langle \tilde{V}_k^{(d)} \right\rangle \right) \times \frac{r^3 f_{\mathbf{V}R}^c (\mathbf{v}, r | \mathbf{x}; t)}{\left\langle R^3 (\mathbf{x}, t) \right\rangle} \mathrm{d}\mathbf{v} \; \mathrm{d}r.$$

When constructing models for terms such as interphase mass, momentum and energy transfer, it is useful to model the Galilean-invariant (GI) forms of these terms because such models are then frame-invariant with respect to Galilean transformations. A Galilean transformation consists of transforming position and time as $\mathbf{x}^* = \mathbf{x} + \mathbf{W}t$ and $t^* = t$, respectively, where $\mathbf{W}$ is a constant translational velocity. If a quantity $\mathbf{Q}$ is Galilean-invariant, then $\mathbf{Q}(\mathbf{x}^*, t^*) = \mathbf{Q}(\mathbf{x}, t)$. The velocity transforms as $\mathbf{U}(\mathbf{x}^*, t^*) = \mathbf{U}(\mathbf{x} + \mathbf{W}t, t) = \mathbf{U}(\mathbf{x}, t) + \mathbf{W}$ and is not Galilean-invariant. If the non-GI forms are modeled, then the resulting models may not be frame-invariant.

The following are GI combinations of unclosed terms:

$$\left\{ \left\langle \widetilde{V_j \Omega} \middle| \mathbf{x}; t \right\rangle - \left\langle \tilde{V}_j \right\rangle \left\langle \tilde{\Omega} \middle| \mathbf{x}; t \right\rangle \right\},$$

and

$$\left\{ \left\langle \widetilde{V_j \Theta} \middle| \mathbf{x}, r = 0_+; t \right\rangle - \left\langle \tilde{V}_j \right\rangle \left\langle \tilde{\Theta} \middle| \mathbf{x}, r = 0_+; t \right\rangle \right\}.$$

Particle method solutions to the ddf equation that model $\langle \mathbf{A} | \mathbf{x}, \mathbf{v}, r; t \rangle$ and $\langle \Theta | \mathbf{x}, \mathbf{v}, r; t \rangle$ automatically guarantee GI modeling of the above terms in the mean momentum equation.

3.6. Second moment equation

The second moment of particle velocity leads to the granular temperature in gas–solid flow, and it is similarly defined for droplets as well. In order to derive the second moment equation in

the LE approach, it is useful to first define the volume-weighted ddf of fluctuating velocity $\tilde{g}(\mathbf{x},\mathbf{w},r,t)$ defined as

$$\tilde{g}(\mathbf{x},\mathbf{w},r,t) = \tilde{f}\left(\mathbf{x},\left\langle\tilde{\mathbf{V}}\middle|\mathbf{x};t\right\rangle+\mathbf{w},r,t\right) = r^3 f(\mathbf{x},\mathbf{v},r,t) \tag{35}$$

$$= \left\langle R^3(\mathbf{x};t)\right\rangle n_s(\mathbf{x};t)\,\tilde{f}^c_{\mathbf{V}R}\left(\left\langle\tilde{\mathbf{V}}\middle|\mathbf{x};t\right\rangle+\mathbf{w},r\middle|\mathbf{x};t\right) \tag{36}$$

$$= \left\langle R^3(\mathbf{x};t)\right\rangle n_s(\mathbf{x};t)\,\tilde{g}^c(\mathbf{w},r|\mathbf{x};t), \tag{37}$$

where

$$\mathbf{w} = \mathbf{v} - \left\langle\tilde{\mathbf{V}}\middle|\mathbf{x};t\right\rangle,$$

where $\tilde{g}^c(\mathbf{w},r|\mathbf{x};t)$ is the r^3-weighted or volume-weighted pdf of fluctuating velocity.

The evolution equation of $\tilde{g}$ can be derived from Eq. (10) (see Appendix A for a derivation):

$$\begin{aligned}&\frac{\partial\tilde{g}}{\partial t}+\left(\left\langle\tilde{V}_k\right\rangle+w_k\right)\frac{\partial\tilde{g}}{\partial x_k}\\&\quad= w_k\frac{\partial\tilde{g}}{\partial w_l}\frac{\partial\left\langle\tilde{V}_l\right\rangle}{\partial x_k}-\frac{\partial}{\partial w_l}\left[\langle A_l|\mathbf{x},\mathbf{v},r;t\rangle\tilde{g}-\tilde{g}\frac{\partial\left\langle\tilde{V}_l\right\rangle}{\partial t}-\tilde{g}\left\langle\tilde{V}_k\right\rangle\frac{\partial\left\langle\tilde{V}_l\right\rangle}{\partial x_k}\right]\\&\qquad-\frac{\partial}{\partial r}\{\langle\Theta|\mathbf{x},\mathbf{v},r;t\rangle\tilde{g}\}+3\langle\Omega|\mathbf{x},\mathbf{v},r;t\rangle\tilde{g}.\end{aligned} \tag{38}$$

The second moment or dispersed-phase Reynolds stress equation can be obtained by multiplying the $\tilde{g}$ evolution equation by $w_i w_j$ (and a factor $\kappa=(4/3)\pi\rho_d$) and integrating over all $[\mathbf{w},r_+]$ space to obtain:

$$\begin{aligned}&\underbrace{\kappa n\left\langle R^3\right\rangle\left\{\frac{\partial\left\langle v_i''^{(d)}\widetilde{v_j''^{(d)}}\right\rangle}{\partial t}+\left\langle\tilde{V}_k\right\rangle\frac{\partial\left\langle v_i''^{(d)}\widetilde{v_j''^{(d)}}\right\rangle}{\partial x_k}\right\}}_{\text{material derivative}}+\underbrace{\kappa\frac{\partial}{\partial x_k}\left[n\left\langle R^3\right\rangle\left\langle v_i''^{(d)}\widetilde{v_j''^{(d)}}v_k''^{(d)}\right\rangle\right]}_{\text{triple velocity correlation}}\\&=\underbrace{-\kappa n\left\langle R^3\right\rangle\left\{\left\langle v_j''^{(d)}\widetilde{v_k''^{(d)}}\right\rangle\frac{\partial\left\langle\tilde{V}_i\right\rangle}{\partial x_k}+\left\langle v_i''^{(d)}\widetilde{v_k''^{(d)}}\right\rangle\frac{\partial\left\langle\tilde{V}_j\right\rangle}{\partial x_k}\right\}}_{\text{production}}+\underbrace{\kappa n\left\langle R^3\right\rangle\left\{\left\langle\widetilde{A_i v_j''^{(d)}}\right\rangle+\left\langle\widetilde{A_j v_i''^{(d)}}\right\rangle\right\}}_{\text{acceleration–velocity covariance}}\\&\quad\underbrace{+\kappa n\left\langle R^3\right\rangle\left[3\left\langle v_i''^{(d)}\widetilde{v_j''^{(d)}}\Omega\middle|\mathbf{x};t\right\rangle+\left\langle v_i''^{(d)}\widetilde{v_j''^{(d)}}\Theta\middle|\mathbf{x},r=0_+;t\right\rangle g^c(r=0_+|\mathbf{x},t)\right]}_{\text{RS change due to mass transfer (1)}}\\&\quad\underbrace{-\kappa n\left\langle R^3\right\rangle\left\langle v_i''^{(d)}\widetilde{v_j''^{(d)}}\right\rangle\left\{3\left\langle\tilde{\Omega}\middle|\mathbf{x};t\right\rangle+\left\langle\tilde{\Theta}\middle|\mathbf{x},r=0_+;t\right\rangle g^c(r=0_+|\mathbf{x},t)\right\}}_{\text{RS change due to mass transfer (2)}}.\end{aligned} \tag{39}$$

In the above equation the material derivative is with the mass-weighted mean dispersed-phase velocity and the production term is due to mean gradients in the dispersed-phase velocity. The fluctuating acceleration–velocity covariance represents the interphase transfer of kinetic energy in fluctuations, and the last two terms correspond to the net Reynolds stress change due to interphase mass transfer. The terms in the above equation are grouped in Galilean-invariant combinations.

3.7. Equivalence and consistency between LE and random field approaches

Establishing the relationships between these two basic approaches used to formulate the theory of multiphase flows is important for developing consistent models and can be of practical use in hybrid simulation approaches [88,89]. A comprehensive derivation of these relations can be found in Pai and Subramaniam [13]. In that work a theoretical foundation for the random field and point process statistical representations of multiphase flows is established in the framework of the probability density function (pdf) formalism. Consistency relationships between fundamental statistical quantities in the EE and LE representations are rigorously established. It is shown that these fundamental quantities in the two statistical representations bear an exact relationship with one another only under conditions of spatial homogeneity. Transport equations for the probability densities in each statistical representation are derived. Governing equations for the mean mass, mean momentum and second moment of velocity corresponding to the two statistical representations are derived from these transport equations. In particular, for the EE representation, the pdf formalism is shown to naturally lead to the widely used ensemble-averaged equations for two-phase flows. Galilean-invariant combinations of unclosed terms in the governing equations which need to be modeled are clearly identified. The correspondence between unclosed terms in each statistical representation is established. Hybrid EE–LE computations can benefit from this correspondence, which serves in transferring information from one representation to the other.

4. Modeling

The evolution equation for the ddf (Eq. (10)) contains conditional expectation terms $\langle A_k|\mathbf{x},\mathbf{v},r;t\rangle$ and $\langle\Theta|\mathbf{x},\mathbf{v},r;t\rangle$ that represent the average particle or droplet acceleration and average radius evolution rate, respectively. These are not closed at the level of the

ddf, i.e., they are not completely determined by the ddf or its moments alone, since they depend on higher order multiparticle statistics (cf. Fig. 1) and carrier-phase properties as well. In the more general form of the ddf evolution (Eq. (11)) that allows for collisions, coalescence and breakup, the corresponding source terms in the ddf equation that are collision integrals with appropriate kernels also need to be modeled.

4.1. Modeled ddf evolution equation

The specification of models for the unclosed terms in the ddf evolution equation results in a *modeled* ddf evolution equation:

$$\frac{\partial f^*}{\partial t}+\frac{\partial}{\partial x_k}[v_k f^*]+\frac{\partial}{\partial v_k}\left[A_k^*(\mathbf{x},\mathbf{v},r,t)f^*\right]+\frac{\partial}{\partial r}\left[\Theta^*(\mathbf{x},\mathbf{v},r,t)f^*\right] = \dot{f}^*_{coll}+\dot{f}^*_{coal}+\dot{f}^*_{bu}, \tag{40}$$

where $A_k^*(\mathbf{x},\mathbf{v},r,t)$, $\Theta^*(\mathbf{x},\mathbf{v},r,t)$ and $\dot{f}^*_{coll/coal/bu}$ represent a family of models for $\langle A_k|\mathbf{x},\mathbf{v},r;t\rangle$, $\langle\Theta|\mathbf{x},\mathbf{v},r;t\rangle$, and $\dot{f}_{coll/coal/bu}$, respectively. The modeled ddf f^*, which is the solution to Eq. (40), is the model for f implied by these model specifications.

For practical multiphase flow problems the solution to the ddf evolution equation is coupled to a Eulerian carrier-phase flow solver [21,29]. Here we primarily consider coupling to a Reynolds-averaged Navier Stokes (RANS) solver, although many of the modeling considerations are equally applicable to LES or DNS coupling as well. The influence of the dispersed phase on the carrier phase is represented by the addition of interphase coupling source terms (cf. Section 3.4) to the usual carrier-phase RANS equations (cf. Eqs. (16)–(20)). When the gas phase is represented by Reynolds-averaged fields, a class of *deterministic* models for the unclosed terms $\langle A_k|\mathbf{x},\mathbf{v},r;t\rangle$ and $\langle\Theta|\mathbf{x},\mathbf{v},r;t\rangle$ may be written as follows:

$$\begin{array}{ll}\text{Unclosed term} & \text{Model}\\ \langle A_k|\mathbf{x},\mathbf{v},r;t\rangle: & A_k^*\left(\left\{\left\langle Q_f(\mathbf{x},t)\right\rangle\right\},\mathscr{M}(f(\mathbf{x},\mathbf{v},r,t))\right)\end{array} \tag{41}$$

$$\langle\Theta|\mathbf{x},\mathbf{v},r;t\rangle: \Theta^*\left(\left\{\left\langle Q_f(\mathbf{x},t)\right\rangle\right\},\mathscr{M}(f(\mathbf{x},\mathbf{v},r,t))\right), \tag{42}$$

where the models A_k^* and Θ^* depend on $\{\langle Q_f(\mathbf{x},t)\rangle\}$ and $\mathscr{M}(f(\mathbf{x},\mathbf{v},r,t))$. Here $\{\langle Q_f(\mathbf{x},t)\rangle\}$ represents the set of averaged fields from the carrier fluid solution (which includes such fields as the turbulent kinetic energy and mean fluid velocity), and $\mathscr{M}(f)$ is any moment of the ddf. The dependence on $\mathscr{M}(f)$ is a general representation of the dependence that the modeled terms might have on quantities like the average dispersed-phase volume fraction density in physical space, which are moments of the ddf (cf. Eq. (13)).

4.2. Solution approaches

In order to solve a general multiphase flow problem using the ddf or NDF approach, Eq. (40) for the modeled ddf is to be numerically solved with appropriate initial and boundary conditions on f^*, for a particular specification of the modeled terms A_k^*, Θ^* and the collisional source terms.

4.2.1. Particle methods

For ease of modeling and computational representation of boundary conditions, a solution approach based on particle methods is commonly used to indirectly solve Eq. (40) in a computationally efficient manner [21]. This solution approach is similar to particle methods used in the probability density function approach to modeling turbulent reactive flows, a thorough exposition of which is given by Pope [4]. As discussed in Refs. [66,74], one can associate an ensemble of N_s *identically* distributed *surrogate* droplets with properties $\{\mathbf{X}^{*(i)}(t),\mathbf{V}^{*(i)}(t),R^{*(i)}(t),i=1,...,N_s(t)\}$, where $\mathbf{X}^{*(i)}(t)$ denotes the ith surrogate droplet's position at time t, $\mathbf{V}^{*(i)}(t)$ represents its velocity, and $R^{*(i)}(t)$ its radius. The properties associated with the ith *surrogate* droplet evolve by the following *modeled* equations:

$$\frac{d\mathbf{X}^{*(i)}}{dt}=\mathbf{V}^{*(i)} \tag{43}$$

$$\frac{d\mathbf{V}^{*(i)}}{dt}=\mathbf{A}^{*(i)} \tag{44}$$

$$\frac{dR^{*(i)}}{dt}=\Theta^{*(i)},\ i=1,\ldots,N_s(t) \tag{45}$$

where $\mathbf{A}^{*(i)}$ is the *modeled* acceleration experienced by the *surrogate* droplet, and $\Theta^{*(i)}$ is its *modeled* rate of radius change due to vaporization.

The correspondence between the surrogate droplets (or surrogate particles) in the LE simulation and the spray droplets (or physical particles) is only at the level of the conditional expectations $\langle A_k|\mathbf{x},\mathbf{v},r;t\rangle$ and $\langle\Theta|\mathbf{x},\mathbf{v},r;t\rangle$. Surrogate particles in the particle method solution to the ddf are not individual physical particles or spray droplets, even though the drag that a surrogate particle experiences is often modeled as the isolated particle or single-droplet drag. In fact the correct interpretation is that $\langle A_k|\mathbf{x},\mathbf{v},r;t\rangle$ is the average drag experienced by a physical particle or droplet in a suspension, and that is different from the isolated particle drag since it includes volume fraction and neighbor particle effects. Conceptualizing surrogate particles as only being statistically equivalent to physical particles or droplets gives considerable flexibility in modeling.

The principle of stochastic equivalence (see Pope [4]) tells us that two systems can evolve such that the individual realizations in each system are radically different, but the two may have identical mean values. Therefore, the system of surrogate droplets (or surrogate particles) may have individual realizations that are vastly different from those of the physical droplets or particles (obeying non-differentiable trajectories, for instance), and yet its implied conditional expectation terms A_k^* and Θ^* can match $\langle A_k|\mathbf{x},\mathbf{v},r;t\rangle$ and $\langle\Theta|\mathbf{x},\mathbf{v},r;t\rangle$ (The principle of stochastic equivalence [4] also reveals that the mapping of particle models to A_k^* and Θ^* is many-to-one, i.e., different particle models can result in the same A_k^* and Θ^*). A direct corollary of the stochastic equivalence principle is that in addition to *deterministic* particle evolution models, one can also use *stochastic* particle models with random terms in the particle property evolution equations (Eqs. (43)–(45)). The addition of random terms (strictly speaking, Wiener process increments) to the computational particle position and velocity evolution results in the appearance of corresponding diffusion terms (in position and velocity space) in the modeled ddf evolution equation that now resembles the Fokker–Planck equation [90].

There is another class of models that can be termed *particle interaction models*, and they are often encountered in modeling the collision term. In these models the surrogate particles within an ensemble may interact. A common misconception in Lagrangian modeling is the assumption that the surrogate particles (or their computational counterparts discussed in Section 5) contain accurate two-particle information. Of course this is not the case if they only correspond to the droplet ensemble at the level of the conditional expectations $\langle A_k|\mathbf{x},\mathbf{v},r;t\rangle$ and $\langle\Theta|\mathbf{x},\mathbf{v},r;t\rangle$. In order for correspondence at the level of two-particle statistics, the surrogate particles would need to match the unclosed terms in the evolution equation for the two-particle density, and also match two-particle statistics at initial time. Another undesirable feature of particle interaction models is that they can develop unphysical correlations over time

[91] due to repeated interactions with neighbors in the same ensemble. Stochastic collision models do not suffer from this drawback [92], and it is easier to ensure their numerical convergence. Besides, the modeling assumptions at the two-particle level appear explicitly in stochastic models. Therefore, even for the collision term it appears that stochastic models are more promising.

4.2.2. Solution of moment equations

Recently Fox et al. [16,17,93] have developed a quadrature method of moments (QMOM) approach to solve the moment equations implied by the ddf in an accurate and efficient manner by discretizing the ddf or NDF in terms of a sum of δ-functions at time-varying abscissa locations with corresponding weights that also evolve in time. This approach is able to successfully represent the crossing of particle jets that is not captured by standard approaches that directly solve the moment equations. By respecting the hyperbolic nature of the collisionless ddf equation, the QMOM approach is able to accurately capture 'shocks' in the dispersed phase and nonequilibrium characteristics of the velocity PDF (whereas moment closures based on KT of gas–solid flow often rely on near-equilibrium assumptions). Results for spray [94] and particle-laden flows [17] obtained using this approach are very promising.

4.3. Modeling challenges

One of the difficulties in developing LE sub-models for average acceleration or rate of radius evolution is that these sub-models interact with each other in a realistic multiphase flow simulation. Therefore, it is virtually impossible to isolate the effect of a sub-model and truly assess its performance in a realistic multiphase flow simulation. For this reason, attempts to improve multiphase flow models using such realistic multiphase flow simulations tend to be inconclusive. However, multiphase flow simulations using a combination of sub-models can be useful in determining the sensitivity of overall multiphase flow predictions to variations in specific sub-models (see for example, the sensitivity study by van Wachem et al. comparing two-fluid sub-models in fluidized bed test cases [95]), and may serve to prioritize modeling efforts for that particular application. It should be noted that this sensitivity is of course highly application-dependent.

Another approach is to test and improve sub-models in an idealized test case using a higher fidelity simulation such as DNS that is believed to be closer to the 'ground truth'. Such an approach can be very useful in assessing a sub-model's performance in isolation (in the absence of interaction with other sub-models), and for further sub-model development. In the rest of this section, this approach will be pursued by taking the acceleration model A_k^* as an example to illustrate modeling challenges. The principal modeling challenges in the LE approach arise from the need to represent the nonlinear, nonlocal, multiscale interactions that characterize multiphase flows. The influence of neighbor particles or droplets, and the importance of fluctuations are also discussed. Nevertheless, it should be borne in mind that the true test of any sub-model is of course its predictive capability in a realistic multiphase flow simulation where it interacts with other sub-models.

4.3.1. Nonlinearity

One of the principal difficulties in modeling the conditional mean acceleration $\langle A_k|\mathbf{x},\mathbf{v},r;t\rangle$ term is its dependence on particle velocity.[6] This nonlinearity is evident in the standard drag law for isolated spherical particles, drops or bubbles [96]. The other source of nonlinearity is the dependence of the conditional mean acceleration on the dispersed-phase volume fraction. DNS of steady flow past fixed assemblies of monodisperse, spherical particles based on continuum Navier–Stokes equations (for example, the DNS approach called Particle-resolved Uncontaminated-fluid Reconcilable Immersed Boundary Method (PUReIBM)) as well as the Lattice Boltzmann Method (LBM) have been useful in developing drag laws that incorporate this volume fraction dependence (see Fig. 5). Some LE simulations [21] use an isolated particle drag correlation for even up to 10% volume fraction on the basis of the flow being dilute.

Fig. 5 shows the dependence of the normalized average drag force F experienced by a particle in a suspension, on solid volume fraction ϕ, at a mean slip Reynolds number $\mathrm{Re}_m \equiv |\langle\mathbf{W}\rangle|(1-\phi)D/\nu_\mathrm{f}$ equal to 100. Here $\langle\mathbf{W}\rangle$ is the mean slip velocity, D is the particle diameter, and ν_f is the fluid kinematic viscosity. The average drag force is normalized by the Stokes drag experienced by a particle at the same superficial velocity $(1-\phi)|\langle\mathbf{W}\rangle|$, such that $F = m\langle A\rangle/3\pi\mu_\mathrm{f}D(1-\phi)|\langle\mathbf{W}\rangle|$, where μ_f is the dynamic shear viscosity of the fluid. The solid black line in Fig. 5 (whose scale is indicated by the y-axis on the right) gives the departure of this average drag force from the isolated drag law ($\varepsilon = (F - F_{isol})/F_{isol}$). It is seen that this departure is nearly 100% at a solid volume fraction of 0.1. The dependence of drag on volume fraction is given by the computational drag laws proposed by various authors [40,79–81]. For example, the following PUReIBM drag law [40]

$$F(\phi,\mathrm{Re}_m) = \frac{F_{isol}(\mathrm{Re}_m)}{(1-\phi)^3} + \frac{5.81\phi}{(1-\phi)^3} + 0.48\frac{\phi^{1/3}}{(1-\phi)^4} + \phi^3\mathrm{Re}_m\left(0.95 + \frac{0.61\phi^3}{(1-\phi)^2}\right), \tag{46}$$

is quite easy to implement in LE codes. In the above equation [40], $F_{isol}(Re_m)$ is the drag on an isolated particle given by the Schiller–Naumann correlation [97]. The dependence of drag on volume fraction is also directly implicated in the growth of instabilities in the dispersed-phase volume fraction [9]. The nonlinear dependence on volume fraction also manifests itself in the interphase momentum coupling term $\alpha_d\rho_d\ \langle\tilde{A}_i\rangle$ (cf. Eq. (30)).

4.3.2. Nonlocal effects

The lack of scale separation in multiphase flows (cf. Fig. 4) that was illustrated by showing that mean fluid temperature may vary on scales comparable to the mesoscale spatial structure of particles has implications for modeling. The form of the models given by Eqs. (41) and (42) is local in physical space, i.e., the modeled term at **x**

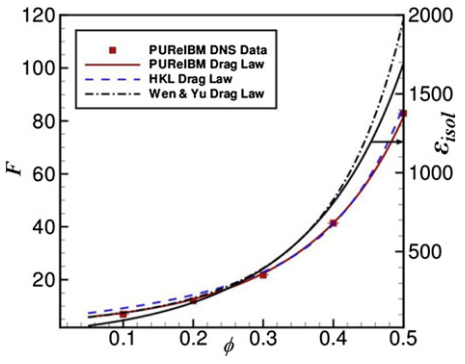

Fig. 5. Variation of average drag force experienced by a spherical particle in a monodisperse suspension as a function of solid volume fraction ϕ. The Reynolds number based on the mean slip velocity is 100.

[6] Note that the conditional acceleration appears inside the velocity derivative in the ddf evolution equation, whereas in the KT of molecular gases the acceleration is independent of velocity and can be taken outside the velocity derivative.

depends only on f and $\langle Q_f \rangle$ at the same physical location $\mathbf{x}$. Models that are local in physical space are strictly valid only if the characteristic length scale of variation of mean quantities (macroscale denoted by ℓ_{macro}) is always greater than a characteristic length scale ℓ_{meso} associated with the particles or droplets (micro- and mesoscales). This is because if scale separation does not exist and $\ell_{meso} \sim \ell_{macro}$, then surface phenomena such as heat transfer and vaporization occurring at a distance ℓ_{meso} from the physical location $\mathbf{x}$ would affect the evolution of mean fields at $\mathbf{x}$. Nonlocal models have been developed for the treatment of near-wall turbulence [98,99], but current multiphase flow models are all of the local type given by Eqs. (41) and (42).

4.3.3. Multiscale effects

The presence of a wide range of length and time scales in both the carrier and dispersed phase poses a significant modeling challenge in multiphase flows. The nature of these interactions is illustrated using the acceleration model as an example.

4.3.3.1. Carrier phase. Turbulence in the carrier phase results in a range of length and time scales. In fact, even laminar multiphase flows can exhibit significant levels of pseudo-turbulent velocity fluctuations with a range of length and time scales, as recently shown by DNS of Tenneti et al. [100]. The density difference between the dispersed and carrier phases results in the dispersed-phase particles or droplets having higher inertia than fluid material volumes or eddies of the same size. Therefore, dispersed-phase particles or droplets may interact dynamically and exchange momentum with fluid eddies that are much larger in size. The particle or droplet momentum response time can be used to calculate the size of a turbulent eddy in the inertial sub-range with the same eddy turnover time. This in turn can be used to define a range of eddy length scales with which the dispersed phase may interact dynamically. It should also be noted that the particles or droplets may not exchange momentum over the same time scale with eddies of all sizes in the carrier fluid turbulent kinetic energy spectrum. These observations motivate the development of multiscale interaction models for particle or droplet acceleration.

4.3.3.2. Dispersed phase. Particles or droplets can preferentially concentrate [101–103] in turbulence, and also organize into clusters and streamers in fluidized bed risers [104,105] depending on the nature of the particle-fluid and interparticle interactions (inelastic collisions, cohesion, electrostatics). This introduces a range of length (and time) scales in the dispersed phase, that can range from macro to meso to microscales as discussed in Section 2.4.3 (cf. Fig. 4). Clearly, momentum transfer between the carrier and dispersed phases is a mutiscale interaction.

At the microscale, the acceleration experienced by individual particles can be affected by their being deep inside a cluster, or in a relatively isolated location. Preferential concentration of $O(1)$ Stokes number particles in low vorticity regions of turbulent flow leads to the formation of mesoscale structures. It is also reported that the average drag experienced by the solid phase can depend significantly on the presence of clusters [108]. It follows that the interphase source terms in the carrier phase that represent momentum coupling should also account for this multiscale interaction.

4.3.4. Effect of neighbors

While it is intuitively clear that the effect of neighbors will become important with increasing dispersed-phase volume fraction, the effect of neighbor particles or droplets on interphase interactions has been difficult to quantify. In the absence of conclusive data these interactions are usually neglected for flows with dispersed-phase volume fraction less than 10%. Chiu et al. [75] have developed models to incorporate neighbor droplet or particle effects, but their accuracy is difficult to establish in the absence of validation data. It was already noted (cf. Fig. 2(d)) that recent DNS of scalar transport in steady flow past fixed particle assemblies show that scalar contours surrounding neighbor particles can interact even at 1% volume fraction. The first-order effect of neighbor particle interactions can be captured by incorporating a dependence of the drag law on volume fraction (which is a first-order statistic). However, the question then arises whether second-order statistics such as the pair correlation function that corresponds to the arrangement (or structure) of neighbor particles or droplets *at the same volume fraction* can affect interphase transfer terms.

To address this question we prepared different particle configurations, each with the same average number density[7] corresponding to solid volume fractions of 0.1, 0.2 and 0.3, but with a different hard-core distance h_c (see Fig. 6). If h_c equals the particle diameter, then the particles can get arbitrarily close until their surfaces touch, but with increasing h_c the particles are forced to be farther away from each other. Fig. 6(b) shows the dependence of the average drag force with increasing hard-core distance h_c, for three different values of the solid volume fraction. It is seen that the drag exhibits an increase with hard-core distance normalized by particle diameter, increasing by as much as 20% as normalized hard-core distance increases from unity to 1.2 (for volume fraction of 0.3 in Fig. 6(b)). DNS studies of turbulent flow past clustered and uniform distributions of particles (at the same volume fraction) [31] indicate that the interphase transfer of energy in velocity fluctuations is also dependent on the statistical distribution of neighboring particles.

4.3.5. Importance of fluctuations

It is clear from visual observation of many multiphase flows that the number of dispersed-phase elements (solid particles, droplets or bubbles), and the geometric volume associated with them, can vary significantly in time and space. In a realization of a multiphase flow we encounter a number $N(\mathscr{V})$ of dispersed particles (or drops or bubbles) in a region $\mathscr{V}$ in physical space. In general $N(\mathscr{V})$ is a random number, although this randomness is not explicitly accounted for in the kinetic theory of granular or gas–solid flow. Kinetic theory was originally developed for the description of molecular gases where this randomness is not significant because fluctuations are negligible on macroscales owing to scale separation. Since this scale separation is not guaranteed in multiphase flows (cf. Fig. 4) it is necessary to account for the randomness in $N(\mathscr{V})$. Fluctuations in number, and the importance of second-order effects, can be assessed through second moment measures of point fields [67]. It is natural to define the variance of N as

$$\mathrm{var}(N) = \left\langle N^2 \right\rangle - \langle N \rangle^2,$$

and the variance captures the effect of fluctuations in N. Fluctuations are closely related to clusters, which is a term loosely used to describe spatial patterns in particle point fields. Here we investigate what influence these fluctuations in number and volume have on particle-fluid interaction that affects $\langle A_k | \mathbf{x}, \mathbf{v}; t \rangle$, the conditional acceleration of a particle due to hydrodynamic forces.

Fig. 7(b) shows a scatter plot of the locally averaged particle acceleration $F(V_m;\omega)$ (which is a random variable that depends on

[7] These configurations correspond to an ensemble where the total number of particles N is a constant.

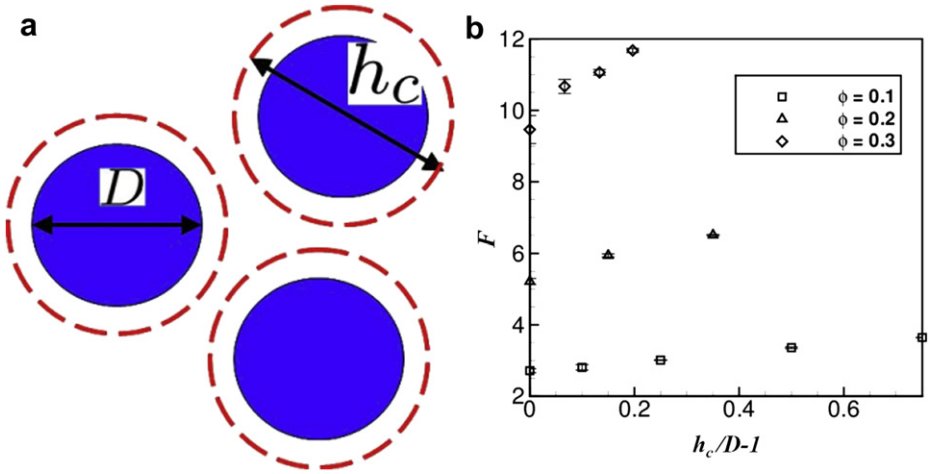

Fig. 6. Variation of average drag force experienced by a particle with varying nearest neighbor distance. The solid volume fraction is kept fixed when the effect of nearest neighbor distance is examined.

the realization) obtained from different measurement volumes V_m with the corresponding local solid volume fraction (which is also a random variable denoted $\Phi(V_m;\omega)$) in those measurement volumes. This scatter is generated from DNS of steady flow past a homogeneous assembly of fixed monodisperse particles at volume fraction of 0.2 and at a mean slip Reynolds number $Re_m = 100$. The measurement volumes ranged from $V_m = D^3$ to $(7.5D)^3$, and were chosen from different locations in the simulation domain of length $L = 12.5D$ with 161 particles in the box. The drag law dependence on volume fraction is shown as a reference value, but clearly this scatter is not captured by the first-order statistical description. These fluctuations in number that arise on each realization of the multiphase flow should not be confused with the statistical error arising from using a finite number of computational particles to represent the ddf, which is also a first-order statistical descriptor. The latter is discussed in detail in Section 5.

These are some of the principal modeling challenges dictated by the physics of multiphase flows that LE models need to address. While the focus in this review has been on modeling the particle acceleration term, similar challenges are faced in the vaporization and collisional source terms as well. The modeling of collisions, coalescence and breakup is particularly challenging because the ddf does not contain two-point information regarding the probability of relative separation of a pair of droplets (or particles) and their relative velocity. Therefore, the collisional terms are closed to obtain a 'kinetic' equation following the classical approaches of Boltzmann and Enskog for the hard-sphere model of a gas. However, the collisions in multiphase flows are complicated by inelastic collisions, deformation and coalescence (of droplets), and the presence of carrier fluid. Quantitative information from DNS that includes all these effects will be needed to assess current models and to examine the validity of scale separation implicit in them. The development of such LE models can be aided by the following guiding principles.

4.4. Guiding principles

LE models should respect the consistency conditions (cf. Section 3.7) arising from the equivalence between the random field and point process statistical descriptions, and should be consistent with the implied moment closures in both approaches (cf. Fig. 1). As such it is easy to ensure Galilean-invariance of LE models if they are formulated in the particle method solution, whereas this needs to be carefully checked in EE models. Finally, all LE sub-models should be formulated such that they are independent of numerical parameters. Often LE implementations are not numerically convergent because the sub-models are formulated by including numerical parameters in such a way as to preclude an asymptotic solution in the limit of infinite numerical resolution. If these guiding principles are followed, then the LE implementation will have consistent sub-models and numerical convergence of the LE method can be established.

4.5. Acceleration model

4.5.1. Deterministic acceleration models

The particle velocity evolution equation (cf. Eq. (44))

$$\mathbf{A}^* = \frac{d\mathbf{V}^*}{dt} = \Omega_p^*(\mathbf{U}_f^* - \mathbf{V}^*) + \mathbf{g} \tag{47}$$

defines a class of Lagrangian models that subsumes the vast majority of models [21,65,109–111] in the literature. This model is applicable to solid particles (although it neglects unsteady acceleration effects), and is often also used for droplets. Note that in the case of droplets [114,115] the effect of vaporization [112,113] and droplet deformation [36,116] could also be important, but these are not represented in this simple model. In Eq. (47), $\mathbf{A}^*$ is the modeled particle acceleration, $\mathbf{U}_f^*$ and $\mathbf{V}^*$ are the modeled gas-phase and dispersed-phase instantaneous velocities respectively, $\mathbf{g}$ is the acceleration due to gravity and Ω_p^* is a characteristic particle response frequency.[8] The particle response frequency depends on the drag coefficient C_D, which is a function of particle Reynolds number Re_p. Models proposed in literature for Ω_p^* (see [21] for example) can be cast in the following form:

$$\Omega_p^* = \frac{1}{\tau_p} f(\mathrm{Re}_p), \tag{48}$$

where $f(Re_p)$ represents a functional dependence of the model for C_D on Re_p. The models in this class differ only in terms of the particle response frequency model, and the model for the gas-phase velocity.

This form (cf. Eq. (47)) of the particle acceleration model is based on the equation for steady motion of a sphere in a fluid under the influence of only drag and body forces, but it is valid over a wide

[8] The superscript '*' in Eq. (47), and in the rest of this work is used to denote modeled quantities, which are only approximations to their exact unclosed counterparts. For example, $\mathbf{A}^*$ in Eq. (47) is a model for $\mathbf{A}$ in Eq. (8).

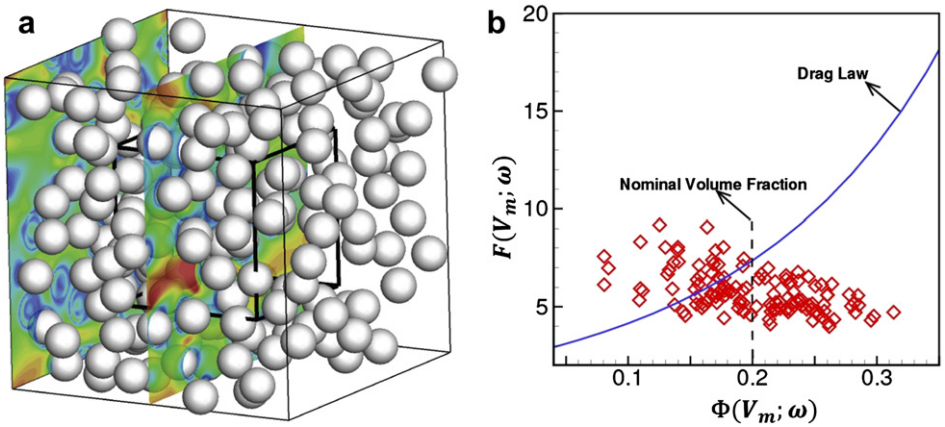

Fig. 7. Importance of local fluctuations in number and volume fraction on average particle acceleration: (a) Local measurement volume V_m in DNS of a homogeneous gas–solid flow, and (b) Scatter plot of locally averaged particle acceleration versus solid volume fraction from different measurement volumes V_m.

range of Re_p. In the case of creeping flow, expressions for particle acceleration that account for the added mass effect, lift force and history terms are available (see for instance, Maxey and Riley [117], Gatignol [118], and Michaelides and Feng [119]). For low values of the carrier to dispersed-phase density ratio ($\sim 10^{-3}$), Crowe et al. [120] justify the simplification of the Basset–Boussinesq–Oseen equation that includes the buoyancy, virtual mass and history force terms to the steady drag form in Eq. (47). However, recent experiments [121–123] in oscillatory flows indicate that the history force can be important even for carrier to dispersed-phase density ratios as low as 0.1 (corresponding to solid particles in liquid). These experiments indicate that the history term should be included in low Reynolds number (~ 2.5, based on the velocity of the oscillating flow) flow for Strouhal numbers between 1 and 20. With increasing particle Reynolds number the steady drag term eventually overwhelms the contribution from the history term.

One of the advantages of the LE approach is that it allows a more accurate description of particle-flow interactions in the Lagrangian frame (see Michaelides [124] for an excellent historical review) by considering the history term [125–127], and virtual mass forces [120]. Vojir and Michaelides [128] used Lagrangian particle simulations to show that history term can be important at high frequencies (high Strouhal number). However, as Michaelides and Feng [119] observed, it is the added computational cost of the history term that has led many to not include it in their study. Li and Michaelides [129] note that adding the history term to a droplet force calculation can increase the instantaneous force by 25%, even though the effect on the time-averaged force is negligible.

Since the carrier phase can be turbulent, the instantaneous gas-phase velocity is decomposed into a mean component $\langle \mathbf{U}_f \rangle^*$, and a fluctuating component $\mathbf{u}_f'^*$, which are related by

$$\mathbf{U}_f^* = \left\langle \mathbf{U}_f \right\rangle^* + \mathbf{u}_f'^*. \tag{49}$$

In the Lagrangian–Eulerian approach, the solution to the averaged Eulerian equations in the gas phase yields a mean gas-phase velocity $\langle \mathbf{U}_f \rangle^*$ while the fluctuation in the gas-phase velocity $\mathbf{u}_f'^*$ is modeled. Together the mean and fluctuating gas-phase velocities form a model for the instantaneous gas-phase velocity $\mathbf{U}_f^*$.

It should be noted that in their calculations of turbulent particle-laden flow using Lagrangian point particles (PP-DNS$^{(p)}$), Elghobashi and Truesdell [34,130,131] included the forces in the Maxey and Riley equation [117] due to fluid pressure gradient and viscous stresses, virtual mass, history and buoyancy effects, in addition to the steady drag term, to ensure accurate computation of transient forces along particle trajectories. This equation is valid only under the restrictions given by Lumley [132], the principal one being that the particle Reynolds number based on the fluctuating fluid velocity should be less than 0.5. Elghobashi and Truesdell [34] found that the history term is always around one order of magnitude smaller than the steady drag term (the other terms are much smaller by orders of magnitude), and its inclusion changes the Lagrangian particle autocorrelation time scale by 3.8%. However, a recent analytical study of particle motion in harmonic Stokes flows by Coimbra and Rangel [133] reports that for particles smaller than the Kolmogorov scale of turbulence, virtual mass effects cannot be modeled using the Maxey and Riley equation [117] for any fluid-to-particle density ratio much different than unity. They also note that the restriction of particle size being smaller than the Kolmogorov scale implies small dimensionless frequencies, or in other words, only particulate flows in the steady Stokes regime satisfy the Kolmogorov length scale restriction. Their conclusion that the history term can be important if the particle radius is not several orders of magnitude smaller than the Kolmogorov scale confirms the findings of Elghobashi and Truesdell [34,130,131]. For non-neutrally buoyant particles, in addition to steady and unsteady contributions to the drag force, the steady and unsteady contributions to lift can be important [134,135].

The following particle acceleration $\mathbf{A}^*$ model belongs to the general class of Lagrangian models considered here (cf. Eq. (47)), and is widely used in many LE implementations [21,22]:

$$\frac{\mathrm{d}\mathbf{V}^*}{\mathrm{d}t} = \frac{3}{8}\frac{\rho_f}{\rho_d}\frac{\left|\left\langle \mathbf{U}_f \right\rangle^* + \mathbf{u}_f'^* - \mathbf{V}^*\right|}{R_p}\left(\left\langle \mathbf{U}_f \right\rangle^* + \mathbf{u}_f'^* - \mathbf{V}^*\right)C_D + \mathbf{g}, \tag{50}$$

where R_p is the radius. The drag coefficient C_D is given by,

$$C_D = \begin{cases} \dfrac{24}{\mathrm{Re}_p}\left(1 + \dfrac{\mathrm{Re}_p^{2/3}}{6}\right) & \mathrm{Re}_p < 1000 \\ 0.424 & \mathrm{Re}_p > 1000 \end{cases}, \tag{51}$$

where the particle Reynolds number

$$\mathrm{Re}_p = \frac{2\rho_f\left|\left\langle \mathbf{U}_f \right\rangle^* + \mathbf{u}_f'^* - \mathbf{V}^*\right|R_p}{\mu_f} \tag{52}$$

and μ_f is the dynamic viscosity of the gas. From Eq. (50) one can infer the instantaneous particle response frequency Ω_p^* as

$$\Omega_p^* = \frac{3}{8}\frac{\rho_f}{\rho_d}\frac{\left|\left\langle \mathbf{U}_f \right\rangle^* + \mathbf{u}_f'^* - \mathbf{V}^*\right|}{R_p} C_D. \tag{53}$$

4.5.1.1. Models for fluctuating gas-phase velocity. Turbulence in the gas phase is usually represented by a k–ε model. This means that in addition to the mean momentum equation in the carrier gas (Eq. (19)), the evolution for the turbulent kinetic energy (TKE) k_f in the fluid phase, and its dissipation rate ε_f is solved for. The form proposed in Refs. [21,22] is widely used. Han and Reitz [136] implemented the RNG k–ε model in LE simulations, which is a more sophisticated single-phase turbulence model. However, the principal issue in the context of LE simulations is the development of *multiphase* turbulence models that address the modeling challenges unique to multiphase turbulence, such as the interphase transfer of TKE. Two-way coupling between the phases requires extension of simpler one-way coupled models [137].

The fluctuating gas-phase velocity $\mathbf{u}_f'^*$ is usually sampled from a joint normal probability density with zero mean and covariance equal to $(2k_f/3)\delta_{ij}$ under the assumption that the turbulence is isotropic. This velocity is kept constant over a time interval, called the turbulence correlation time, which is taken to be the minimum of an eddy traverse time t_R and an eddy life time t_E. At the end of the time interval the renewal time is reached, and a new value of fluctuating velocity $\mathbf{u}_f'^*$ is sampled. This is intended to capture the effect of crossing trajectories as a particle shoots across successive eddies. Such models for the fluctuating gas-phase velocity are commonly known as *eddy life time* models (ELT). Brown and Hutchinson [110], and Gosman and Ioannides [111] used a linearized form of the equation of motion of a droplet to arrive at an eddy traverse time $t_R = -\tau_p \ln\left(1.0 - l_e/(\tau_p|\mathbf{U}_f^* - \mathbf{V}^*|)\right)$, where the characteristic length scale of the eddy $l_e = C_\mu^{1/2} k_f^{3/2}/\varepsilon_f$. They also proposed a model for the eddy life time as $t_E = l_e/|\mathbf{u}_f'^*|$. Ormancey and Martinon [109] proposed that the time intervals over which $\mathbf{u}_f'^*$ remains constant be exponentially distributed (Poisson model), with the mean time interval equal to the Lagrangian integral time scale of turbulence T_L. The KIVA family of codes [21] uses a model similar to Hutchinson's but with $t_E = k_f/\varepsilon_f$ and $t_R = C_{ps}(k_f^{3/2}/\varepsilon_f)|\langle \mathbf{U}_f\rangle^* + \mathbf{u}_f'^* - \mathbf{V}^*|^{-1}$, where C_{ps} is a model constant equal to 0.164 $(= C_\mu^{3/4})$.

The foregoing discussion applies to turbulent carrier flow with dispersed-phase particles or droplets that are smaller than the Kolmogorov scale of turbulence. As was noted earlier, even laminar multiphase flows can exhibit significant velocity fluctuations in the carrier phase merely due to the presence of dispersed-phase particles [100] or droplets. The physical mechanisms for these fluctuations are completely different in the two cases, and the modeling of these pseudo-turbulent velocity fluctuations in the latter case is still in its infancy.

4.5.2. Decomposition of acceleration model into mean and fluctuation

It is useful to decompose the acceleration model $\mathbf{A}^*$ into mean $\langle \mathbf{A}\rangle^*$ and fluctuating $\mathbf{A}'^*$ contributions, because this identifies the implied models for mean interphase momentum transfer and interphase transfer of TKE (cf. Eqs. (33) and (39)). It also reveals that the Lagrangian acceleration model implies a modeled evolution equation for the second moments of dispersed-phase velocity and the Lagrangian (temporal) velocity autocorrelation of the dispersed-phase. The model predictions of these quantities can be compared with DNS results to assess and improve the Lagrangian acceleration model.

For simplicity if we consider a statistically homogeneous multiphase flow with no interphase mass transfer, then the particle velocity evolution equation (Eq. (47)) can be rewritten as

$$\frac{\mathrm{d}\mathbf{V}^*}{\mathrm{d}t} = \frac{\mathrm{d}\langle \mathbf{V}\rangle^*}{\mathrm{d}t} + \frac{\mathrm{d}\mathbf{v}'^*}{\mathrm{d}t}, \tag{54}$$

with

$$\frac{\mathrm{d}\langle \mathbf{V}\rangle^*}{\mathrm{d}t} = \langle \mathbf{A}\rangle^*, \tag{55}$$

and

$$\frac{\mathrm{d}\mathbf{v}'^*}{\mathrm{d}t} = \mathbf{A}'^*. \tag{56}$$

A model for acceleration of the dispersed phase implies an average interphase transfer of momentum between the dispersed phase and the carrier flow. The evolution equation for the particle velocity implies a modeled evolution equation for the ddf of fluctuating velocity (cf. Appendix A) and the second moment of fluctuating velocity Eq. (39). Fluctuations in the modeled velocity imply an evolution of the dispersed-phase turbulent kinetic energy that is governed by the acceleration–velocity covariance $\langle \mathbf{A}'^*\mathbf{v}'^*\rangle$ in statistically homogeneous flows. The deterministic model in Eq. (56) implies an acceleration–velocity covariance model $\langle \mathbf{A}'^*\mathbf{v}'^*\rangle$ in terms of a 'fluid-particle' velocity correlation $\langle \mathbf{u}_f'^*\mathbf{v}'^*\rangle$ [9,138]. While this single-point 'fluid-particle' velocity correlation may admit some coarse-grained interpretation, it does not exist in any multiphase flow with finite-sized droplets or particles because fluid and particle cannot coexist at the same physical location at the same time instant [65,139]. Stochastic models for the particle velocity increment offer a promising route to remedy this problem.

4.5.3. Stochastic models

Evidence from DNS of gas–solid flow also suggests that stochastic models for the particle velocity increment might represent particle acceleration statistics more faithfully than deterministic models. Statistical variability in particle acceleration, as characterized by scatter plots of particle acceleration and particle velocity in Tenneti et al. [15] and of particle acceleration and solid volume fraction in Fig. 7(b), suggest that a stochastic model is more capable of capturing the physics of multiphase flow than the deterministic model already discussed.

Stochastic models are written in terms of the particle velocity increment, such as the following Langevin model [90,100]:

$$\mathrm{d}V_i^* = -\beta\langle W_i\rangle \mathrm{d}t - \gamma v_i'^* \mathrm{d}t + B\mathrm{d}\mathscr{W}_i, \tag{57}$$

where $\mathrm{d}V_i^*$ is the increment in the particle velocity, $v_i'^*$ is the fluctuation in the particle velocity and $\mathrm{d}\mathscr{W}_i$ is a Wiener process increment. Fluctuations in the particle velocity are defined about the mean particle velocity, i.e. $v_j'^* = V_j^* - \langle V_j\rangle^*$. The first term on the right hand side of Eq. (57) accounts for the effect of the mean slip velocity. The mean slip velocity, defined as $\langle \mathbf{W}\rangle = \langle \mathbf{V}\rangle^* - \langle \mathbf{U}_f\rangle^*$, is the relative velocity between the solid phase mean velocity and the fluid-phase mean velocity. The second term in Eq. (57) accounts for the fluctuation in particle velocity and the last term models the effect of hydrodynamic interaction with neighboring particles. The coefficient γ is the inverse of the Lagrangian particle velocity autocorrelation time. It quantifies how long a particle retains memory of its initial velocity. These coefficients are functions of volume fraction (ϕ), mean flow Reynolds number (Re_m) and particle to fluid density ratio (ρ_p/ρ_f). DNS of freely evolving suspensions where particles move under the influence of the surrounding fluid and interparticle collisions can be performed using the DNS methodology to extract a functional form for the Langevin model coefficients [100].

4.5.4. Mean momentum transfer

The nonlinear dependence of particle acceleration on particle velocity is fully represented in the LE model (cf. Eq. (50)). The interphase mean momentum source term in Eq. (20) corresponding to the LE acceleration model given by Eq. (50) can be calculated using Eqs. (24), (26), (27) and (30). It is noteworthy that the time scale associated with the mean acceleration $\langle \mathbf{A} \rangle^* / \langle \mathbf{V} \rangle^*$ is not the reciprocal of

$$\left\langle \Omega_p^* \right\rangle = \frac{3}{8}\frac{\rho_f}{\rho_d}\left\langle \frac{\left| \left\langle \mathbf{U}_f \right\rangle^* + \mathbf{u}_f'^* - \mathbf{V}^* \right|}{R_p} C_D \right\rangle,$$

but represents a weighted integral over the distribution of all particle response time scales.

4.5.5. Dispersed-phase velocity fluctuations

Here we first consider the case of dispersed-phase particles or droplets smaller than the Kolmogorov scale of carrier flow turbulence evolving in a dilute flow with elastic collisions (or negligible collisional dissipation). Pai and Subramaniam [14] showed that one of the drawbacks of the acceleration model given by Eq. (50) is its inability to reproduce the trends in decay of velocity fluctuations with Stokes number that are observed in PP-DNS of homogeneous turbulent two-phase flow [65]. This is because the acceleration model implies an equation for the trace of the second moment of the dispersed-phase velocity fluctuations that evolves on the particle or droplet response time scale $\tau_p = 2\rho_d R_p^2/9\mu_f$. In reality, particles or droplets respond differently to gas-phase turbulent eddies depending on the ratio of the particle or droplet response time to the eddy turnover time. Pai and Subramaniam [14] proposed a different model for the droplet velocity fluctuation $\mathbf{v}'^*$,

$$\frac{\mathrm{d}\mathbf{v}^{*\prime}}{\mathrm{d}t} = \frac{\mathbf{u}_f'^* - \mathbf{v}'^*}{\langle \tau_{\mathrm{int}} \rangle}, \tag{58}$$

that evolves on a multiscale interaction time scale $\langle \tau_{\mathrm{int}} \rangle$.

4.5.5.1. Multiscale interaction timescale model. In the spectral description of particle–turbulence interaction, a dispersed particle interacts with a range of eddies which in turn corresponds to a range of wavenumbers in the fluid-phase TKE spectrum. One may define a Stokes number St_κ as the ratio of the particle response timescale τ_p to the timescale τ_κ corresponding to the eddies of wavenumber κ. Some eddies (say, type A) in this range have a timescale such that $St_\kappa > 1$, while the others (say, type B) in this range have a timescale such that $St_\kappa < 1$. The particle responds immediately to eddies that have a timescale such that $St_\kappa < 1$, while it responds slowly to eddies that have a timescale such that $St_\kappa > 1$. In the former case, the timescale for interphase TKE transfer is influenced more by the timescale corresponding to the eddies with wavenumber κ, while in the latter case the timescale for interphase TKE transfer is influenced more by the particle response timescale τ_p. Thus, the effective timescale for particle–turbulence interaction is obtained by integrating the effects of the two wavenumber ranges identified above, over the energy spectrum of fluid-phase turbulence in the two-phase flow. The multiscale interaction timescale $\langle \tau_{\mathrm{int}} \rangle$ presented here is a single-point analogue of the above spectral model.

Let $\mathbf{u}_f'^*$ be a model for the Eulerian gas-phase velocity fluctuation in Eq. (49) (an example is given in Eq. (64)). If z is the sample space variable corresponding to the random variable $Z = |\mathbf{u}_f'^*|$, the multiscale interaction timescale $\langle \tau_{\mathrm{int}} \rangle$ is given by

$$\langle \tau_{\mathrm{int}} \rangle = \int_{|u|^\dagger}^{\infty} \langle \tau_{\mathrm{int}} | Z = z \rangle f_Z(z)\mathrm{d}z + \int_0^{|\mathbf{u}|^\dagger} \tau_p f_Z(z)\mathrm{d}z, \tag{59}$$

where $f_Z(z)$ the pdf of Z. The conditional mean $\langle \tau_{\mathrm{int}} | z \rangle$ is given by

$$\langle \tau_{\mathrm{int}} | z \rangle = St_l(\tau_p - \tau) + \tau \tag{60}$$

for $|\mathbf{u}|^\dagger \le |\mathbf{u}_f'^*| \le \infty$, while $\langle \tau_{\mathrm{int}} | z \rangle = \tau_p$ for $0 \le |\mathbf{u}_f'^*| \le |\mathbf{u}|^\dagger$. Here, a Stokes number valid in the inertial range is given by

$$St_l = \frac{\tau_p}{\tau_l}, \tag{61}$$

where τ_l is computed as

$$\tau_l = \frac{|\mathbf{u}_f'^*|^2}{\varepsilon_f}. \tag{62}$$

In order to complete the specification of the multiscale interaction timescale, the pdf of $|\mathbf{u}_f'^*|$ is required. Using Eq. (64) the pdf of $\mathbf{u}_f'^*$ can be computed directly from the solution. However, if $\mathbf{u}_f'^*$ is assumed to obey a joint normal distribution with zero mean and covariance $\sigma_f^2\delta_{ij}$, where $\sigma_f^2 = (2/3)k_f$ and δ_{ij} is the Kronecker delta as is done in recent studies [14,141], then the pdf of $Z = |\mathbf{u}_f'^*|$ is

$$f_Z(z) = \sqrt{\frac{2}{\pi}}\frac{1}{\sigma_f^3} z^2 \exp\left(-z^2/2\sigma_f^2\right). \tag{63}$$

As noted above, Eq. (62) is based on an inertial sub-range scaling where eddies have a characteristic length scale l. The Stokes number St_l defined in Eq. (61) using the characteristic length scale is the single-point analogue of St_κ. For a value of $St_l > 1$, the particle responds slowly to the eddies and the timescale of energy transfer is influenced more by the particle response time τ_p. On the other hand, if $St_l < 1$, the particle responds immediately to the flow, and the timescale of energy transfer is influenced more by the eddy turnover timescale τ. Thus, the pdf of $|\mathbf{u}_f'^*|$ for a Gaussian $\mathbf{u}_f'^*$(see Fig. 8) can be divided into two regions: one that represents $St_l > 1$, and the other that represents $St_l < 1$, with $|\mathbf{u}|^\dagger$ representing the transition between the two regions at $St_l = 1$. Thus, $|\mathbf{u}|^\dagger$ is uniquely determined by the relation $(|\mathbf{u}|^\dagger)^2 = \tau_p\varepsilon_f$.

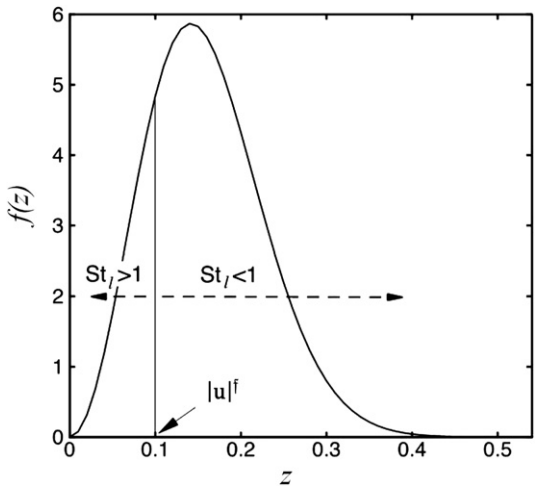

Fig. 8. A schematic probability density function of $|\mathbf{u}_f'^*|$ that is used in the derivation of the multiscale interaction timescale $\langle \tau_{\mathrm{int}} \rangle$. The sample space variable corresponding to $|\mathbf{u}_f'^*|$ is z.

It is interesting to note that Eq. (59) has the correct behavior for limiting values of St_l and $|\mathbf{u}|^\dagger$. In the limit $|\mathbf{u}|^\dagger \to 0$, there are no eddies in the system with $St_l > 1$. The dispersed particles are simply convected by the flow and the correct timescale for interphase TKE transfer in this limit is τ. In the limit $|\mathbf{u}|^\dagger \to \infty$, practically all the eddies in the system satisfy $St_l > 1$, which implies that there are no eddies energetic enough to convect the particles. The correct timescale for interphase TKE transfer in this limit is the particle response timescale τ_p.

The multiscale interaction time scale model as implemented in the LE framework by Pai and Subramaniam [14] correctly reproduces the DNS trends in decay of velocity fluctuations with Stokes number for homogeneous turbulent two-phase flow with zero mean slip velocity. Note that this is still a deterministic model that results in the anomalous 'fluid-particle' velocity correlation. A stochastic version of the same model that incorporates the multiscale interaction time scale concept but that does not result in the anomalous 'fluid-particle' velocity correlation is described in the following section. In a general multiphase flow problem the effects of inhomogeneous mean flow and gravity introduce additional phenomena that manifest as anisotropy in the second moments of droplet fluctuation velocity.

4.6. Position evolution model

The simplest position evolution model is (cf. Eq. (43)),

$$\frac{\mathrm{d}\mathbf{X}^*}{\mathrm{d}t} = \mathbf{V}^*$$

but in some works it is modified to include a random term [142]. The justification for adding this random term is to represent the effect of droplet dispersion due to random motion of the turbulent eddies. It is well known that adding a random term (Wiener process increment, to be precise) makes the position evolution equation (Eq. (43)) a stochastic differential equation (SDE). The corresponding change to the modeled ddf evolution equation is the addition of a term representing diffusion in physical space (as in the Fokker–Planck equation corresponding to the SDE [61,143,144]).

It is well established from analyses of the system of SDE's that arise in both turbulent single-phase flows and Brownian dynamics, that diffusion arises from the effect of velocity autocorrelation. In the limit of rapid momentum relaxation, the system of equations can be simplified to a Langevin equation for position [145,146]. The assumption of fast momentum relaxation is generally not applicable to spray droplets because that would imply that the droplet velocity distribution relaxes to an equilibrium Maxwellian distribution, which is obviously not true for the strongly nonequilibrium situation in sprays. Also retaining both the velocity SDE and the position SDE will result in two sources of diffusion, which in turbulent single-phase flows can be meaningfully interpreted as the sum of molecular diffusion arising from the position equation and turbulent diffusion arising from the velocity equation [144]. A similar analogy does not exist in the case of multiphase flow. In the following section, a summary of approaches to modeling particle or droplet dispersion is presented.

4.6.1. Droplet dispersion

Dispersion of spray droplets and the modulation of turbulence in the ambient gas by the dispersing droplets are two coupled phenomena that are closely linked to the evolution of global spray characteristics, such as the spreading rate of the spray and the spray cone angle. PP-DNS$^{(p)}$ of turbulent gas flows laden with sub-Kolmogorov size particles, in the absence of gravity, report that dispersion statistics and turbulent kinetic energy (TKE) evolve on different time scales.

Particles with high Stokes number lose energy faster than particles with low Stokes number in freely decaying turbulence [65]. On the other hand, particles with high Stokes number lose correlation with their initial velocities slower than particles with low Stokes number in stationary turbulence [41,45]. The disparate behavior of the velocity autocorrelation and TKE time scales affects the dispersion characteristics of a spray.

Lu [147] uses a time-series analysis involving fluid-phase temporal and spatial Eulerian velocity correlations to arrive at a stochastic model for the fluid velocity at the particle location, in the limit of one-way coupled turbulence. Spray droplet interactions with the gas phase are, however, strongly two-way coupled. Nevertheless, testing the behavior of a two-phase model in the limit of one-way coupled spray configurations is indeed necessary. Lu reports good agreement between model results and theoretical results of Csanady [148], and particle-laden grid-generated turbulence results of Snyder and Lumley [149] in predicting particle diffusion coefficients and velocity autocorrelations. Mashayek and Jaberi [45] used Lu's time-series approach to predict particle velocity autocorrelation functions and asymptotic diffusion coefficients for non-evaporating and evaporating droplets laden in one-way coupled stationary turbulence, again reporting overall reasonable agreement with PP-DNS data [150]. An extension of the time-series model has been tested by Gao and Mashayek [151] in compressible homogeneous shear flows with interphase mass transfer due to evaporating droplets. They report good agreement of predicted droplet velocity correlations and droplet-fluid velocity cross-correlations with PP-DNS of evaporating droplets in a low Mach number turbulent shear flow [44].

Pozorski and Minier [152] modified the Lagrangian integral time scale in the generalized Langevin model proposed by Haworth and Pope [153] to arrive at the fluid velocity "seen" by the particles. To our knowledge, no validation tests are available in the literature that quantify the predictive capability of this model in canonical particle-laden flows. Chagras et al. [154] employ a Langevin-type equation that uses the Lagrangian integral time scale of the fluid "seen" by the particles and the fluid-phase Reynolds stresses to arrive at a model for $\mathbf{u}_f'$. They analyze several cases of two-way coupled gas–solid pipe flow with large mass loading and report overall agreement of temperature profiles and instantaneous velocities with experimental results. Chen and Pereira [155] use an assumed probability density function (pdf) for the spatial distribution of the particles whose variance evolves in time by an ordinary differential equation containing an assumed fluid-phase Lagrangian velocity autocorrelation of the Frenkiel form [156]. They report good match of predicted dispersed-phase velocities from their two-way coupled simulations with results from experiments conducted on particle-laden planar mixing layers and co-flowing planar jets.

With the exception of Mashayek and Jaberi [45], there is no evidence in the literature of tests conducted with the aforementioned models in simple canonical two-phase flows (such as stationary or freely decaying particle-laden turbulence) to test their capability in simultaneously capturing the energy and dispersion time scales as observed in PP-DNS. However, the time-series model [147] used by Mashayek [45] relies on statistics of the fluid phase that are valid only in the limit of one-way coupled two-phase flows. Extending the time-series model to two-phase flows with significant two-way coupling effects will require the knowledge of the Eulerian spatial correlation of gas-phase velocity which is a non-trivial quantity to measure or model in such flows. Also, the extension of the time-series model proposed by Gao and Mashayek [151] involves correlations among the velocity components, temperature and mass fraction, with the assumption that all these correlations evolve on the same Eulerian fluid integral time scale.

4.6.1.1. Coupled stochastic model. The coupled stochastic model (CSM) for homogeneous turbulent two-phase flows [187] consists of two coupled stochastic differential equations (SDE) for the modeled fluctuating Lagrangian gas-phase velocity **u** and fluctuating Lagrangian dispersed-phase velocity **v**. This model possesses a unique feature that the implied TKE and velocity autocorrelation in each phase evolve on different time scales. Consequently, this model has the capability of simultaneously predicting the disparate Stokes number trends in the evolution of dispersion statistics, such as velocity autocorrelations, and TKE in each phase. Predictions of dispersion statistics and TKE from the new model show good agreement with published PP-DNS of non-evaporating and evaporating droplet-laden turbulent flow.

The proposed system of SDEs in CSM is

$$\mathrm{d}u^{\prime *}_{f,i} = -\left[\frac{1}{2\tau_1}+\left(\frac{1}{2}+\frac{3}{4}C_0\right)\frac{\varepsilon_f}{k_f}\right]u^{\prime *}_{f,i}\mathrm{d}t+\left[C_0\varepsilon_f+\frac{2}{3}\frac{k_f}{\tau_1}+\frac{2}{3}\left(\frac{k^e_f-k_f}{\tau_2}\right)\right]^{1/2}\mathrm{d}W^u_i \tag{64}$$

$$\mathrm{d}v^{\prime *}_i = -\frac{1}{2\tau_3}v^{\prime *}_i\mathrm{d}t+\left[\frac{2}{3}\frac{k_d}{\tau_3}+\frac{2}{3}\left(\frac{k^e_d-k_d}{\tau_4}\right)\right]^{1/2}\mathrm{d}W^v_i, \tag{65}$$

where τ_1, τ_2, τ_3 and τ_4 are time scales that appear in the drift and diffusion coefficients[9] of each SDE, while $\mathrm{d}W^u_i$ and $\mathrm{d}W^v_i$ are independent Wiener processes [157]. The subscript i denotes the Cartesian components. The TKE in the dispersed phase is denoted k_d and the TKE in the gas phase is denoted k_f, with a superscript 'e' to denote their 'equilibrium' values (the concept of 'equilibrium' is explained in Refs. [14,141,187]).[10] Also, ε_f is the gas-phase dissipation enhanced by the presence of the dispersed phase. The constant $C_0 = 2.1$, which is identical to that used in the Simplified Langevin model (SLM) [61]. Mean velocity in either phase, and hence the mean slip velocity, is assumed to be zero for simplicity, although this is not an inherent limitation of CSM. The fluid-phase SDE can be viewed as an extension of the SLM [61,153] to two-phase flows, but with an important difference being the introduction of drift and diffusion time scales that are different from each other. Also, additional terms involving k^e_f and k^e_d (in parentheses) that represent interphase interactions have been added. The coupling between the two phases is only through moments of the velocities in each phase like TKE (k_f and k_d) and the dissipation ε_f, and not explicitly through the instantaneous values of $u^{\prime *}_{f,i}$ and $v^{\prime *}_f$.

Note that for widely used LE models, the interphase TKE transfer evolves on the particle response time scale τ_p, which was found to be inadequate to capture the multiscale nature of particle–turbulence interaction [14]. The specification of the drift time scales τ_1 and τ_3 in Eqs. (64) and (65) is summarized here. Detailed justification for these choices is given in Ref. [158,187]. The specification for the drift time scale τ_3 is

$$\frac{1}{\tau_3} = 2\left[\frac{1}{2\tau_1}+\left(\frac{1}{2}+\frac{3}{4}C_0\right)\frac{1}{\tau}\right]\frac{1}{1+St_\eta C_3}, \tag{66}$$

where C_3 is a model constant ($C_3 = 0.1$) and $\tau = k_f/\varepsilon_f$ is the fluid-phase eddy turnover time scale. This specification for τ_3 obeys the correct limiting behavior in the limit of zero Stokes number ($St_\eta \to 0$), where the droplets respond immediately to the surrounding fluid and the fluid-phase velocity autocovariance and the dispersed-phase velocity autocovariance must match. The drift time scale τ_1 is prescribed to be

$$\frac{1}{\tau_1} = \frac{C_1\varphi}{\tau},$$

where C_1 is a model constant ($C_1 = 0.5$). In the limit of zero mass loading, the time scale τ_1, which essentially represents the modification to the fluid velocity autocorrelation time scale due to the presence of dispersed phase, should tend to infinity. In this limit the drift time scale in Eq. (64) approaches the specification for the single-phase simplified Langevin model [61].

The time scales τ_2 and τ_4 govern the evolution of TKE in each phase, which are

$$\frac{\mathrm{d}k_f}{\mathrm{d}t} = -\frac{k_f-k^e_f}{\tau_2}-\varepsilon_f \tag{67}$$

$$\frac{\mathrm{d}k_d}{\mathrm{d}t} = -\frac{k_d-k^e_d}{\tau_4}. \tag{68}$$

In accordance with the 'equilibration of energy' concept, and to introduce the capability to capture the multiscale nature of a turbulent two-phase mixture into CSM, the time scales τ_2 and τ_4 are chosen to be equal to $\tau_\pi = \langle\tau_{\mathrm{int}}\rangle/C_\pi$, where $\langle\tau_{\mathrm{int}}\rangle$ is a multiscale interaction time scale for interphase TKE transfer proposed by Pai and Subramaniam [14]. It was shown in Ref. [14] that the new time scale accurately captures the dependence of the interphase TKE transfer on St_η. This time scale has been successfully employed in the context of EE two-phase turbulence modeling by Xu and Subramaniam [141]. The constant C_π is chosen to be 2.5.

4.7. Other sub-models

There are many other physical phenomena that are important in multiphase flows, including heat transfer, vaporization, and collisions. These require sub-models that need to be incorporated into the LE simulation code. Considerable progress has been made in modeling these physical phenomena using Lagrangian sub-models. These sub-models are not discussed here because authoritative reviews are available for the interested reader. The development of a predictive LE simulation will require systematic testing of each of these sub-models using the criteria and guiding principles described in Section 4.4.

5. Numerical implementation

In LE simulations that are a particle method solution to the modeled ddf evolution (PP-DNS$^{(s)}$ and RANS in Table 1), the ensemble of N_s *surrogate* droplets is indirectly represented by N_c computational particles (also called 'parcels' in the spray literature). The number of computational particles N_c does not necessarily have to equal the average number of physical particles or droplets $\langle N_s\rangle$ that is represented by the ddf.[11] To reduce computational cost N_c is chosen to be smaller than $\langle N_s\rangle$ (sometimes by even several orders of magnitude), and the correspondence between the computational representation and the surrogate ensemble is enforced at the level of the modeled ddf [107]. This reduction in computational cost is

[9] The terms 'drift' and 'diffusion' are used in the sense of stochastic differential equation theory.

[10] The subscript f stands for the gas phase or fluid phase, and the subscript d stands for the dispersed phase.

[11] The average number of physical particles or droplets $\langle N_s\rangle$ is the same in the physical system and the surrogate ensemble, so we do not distinguish between the two when it is not necessary.

accomplished by assigning a statistical weight to the computational particles, and it is a valid approach as long as the computed solution converges to the modeled ddf that evolves by Eq. (40).

These N_c computational particles are represented in a Lagrangian frame at time t by a set of properties $\{\mathbf{X}_c^{(i)}(t), \mathbf{V}_c^{(i)}(t), R_c^{(i)}(t), W^{(i)}, i = 1,...,N_s(t)\}$, where $\mathbf{X}_c^{(i)}(t)$ denotes the ith computational particle's position, $\mathbf{V}_c^{(i)}(t)$ its velocity, $R_c^{(i)}(t)$ its radius, and $W^{(i)}$ its statistical weight. The statistical weight is defined as the average number of droplets represented by a computational particle. The summation of statistical weights over all computational particles equals the expected total number of droplets

$$\sum_{i=1}^{N_c(t)} W^{(i)} = \langle N_s(t) \rangle. \tag{69}$$

As already noted earlier, the surrogate droplets (or particles) do not have to evolve identically to their physical counterparts because the equivalence of the modeled surrogate system and physical system is in a (weak [159]) statistical sense (sample paths do not have to match). Since the N_c computational particles efficiently solve the evolution of the surrogate ensemble, they too do not have to evolve identically to their physical counterparts. If the statistical weighting is uniform in position, velocity and radius space, then the computational particles evolve identically to their surrogate counterparts as given by Eqs. (43)–(45). The position, velocity and radius of the computational particles evolve by

$$\frac{d\mathbf{X}_c^{(i)}}{dt} = \mathbf{V}_c^{(i)} \tag{70}$$

$$\frac{d\mathbf{V}_c^{(i)}}{dt} = \mathbf{A}_c^{(i)} = \mathbf{A}^{*(i)} \tag{71}$$

$$\frac{dR_c^{(i)}}{dt} = \Theta_c^{(i)} = \Theta^{*(i)} \tag{72}$$

$$\frac{dW^{(i)}(t)}{dt} = -\omega^{(i)}(t) W^{(i)}(t), \quad , i = 1, \ldots, N_c(t), \tag{73}$$

where $\mathbf{A}_c^{(i)}$ is the instantaneous acceleration experienced by the ith computational particle, $\Theta_c^{(i)}$ is the rate of change of particle radius due to vaporization, and $\omega^{(i)}$ represents the fractional rate of change of statistical weight. Note that the statistical weights may evolve in time, although in traditional LE simulations they do not [107]. In some LE spray simulations [21] the statistical weight initially assigned to the computational particle depends on the droplet radius so as to preferentially sample larger radius drops relative to smaller ones [21,160]. This procedure is called 'importance sampling' and it is often used solely in the initialization procedure (as in Ref. [21]), in which case the sampling can degrade in time [160]. If it is desired that a particular weight distribution be maintained at all time, then in that case the evolution equations for the computational particle can differ from their counterparts in the surrogate droplet ensemble so as to maintain equivalence at the level of the modeled ddf [161].

5.1. Interpretation of results

Based on the preceding discussion, it is clear that it is not meaningful to compare scatter plots of computational particles from a single realization of LE simulation with instantaneous snapshots of spray droplets or solid particles from spray or particle-laden experiments because computational particles in the LE simulation can have different statistical weights. It is only meaningful to compare moments (e.g., average, covariance) and other statistical quantities, once numerical convergence of the LE simulations have been established.

5.2. Numerical convergence

Numerical convergence and accuracy of LE simulations have been critically examined by many researchers [23,24,162,163]. Accurate calculation of the interphase transfer terms (corresponding to mass, momentum and energy, cf. Eqs. (25)–(31)) that couple the Lagrangian particle representation to the Eulerian gas-phase equations is crucial for predicting qualitatively correct physical behavior, as well as for quantitative comparison with experiments or higher fidelity simulations. One of the principal differences between numerical convergence of LE simulations and standard Eulerian CFD simulations is that in addition to the grid resolution and time step that are numerical parameters common to both simulations, the number of computational particles N_c is an additional numerical parameter in LE simulations.

In traditional LE (TLE) simulations [48,83,130,164] the dispersed phase is represented by a fixed number of computational particles. If a fixed number of computational particles N_c is used to represent the dispersed phase on a grid with total number of grid cells M, then the statistical error in a grid-based estimate of any mean field quantity increases with grid refinement, resulting in a non-convergent LE simulation. This is because as the grid is refined, fewer and fewer particles are available in each grid cell to form the grid-based mean field estimate. Note that for fixed N_c, the nominal number of particles per grid cell $N_{pc} = N_c/M$ decreases as the grid is refined. Therefore the statistical error, which is inversely proportional to the square root of number of particles per cell, increases. This increase in statistical error eventually overwhelms the reduction in spatial discretization error that is achieved by grid refinement. As a result, the total numerical error increases with grid refinement leading to non-converged TLE solutions.

The other issue with numerical convergence of LE simulations pertains to the spatial distribution of computational particles. In many multiphase flow problems, especially with finite Stokes number droplets or particles, the spatial distribution of physical droplets or particles can be highly nonuniform.

Fig. 9 shows the spatial distribution of particles in lid-driven cavity flow simulation [107] for a Stokes number equal to 0.8. It

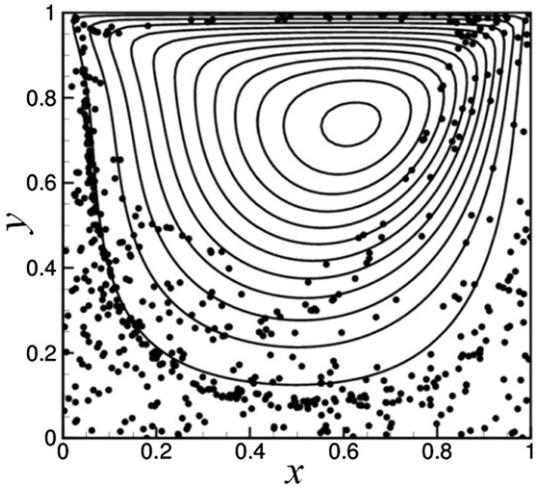

Fig. 9. Snapshot of a one-way coupled lid-driven cavity flow simulation at non-dimensional time tU/L equal to 10. The important flow parameters are $Re = UL/\nu = 100$, $St = \tau_p/\tau_F = 0.8$. The solid lines represent the fluid-phase stream function contours and black dots represent the dispersed-phase particles.

can be seen that the particles have preferentially concentrated in regions of the flow field with high rate of strain. Therefore, for finite Stokes number, the computational particles also preferentially concentrate just like the real particles. In TLE simulations the computational particles follow this nonuniform distribution, resulting in high statistical error in regions populated by few particles, and solutions that do not converge with grid refinement [107].

The problem of LE numerical convergence is now briefly described and solutions to ensure numerical convergence and accuracy are outlined. For two-way coupled multiphase flows, accurate calculation of the interphase transfer terms is necessary for proper representation of the flow physics in an LE simulation. As an example let us consider the mean interphase momentum transfer term $\langle \mathbf{F}^{fd}(\mathbf{x},t)\rangle$ in Eq. (15) for a monodisperse particle-laden flow, which needs to be accurately computed from the LE solution, i.e., the mean fluid velocity field $\mathbf{U}^{f}(\mathbf{x},t)$, and the position and velocity of the computational particles $\{\mathbf{X}_c^{(i)}(t),\ \mathbf{V}_c^{(i)}(t),\ i = 1,...,N_s(t)\}$. The mean interphase momentum transfer term $\langle \mathbf{F}^{fd}(\mathbf{x},t)\rangle$ at Eulerian grid nodes is estimated from this solution data in two steps:

1.Calculation of particle forces $\mathbf{f}_c^{(i)}$:

This requires calculation of the fluid velocity at the particle location $\mathbf{U}^{(f)}(\mathbf{X}_c^{(i)},t)$ in Eq. (75) from the fluid velocity at Eulerian grid nodes. The numerical estimate of the fluid velocity field $\mathbf{U}^{(f)}(\mathbf{x},t)$ at the particle location $\mathbf{X}_c^{(i)}$ using a representation of $\mathbf{U}^{(f)}$ at M grid nodes is denoted $\{\mathbf{U}^{(f)}(\mathbf{X}_c^{(i)},t)\}_M$, and is obtained through *forward interpolation/approximation* as:

$$\left\{\mathbf{U}^{(f)}(\mathbf{X}_c^{(i)},t)\right\}_M = \mathscr{T}\{\mathbf{U}_m^{(f)}, m = 1,\ldots,M; \mathbf{X}_c^{(i)}\}, \tag{74}$$

where the fluid velocity at the mth Eulerian grid node is denoted $\mathbf{U}_m^{(f)}$, and $\mathscr{T}$ is a generic interpolation/approximation operation. The particle force $\mathbf{f}_c^{(i)}$ is then obtained by substituting $\{\mathbf{U}^{(f)}(\mathbf{X}_c^{(i)},t)\}_M$ for $\mathbf{U}^{(f)}(\mathbf{X}_c^{(i)},t)$ in a general form of the particle force model that subsumes different drag force correlations, which reads:

$$\mathbf{f}_c^{(i)}(t) = \mathbf{f}\left(\mathbf{U}^{(f)}(\mathbf{X}_c^{(i)}(t),t), \mathbf{V}_c^{(i)}, \rho_f, \nu_f, \rho_p, D_p\right), \tag{75}$$

where ρ_f and ν_c is the fluid-phase density and kinematic viscosity, respectively.

2. Mean interphase momentum transfer $\mathbf{F}^{fd}(\mathbf{x},t)$ from particle forces $\mathbf{f}_c^{(i)}$:

The numerical procedure to calculate the Eulerian mean field $\mathbf{F}^{fd}(\mathbf{x},t)$ from particle data $\{\mathbf{X}_c^{(i)}(t),\ \mathbf{f}_c^{(i)}(t),\ i = 1,...,N_c\}$ is *described* variously as mean estimation from particle data, projection of fluid-particle interaction forces onto the Eulerian grid, or backward estimation. The numerical estimate for the mean interphase momentum transfer $\langle \mathbf{F}^{fd}(\mathbf{x},t)\rangle$ at the mth Eulerian grid node is denoted $\{\mathbf{F}_m^{fd}\}$, and the general form of its estimate from the particle data is:

$$\{\mathbf{F}_m^{fd}\} = \mathscr{E}\left\{\mathbf{X}_c^{(i)}, \mathbf{f}_c^{(i)}, W^{(i)},\ i = 1,\ldots,N_c(t)\right\}, \tag{76}$$

where $\mathscr{E}$ like $\mathscr{T}$ is another generic interpolation/approximation operator.

Numerical error in the interphase momentum transfer calculation arises from both forward interpolation/approximation of fluid velocity at grid nodes to particle locations, and from backward estimation of the interphase momentum transfer term at particle locations to grid nodes. Both forward interpolation [48,165,166] and the calculation of mean fields from particle data [83,130,164,167–170] have been studied by many researchers. Garg et al. [106] proposed and validated a model for the numerical error incurred in calculating the interphase transfer terms by decomposing the error into statistical, bias and discretization components [106]. They explicitly characterized the total numerical error ε_F in calculating the interphase force $\{\mathbf{F}_m^{fd}\}$ in terms of numerical parameters (grid size M and number of particles per cell N_{pc}) as:

$$\varepsilon_F = \frac{c_F\theta}{\sqrt{N_{pc}}} + \frac{b_F(M)}{N_{pc}} + \frac{a_F}{M^p},$$

where a_F, b_F and c_F are coefficients that characterize the spatial discretization error, bias error, and statistical error, respectively. The error model shows that in order to obtain numerically converged results, it is imperative to simultaneously reduce the statistical and deterministic error components that result from backward estimation. The bias and statistical error components depend on the number of particles per cell. Therefore, numerical convergence cannot be achieved by grid refinement with a fixed total number of computational particles because the number of particles per cell keeps decreasing. This is because the bandwidth of most numerical schemes scales with the grid spacing.

Garg et al. [106] performed comprehensive tests of numerical schemes used to calculate mean interphase transfer terms in LE simulations using a test problem that admits an analytical solution. This allowed characterization of numerical convergence as well as accuracy. They demonstrated that with very high number of particles per cell (100–400), and with multiple independent realizations (100–400), the various schemes they tested are indeed numerically convergent and accurate for the simple static test problem they devised. Such high numerical resolution is impractical in LE simulations of realistic multiphase flows, where typical values for the nominal number of particles per cell N_{pc} in 3D LE simulations range from 0.0156 to 0.125 in Sundaram and Collins [65] to exactly 1 in Boivin et al. [48]. In 2D calculations higher N_{pc} values have been used: 3–30 in Narayanan et al. [170] and 16–500 in Lakehal and Narayanan [162]. In all but one of these studies (Lakehal and Narayanan [162]), only one realization is simulated. Garg et al. [106] found that for realistic resolution using 5 particles per cell with only one realization, some schemes can give errors as high as 80% [106]. They also found that alternative numerical schemes that employ kernel-based estimators to decouple the calculation of mean particle fields from the Eulerian grid resulted in total numerical error of only 20% at the same resolution, and these are briefly described in the next subsection.

5.3. Grid-free estimation

A key ingredient to the solution of the LE numerical convergence problem is the use of *grid-free* kernel-based estimators that Garg et al. [106] adapted from particle methods for PDF-based approaches to turbulent reactive flows [171,172]. Similar ideas have been used in collision calculations, such as the 'collision grid' concept [26]. The particular grid-free estimator that Garg et al. [106] used to demonstrate accuracy and convergence in LE simulations is a two-stage estimator (TSE) algorithm developed by Dreeben and Pope [171]. For forward interpolation it uses a second-order Lagrange polynomial interpolation scheme that is formally second-order accurate, and which is essentially a trilinear interpolation scheme that is identical to the PNN method [48,130,164]. For backward estimation it employs a grid-free two-stage algorithm. In the first stage, it estimates weighted values of the particle property (e.g., interphase force) using a linear kernel of user-specified bandwidth at knot locations that depend on where the

particles are located. The second stage involves least-squares fitting of locally linear or quadratic functions to these knot values. The advantage of this method is that its convergence characteristics are not tied to the Eulerian grid (in fact it does not need an Eulerian grid at all!), but by adjusting the bandwidth of the kernel the user can balance the contribution from truncation and statistical errors.

While kernel-based grid-free estimation reduces statistical error independently of the grid resolution and facilitates convergence, it does not address the issue of large numerical errors arising from spatial nonuniformity in the distribution of computational particles as shown in Fig. 9.

5.4. Improved LE simulation method

The non-convergence of TLE simulations for spatially nonuniform particle distributions such as those shown in Fig. 9 for a lid-driven cavity problem has led to the development of the improved LE (ILE) simulation method. The ILE simulation uses a computational particle number density control algorithm which is similar to those used in various other particle-based simulations [3,4,172–175]. The computational particle number density control algorithm ensures a near-uniform distribution of computational particles during the entire course of simulation. However, as a result of ensuring near-uniform distribution of computational particles, the statistical weights now need to be evolved in time in order to solve the same physical problem. This is achieved by annihilating (in case of excess) and cloning (in case of deficient) computational particles in each cell, resulting in nominally equal number of computational particles per cell at all times [3]. Thus, the ILE method ensures that the statistical error remains nearly spatially uniform. The computational particle number density control procedure relies on the principle of *statistical equivalence* between the ILE computational ensemble (with unequal and time-evolving statistical weights) and the modeled ddf representation of the physical system.

Analogous to the modeled ddf $f^*(\mathbf{x},\mathbf{v},r,t)$ that was defined earlier for the surrogate droplets, a weighted density function $h(\mathbf{x},\mathbf{v},r,t)$ for the computational particles is defined as

$$h(\mathbf{x},\mathbf{v},r,t) \equiv \left\langle \sum_{i=1}^{N_c(t)} W^{(i)} \delta(\mathbf{x}-\mathbf{X}_c^{(i)}(t)) \delta(\mathbf{v}-\mathbf{V}_c^{(i)}(t)) \delta\left(r-R_c^{(i)}(t)\right) \right\rangle. \tag{77}$$

The validity of using computational particles rests on the equivalence between h and f^* at all time. Statistical equivalence is ensured by enforcing consistency at all times between

(i) the number density implied by the computational ensemble and the number density corresponding to the physical system, and
(ii) the particle velocity distribution implied by the computational ensemble and the particle velocity distribution corresponding to the physical system.

The combination of ILE with the kernel-based grid-free TSE estimator is shown to yield accurate solutions to a two-phase flow test problem that admits an analytical solution for the mean interphase momentum transfer term [107]. The same ILE approach is also successful in maintaining near-uniform computational particle number density, resulting in a numerically convergent solution to the particle-laden lid-driven cavity problem [107]. It is worth noting that with an efficient parallelization strategy based on domain decomposition, the ILE simulations result in better load-balancing than the TLE simulations. Therefore, the combination of ILE with the TSE estimator is shown to be a promising approach to obtain numerically convergent and accurate results for LE simulation of multiphase flows.

5.5. Summary of LE numerical solution

1. The two major limitations of TLE simulations: (i) increase in statistical error with grid refinement, and (ii) nonuniform spatial distribution of statistical error, are effectively addressed by kernel-based grid-free estimation using TSE, and the ILE approach that maintains a near-uniform spatial distribution of computational particles.
2. As noted earlier, numerical non-convergence of LE simulations often results from LE sub-models that are not numerically consistent, i.e. such sub-models do not admit a unique solution to the modeled ddf in the limit of numerical parameters tending to their asymptotic values because these sub-models have numerical parameters mixed up with physical parameters. This is easily remedied by appropriately reformulating the sub-model to ensure it is numerically consistent, and the modeling deficiency should not be misinterpreted as indicative of any fundamental difficulty in obtaining numerically converged LE solutions.
3. Although ILE with TSE results in numerically converged and accurate solutions for a given particle force *model*, it does not address the larger question of what constitutes an accurate coarse-graining of particle forces from a DNS? For instance, Moses and Edwards [84] showed that the particle force computed from DNS is better represented by a doublet, rather than a point force. It is also not clear whether the pressure field in the Eulerian representation of the carrier flow is an appropriate coarse-graining of the pressure field from DNS.
4. In particle method solutions to turbulent reactive flows a consistency requirement is imposed at the end of each time step to reconcile the particle representation to the implied mean fields [4], whereas the same has not received as much attention in LE simulations. The decoupled advancement of Eulerian carrier-phase equations and Lagrangian equations for computational particle properties over a time step, and any dependence of the numerical solution on the sequence in which these equations are advanced, needs to be examined more closely.
5. Numerical studies of LE simulations reveal that the numerical schemes used to advance the computational particles can strongly influence higher order statistics, such as nearest neighbor distance and pair correlation statistics (of the computational particles) [176]. This can be significant for LE simulations that use particle interaction models.
6. The foregoing discussion on LE numerical solution is restricted to LE with RANS for the Eulerian carrier flow or PP-DNS$^{(s)}$ in Table 1, but other considerations could prevail for the other LE simulation approaches.

6. Lagrangian–Eulerian simulations of multiphase flow

Selected LE simulations representative of the state-of-the-art are highlighted in this section. Fig. 10 shows LE simulations (of type LES$^{(p)}$ in Table 1) of a gas–solid flow in the riser section of a fluidized bed by Desjardins' group. The gas phase is solved using an LES formulation with the standard dynamic Smagorinsky subgrid model [177]. Particles evolve by a modeled drag law and interact on contact according to a modified version of Cundall and Strack's soft-sphere discrete element model [58]. The Euler–

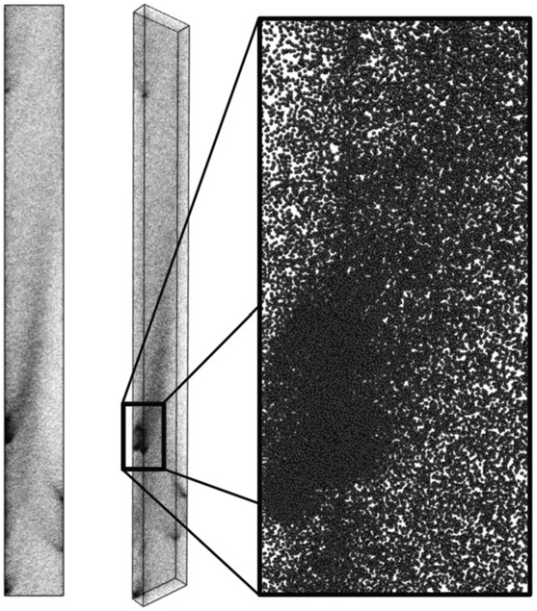

Fig. 10. Example of an LE simulation of gas–solid flow showing particles in a riser. The flow is established by imposing a uniform pressure gradient in the fluid phase in the vertical direction. The gas phase is solved using an LES formulation while particles evolve by a drag law and undergo soft-sphere collisions, corresponding to an LE simulation of type LES$^{(p)}$ (cf. Table 1).

Lagrange simulation strategy has been validated extensively for the dense regime [178]. The purpose of this study was to extend the scheme to dilute flows in fast fluidization environments and assess its capability to generate particle clustering. Clusters were observed to fall at the walls at a constant rate, and cluster velocities showed excellent agreement with experimental correlations [179]. This simulation uses 1,536,000 grid cells for the gas phase with 266,760 particles and takes approximately 11,520 CPU hours (5 days) on 96 cores.

Fig. 11 shows LE simulations (of type PP-DNS$^{(p)}$ in Table 1) of a droplet-laden mixing layer by Bellan's group [52]. The gas phase is solved using a DNS formulation, while the droplets are modeled as point sources of mass and momentum and energy. Collisions are neglected because the flow is dilute (volumetric loading is $O(10^{-3})$ and mass loading is 0.2). This simulation uses $288 \times 320 \times 176$ grid cells for the gas phase with 2,993,630 drops and takes approximately 2252 CPU hours on 64 processors of an SGI Origin2000.

Results from this PP-DNS of a temporal mixing layer laden with evaporating drops are compared with PP-LES to assess the ability of the multiphase PP-LES to reproduce detailed characteristics of PP-DNS. The PP-LES used computational drops, each of which represented eight physical drops, and a reduced flow field resolution using a grid spacing four times larger than that of the DNS. The LES also used models for the filtered source terms, which express the coupling of the drops with the flow, and for the unresolved subgrid-scale fluxes of species mass, momentum, and enthalpy. Different subgrid models were evaluated. It was found that for this dilute droplet-laden flow, all LESs captured the largest-scale vortex, the global amount of vapor emanating from the drops, and the overall size distribution of the drops. All LESs tended to underpredict the global amount of irreversible entropy production (dissipation). The subgrid models differed in their ability to capture the global or local vorticity variation and in predicting the spatial distribution of drops.

Variants of the LE approach as described in Table 1 have been developed by many researchers. Notably, Jaberi et al. [174] and Gutheil et al. [180] have extended the LE approach by incorporating a particle-based solution for the composition PDF in the gas phase.

7. Extension of the LE approach

As noted in Section 4.3.3, preferential concentration and clustering are important multiphase flow phenomena that need to be accurately captured by simulations. This can be a challenge for LE simulations because accurate prediction of preferential concentration requires modeling two-particle statistics that are not represented in the LE approach (cf. Section 4.3.3).

However, a two-particle statistical theory can be derived from the point process representation detailed in Section 2.4. Two-particle statistics have been used by other researchers in sprays [75], Brownian dynamics simulation [181] and to model coagulation [188]. In order to characterize structural properties of the dispersed-phase droplets or particles using quantities such as the pair correlation function, we need to consider the two-particle density $\rho^{(2)}(\mathbf{x}_1,\mathbf{x}_2,\mathbf{v}_1,\mathbf{v}_2,t)$, which is defined as

$$\rho^{(2)}(\mathbf{x}_1,\mathbf{x}_2,\mathbf{v}_1,\mathbf{v}_2,t) \equiv \langle f_1' f_2' \rangle, \tag{78}$$

where $f_1' f_2'$ is the two-particle counterpart of the one-point fine-grained density in the Klimontovich approach [182]:

$$f_1' f_2' = \sum_{i=1}^{N} f_1'^{(i)} \sum_{\substack{j=1 \\ j\neq i}}^{N} f_2'^{(j)} = \sum_{i=1}^{N} \delta\left(\mathbf{x}_1 - \mathbf{X}^{(i)}(t)\right)\delta\left(\mathbf{v}_1 - \mathbf{V}^{(i)}(t)\right) \times \sum_{\substack{j=1 \\ j\neq i}}^{N} \delta\left(\mathbf{x}_2 - \mathbf{X}^{(j)}(t)\right)\delta\left(\mathbf{v}_2 - \mathbf{V}^{(j)}(t)\right). \tag{79}$$

In the above expression $[\mathbf{x}_k, \mathbf{v}_k, k = 1,2]$ are the Eulerian coordinates of the position-velocity phase space for the particle pair. The summation over distinct pairs $j \neq i$ is necessary for the definition of the two-particle density, whose integral is the second factorial measure. If all pairs are included, an atomic contribution arises in the second moment measure that does not have a density [71,72]. The ensemble average of the two-particle fine-grained density function $f_1' f_2'$ is the two-particle density. Integrating the two-particle density over the velocity spaces results in the unnormalized pair correlation function

$$\rho^{(2)}(\mathbf{x}_1,\mathbf{x}_2,t) = \int \rho^{(2)}(\mathbf{x}_1,\mathbf{x}_2,\mathbf{v}_1,\mathbf{v}_2,t)\mathrm{d}\mathbf{v}_1\mathrm{d}\mathbf{v}_2. \tag{80}$$

Substituting Eq. (79) into Eq. (78), and differentiating Eq. (78) with respect to time results in the evolution equation for the two-particle density $\rho^{(2)}(\mathbf{x}_1,\mathbf{x}_2,\mathbf{v}_1,\mathbf{v}_2,t)$:

$$\frac{\partial \rho^{(2)}}{\partial t} = -\frac{\partial}{\partial \mathbf{x}_1}\left(\mathbf{v}_1 \rho^{(2)}\right) - \frac{\partial}{\partial \mathbf{x}_2}\left(\mathbf{v}_2 \rho^{(2)}\right) - \frac{\partial}{\partial \mathbf{v}_1}\left(\left\langle \mathbf{A}^{(1)} \middle| \mathbf{x}_1,\mathbf{x}_2,\mathbf{v}_1,\mathbf{v}_2,t \right\rangle \rho^{(2)}\right) - \frac{\partial}{\partial \mathbf{v}_2}\left(\left\langle \mathbf{A}^{(2)} \middle| \mathbf{x}_1,\mathbf{x}_2,\mathbf{v}_1,\mathbf{v}_2,t \right\rangle \rho^{(2)}\right). \tag{81}$$

Introducing the pair relative separation $\mathbf{r} = \mathbf{x}_2 - \mathbf{x}_1$ and the pair relative velocity $\mathbf{w} = \mathbf{v}_2 - \mathbf{v}_1$, and assuming statistical homogeneity in physical space and velocity space, leads to the following form for the evolution of the two-particle density

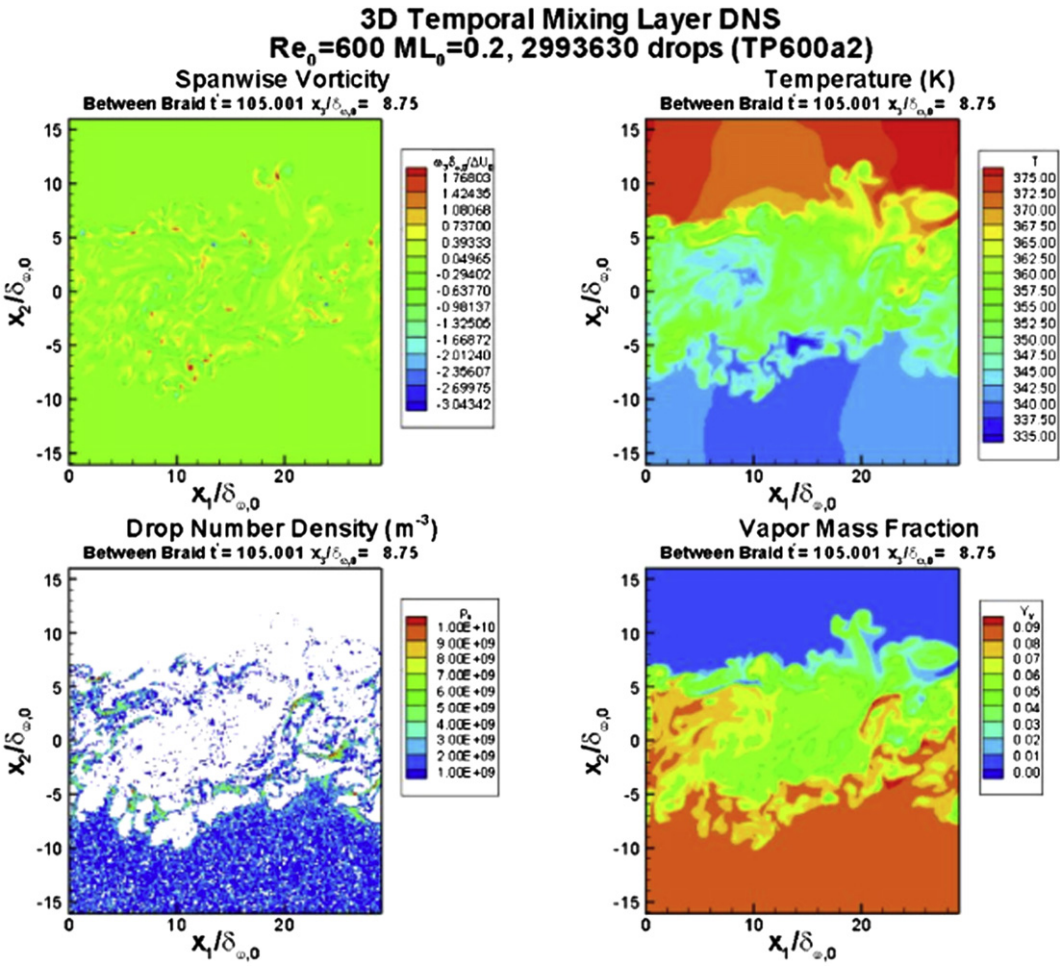

Fig. 11. Example of an LE simulation of droplet-laden mixing layer. The gas phase is solved using point particle DNS while the droplets evolve as point sources of mass, momentum and energy corresponding to an LE simulation of type PP-DNS$^{(p)}$ (cf. Table 1). The droplets are initialized in the lower half plane with a Gaussian distribution of Stokes number with mass loading 0.2.

$$\frac{\partial \rho^{(2)}}{\partial t} + \frac{\partial}{\partial \mathbf{r}}\left[\mathbf{w}\rho^{(2)}\right] + \frac{\partial}{\partial \mathbf{w}}\left[\left\langle \Delta\mathbf{A}^{(2)(1)} \middle| \mathbf{r}, \mathbf{w}; t \right\rangle \rho^{(2)}\right] = 0, \tag{82}$$

where

$$\left\langle \Delta\mathbf{A}^{(2)(1)} \middle| \mathbf{r}, \mathbf{w}; t \right\rangle = \left\langle \mathbf{A}^{(2)} \middle| \mathbf{x}_1, \mathbf{x}_2, \mathbf{v}_1, \mathbf{v}_2, t \right\rangle - \left\langle \mathbf{A}^{(1)} \middle| \mathbf{x}_1, \mathbf{x}_2, \mathbf{v}_1, \mathbf{v}_2, t \right\rangle$$

is the conditionally averaged relative acceleration between particles 1 and 2. The angle brackets represent averaging over all three-particle (and higher multiparticle) statistics.

Extending LE simulations to faithfully represent two-particle statistics requires (i) initializing the computational particle ensemble to match *both* the ddf *and* the two-particle density, and (ii) models for the average relative acceleration between particle pairs. Such an approach has been successfully employed to model nanoparticle aggregation [183,189].

8. Summary points

1. *Mathematical formulation*: The LE approach is shown to be well suited for modeling the effects of polydispersity and dispersed-phase inertia in multiphase flows that result in nonlinear, multiscale interactions and nonequilibrium effects leading to complex flow behavior. The LE approach is shown to belong to a hierarchy of statistical models for multiphase flow, and LE closure models imply a set of moment equations in the Eulerian two-fluid theory. The mathematical formulation of the LE approach that is based on a stochastic point process theory is general enough to extend to dense multiphase flows. It is shown that the point particle assumption is not necessary in LE formulations, and that the mathematical formulation accounts for finite-sized particles, provided appropriate closure models are chosen and volume–displacement effects in the carrier phase are accounted for. It is emphasized that two-particle effects are not represented in the first-order LE formulation, but are modeled. Two-particle information is primarily needed to compute collisional effects that are modeled in the LE approach. However, recent DNS also reveal the importance of neighbor particle effects and fluctuations in number of particles or droplets (compared to the mean). Representation of both these phenomena requires two-particle information, so they must also be modeled in a first-order LE formulation.
2. *Closure models*: The LE particle method solution to the NDF can be interpreted as a computational solution to the evolution of an ensemble of identically distributed surrogate droplets (or particles). Conceptualizing surrogate particles as only being statistically equivalent to physical particles or droplets gives considerable flexibility in modeling. One of the advantages of

the LE particle method solution is that it is easy to ensure that models are realizable and Galilean-invariant. While models for particle or droplet velocity can be deterministic or stochastic, recent evidence from DNS of gas–solid flow suggests that stochastic models for the particle velocity increment might represent particle acceleration statistics more faithfully than deterministic models. Implied models for the mean and fluctuating dispersed-phase velocity should capture mean momentum transfer and transfer of TKE over a range of volume fraction, Stokes number and Reynolds number. Position evolution and droplet dispersion models should capture the dependence of dispersion statistics on volume fraction, Stokes number and Reynolds number. The opposite trends of particle dispersion and interphase TKE transfer on Stokes number can be captured using a timescale that incorporates multiscale effects.

3. *Numerical solution*: Accurate calculation of the interphase transfer terms corresponding to mass, momentum, and energy coupling between the Lagrangian particle representation and the Eulerian gas-phase equations is crucial for predicting qualitatively correct physical behavior, as well as for quantitative comparison with experiments or higher fidelity simulations. An error model for LE simulations is proposed that decomposes the total numerical error into discretization, statistical, and bias error contributions. In TLE simulations where a fixed number of computational particles N_c is used to represent the dispersed phase on a grid, the statistical error in a grid-based estimate of any mean field quantity increases with grid refinement, resulting in non-convergent LE simulations. Without the use of special numerical algorithms, the statistical error can overwhelm the calculation of physical quantities such as the mean interphase momentum transfer. A solution to the LE numerical convergence problem is the use of *grid-free* kernel-based estimators. With grid-free estimation methods the Eulerian grid for the carrier phase can be refined independently of the number of computational parcels that represent the dispersed phase in the Lagrangian frame. Since in this approach the Eulerian grid does not need to be tied to particle size it always results in convergent estimates, whereas with grid-based estimation methods the computed local dispersed-phase volume fraction appears to not converge with increasing grid refinement. Another source of numerical error in LE simulations is spatial nonuniformity in the distribution of computational particles. A computational particle number density control algorithm that employs time-evolving statistical weights ensures a near-uniform distribution of computational particles to remedy this problem. Therefore, the two major limitations of TLE simulations: (i) increase in statistical error with grid refinement, and (ii) nonuniform spatial distribution of statistical error, are effectively addressed by kernel-based grid-free estimation, and computational particle number density control, respectively.
4. *Variants and extensions*: Since two-particle statistics are not incorporated in the first-order LE formulation, inferring the physics of phenomena such as preferential concentration phenomena from LE simulations is questionable. Extending LE simulations to faithfully represent two-particle statistics requires (i) initializing the computational particle ensemble to match *both* the ddf *and* the two-particle density, and (ii) models for the average relative acceleration between particle pairs.

9. Future directions

1. *Mathematical formulation*: One important extension of the current first-order LE approach is to formally include two-particle effects. Based on the results in Fig. 6(b) we conclude that it may not be possible to propose a closure for the conditional acceleration of a particle due to hydrodynamic forces $\langle A_k|\mathbf{x},\mathbf{v};t\rangle$ that is dependent purely on first-order statistics. Since the kinetic theory or ddf description does not contain a description of second-order statistics, this suggests it may be an inadequate level of closure for multiphase flows in which fluctuations of number and volume are significant. The other extension is the formal inclusion of joint particle (or droplet) and carrier fluid-phase statistics. For particles and droplets of finite size this also requires extension to two-particle statistics.
2. *Closure models*: It is anticipated that the development of models from DNS will play a major role in improvement of LE closures. Development of models for LES will depend on the filtering approach, with the recently introduced self-conditioned LES approach appearing to be the most consistent and promising [1,184]. The development of stochastic collision models along the Enskog Simulation Monte Carlo (ESMC) approach [185,186] will be useful for LE simulation of dense flows. Furthermore, there is still scope for development of multiscale models for LE simulation of multiphase flows.

Acknowledgments

The author's understanding of LE methods has developed through interactions with many colleagues and students. In particular, the author is especially grateful to Peter O'Rourke, Christopher Jarzynski, Mario Trujillo, Lance Collins and Rodney Fox for the theoretical aspects, and Stephen Pope, Daniel Haworth, Thomas Dreeben, and David Schmidt for the aspects pertaining to numerical methods. Collaboration with Chidambaram Narayanan on development of the STEINLI code is gratefully acknowledged, as well as Rahul Garg and Madhusudan Pai's contributions to LE numerics and multiscale modeling, respectively. The author is grateful to Olivier Desjardins for providing Fig. 10 and to Josette Bellan for providing Fig. 11. Bo Sun and Sudheer Tenneti assisted with preparation of the figures, and Ravi Kolakaluri helped collate the references. Financial support has been provided by the US Department of Energy through the Early Career Principal Investigator Program Grant No. DE-FG02-03ER25550, and through grants DE-FC26-07NT43098, DE-FG26-07NT43070 & DE-FE0007260 administered by the National Energy Technology Laboratory. The US National Science Foundation provided financial support through the following grants: NSF CMMI 0927660, NSF CBET 1034307, and NSF CBET 1134500.

Appendix A. Evolution equation for the volume-weighted ddf of fluctuating velocity

The evolution equation for the volume-weighted ddf of fluctuating velocity $\tilde{g}$ is derived in this section. Using the chain rule, we first form the time and spatial derivatives of the r^3-weighted ddf $\tilde{f}$:

$$\frac{\partial \tilde{f}}{\partial t} = \frac{\partial \tilde{g}}{\partial t} - \frac{\partial \tilde{g}}{\partial w_j}\frac{\partial \widetilde{\langle V_j \rangle}}{\partial t} \tag{83}$$

$$\frac{\partial \tilde{f}}{\partial x_k} = \frac{\partial \tilde{g}}{\partial x_k} - \frac{\partial \tilde{g}}{\partial w_j}\frac{\partial \widetilde{\langle V_j \rangle}}{\partial x_k} \tag{84}$$

The above two expressions can be combined as follows:

$$\frac{\partial \tilde{f}}{\partial t}+\left(\widetilde{\langle V_k\rangle}+w_k\right)\frac{\partial \tilde{f}}{\partial x_k}=\frac{\partial \tilde{g}}{\partial t}+\left(\widetilde{\langle V_k\rangle}+w_k\right)\frac{\partial \tilde{g}}{\partial x_k}-\frac{\partial \tilde{g}}{\partial w_j}\left[\frac{\partial \widetilde{\langle V_j\rangle}}{\partial t}+\left(\widetilde{\langle V_k\rangle}+w_k\right)\frac{\partial \widetilde{\langle V_j\rangle}}{\partial x_k}\right]. \tag{85}$$

Multiplying Eq. (10) on both sides by r^3, the evolution equation for $\tilde{f}=r^3 f$ can be derived:

$$\frac{\partial \tilde{f}}{\partial t}+v_k\frac{\partial \tilde{f}}{\partial x_k}=-\frac{\partial}{\partial v_k}\left[\langle A_k|\mathbf{x},\mathbf{v},r;t\rangle\tilde{f}\right]-\frac{\partial}{\partial r}\left[\langle\Theta|\mathbf{x},\mathbf{v},r;t\rangle\tilde{f}\right]+3r^2\langle\Theta|\mathbf{x},\mathbf{v},r;t\rangle. \tag{86}$$

Note that since v_k is a sample space variable, it can be taken outside the derivative in the second term on the left hand side. Equating the right hand sides of Eqs. (85) and (86), and rearranging results in the transport equation for the r^3-weighted ddf of fluctuating velocity Eq. (38).

References

[1] Fox RO. Large-eddy-simulation tools for multiphase flows. Annu Rev Fluid Mech 2012;44(1):47–76.
[2] Libby PA, Williams FA. Turbulent reacting flows. New York: Academic Press, Harcourt Brace and Co.; 1993.
[3] Fox RO. Computational models for turbulent reacting flows. Cambridge University Press; 2003.
[4] Pope SB. PDF methods for turbulent reactive flows. Prog Energy Combust Sci 1985;11:119–92.
[5] Faeth GM. Evaporation and combustion of sprays. Prog Energy Combust Sci 1983;9:1–76.
[6] Law CK. Recent advances in droplet vaporization and combustion. Prog Energy Combust Sci 1982;8:171–201.
[7] Sirignano WA. Fluid dynamics of sprays – 1992 Freeman scholar lecture. J Fluids Eng – Trans ASME 1993;115:345–78.
[8] Williams FA. Spray combustion and atomization. Phys Fluids 1958;1(6):541–5.
[9] Koch DL. Kinetic theory for a monodisperse gas–solid suspension. Phys Fluids A 1990;2(10):1711–23.
[10] Drew DA. Mathematical modeling of two-phase flow. Annu Rev Fluid Mech 1983;15:261–91.
[11] Drew DA, Passman SL. Theory of multicomponent fluids, applied mathematical sciences. New York: Springer; 1998.
[12] Enwald H, Peirano E, Almstedt AE. Eulerian two-phase flow theory applied to fluidization. Int J Multiphase Flow 1996;22:21–66.
[13] Pai MG, Subramaniam S. A comprehensive probability density function formalism for multiphase flows. J Fluid Mech 2009;628:181–228.
[14] Pai MG, Subramaniam S. Modeling interphase turbulent kinetic energy transfer in Lagrangian–Eulerian spray computations. Atom Sprays 2006;16(7):807–26.
[15] Tenneti S, Garg R, Hrenya CM, Fox RO, Subramaniam S. Direct numerical simulation of gas–solid suspensions at moderate Reynolds number: quantifying the coupling between hydrodynamic forces and particle velocity fluctuations. Powder Technol 2010;203:57–69.
[16] Fox RO. A quadrature-based third-order moment method for dilute gas-particle flows. J Comput Phys 2008;227(12):6313–50.
[17] Desjardins O, Fox RO, Villedieu P. A quadrature-based moment method for dilute fluid-particle flows. J Comput Phys 2008;227(4):2514–39.
[18] Lakehal D, Narayanan C. Numerical analysis of the continuum formulation for the initial evolution of mixing layers with particles. Int J Multiphase Flow 2003;29(6):927–41.
[19] Narayanan C, Lakehal D. Particle transport and flow modification in planar temporally evolving laminar mixing layers. I. Particle transport under one-way coupling. Phys Fluids 2006;18(9):093302.
[20] Gondret P, Lance M, Petit L. Bouncing motion of spherical particles in fluids. Phys Fluids 2002;14(2):643.
[21] Amsden AA, O'Rourke PJ, Butler TD. KIVA–II: a computer program for chemically reactive flows with sprays, Tech. rep. LA-11560-MS, Los Alamos National Laboratory. May 1989.
[22] Amsden AA. KIVA-3: A KIVA program with block-structured mesh for complex geometries, Tech. rep. LA-12503-MS, Los Alamos National Laboratory: Los Alamos, NM 87545, USA. March 1993.
[23] Iyer V, Abraham J. Penetration and dispersion of transient gas jets and sprays. Combust Sci Technol 1997;130:315–34.
[24] Aneja R, Abraham J. How far does the liquid penetrate in a diesel engine: computed results vs. measurements. Combust Sci Technol 1998;138(1–6):233–56.
[25] Subramaniam S, O'Rourke PJ. Numerical convergence of the KIVA-3 code for sprays and its implications for modeling. Unclassified report LAUR 98-5465. Los Alamos, NM: Los Alamos National Laboratory; 1998. p. 87545.
[26] Schmidt DP, Rutland CJ. A new droplet collision algorithm. J Comput Phys 2000;164(1):62–80.
[27] Zhang DZ, Prosperetti A. Ensemble phase-averaged equations for bubbly flows. Phys Fluids 1994;6(9):2956–70.
[28] O'Rourke PJ. Collective drop effects on vaporizing liquid sprays, Ph.D. thesis, Princeton University. 1981.
[29] O'Rourke PJ. The KIVA computer-program for multidimensional chemically reactive fluid-flows with fuel sprays. Lecture Notes Phys 1985;241:74–89.
[30] Dukowicz JK. A particle-fluid numerical model for liquid sprays. J Comput Phys 1980;35(2):229–53.
[31] Xu Y, Subramaniam S. Effect of particle clusters on carrier flow turbulence: a direct numerical simulation study. Flow Turbulence Combust 2010;85(3–4):735–61.
[32] Bagchi P, Balachandar S. Effect of turbulence on the drag and lift of a particle. Phys Fluids 2003;15(11):3496.
[33] Uhlmann M. An immersed boundary method with direct forcing for the simulation of particulate flows. J Comput Phys 2005;209(2):448–76.
[34] Elghobashi SE, Truesdell GC. Direct simulation of particle dispersion in a decaying isotropic turbulence. J Fluid Mech 1992;242:655–700.
[35] Zhang Z, Prosperetti A. A second-order method for three-dimensional particle simulation. J Comput Phys 2005;210(1):292–324.
[36] Quan S, Schmidt DP, Hua J, Lou J. A numerical study of the relaxation and breakup of an elongated drop in a viscous liquid. J Fluid Mech 2009;640:235.
[37] Gorokhovski M, Herrmann M. Modeling primary atomization. Annu Rev Fluid Mech 2008;40(1):343–66.
[38] Herrmann M. A balanced force refined level set grid method for two-phase flows on unstructured flow solver grids. J Comput Phys 2008;227(4):2674–706.
[39] Esmaeeli A, Tryggvason G. Direct numerical simulation of bubbly flows. Part 1. Low Reynolds number arrays. J Fluid Mech 1998;377:313–45.
[40] Tenneti S, Garg R, Subramaniam S. Drag law for monodisperse gas–solid systems using particle-resolved direct numerical simulation of flow past fixed assemblies of spheres. Int J Multiphase Flow 2011;37(9):1072–92.
[41] Squires KD, Eaton JK. Measurements of particle dispersion obtained from direct numerical simulations of isotropic turbulence. J Fluid Mech 1991;226:1–35.
[42] Squires KD, Eaton JK. Lagrangian and Eulerian statistics obtained from direct numerical simulations of homogeneous turbulence. Phys Fluids 1991;3(1):130–43.
[43] Wang L-P, Rosa B, Gao H, He G, Jin G. Turbulent collision of inertial particles: point-particle based, hybrid simulations and beyond. Int J Multiphase Flow 2009;35(9):854–67.
[44] Mashayek F. Direct numerical simulations of evaporating droplet dispersion in forced low Mach number turbulence. Int J Heat Mass Transf 1998;41(17):2601–17.
[45] Mashayek F, Jaberi FA. Particle dispersion in forced isotropic low-Mach-number turbulence. Int J Heat Mass Transf 1999;42(15):2823–36.
[46] Sundaram S, Collins LR. Collision statistics in an isotropic particle-laden turbulent suspension. Part I. Direct numerical simulations. J Fluid Mech 1997;379:75–109.
[47] Miller RS, Bellan J. Direct numerical simulation of a confined three-dimensional gas mixing layer with one evaporating hydrocarbon-droplet-laden stream. J Fluid Mech 1999;384:293–338.
[48] Boivin M, Simonin O, Squires K. Direct numerical simulation of turbulence modulation by particles in isotropic turbulence. J Fluid Mech 1998;375:235–63.
[49] Okong'o NA, Bellan J. A priori subgrid analysis of temporal mixing layers with evaporating droplets. Phys Fluids 2000;12(6):1573–91.
[50] Apte SV, Mahesh K, Moin P, Oefelein J. Large-eddy simulation of swirling particle-laden flows in a coaxial-jet combustor. Int J Multiphase Flow 2003;29(8):1311–31.
[51] Almeida T, Jaberi F. Large-eddy simulation of a dispersed particle-laden turbulent round jet. Int J Heat Mass Transf 2008;51(3–4):683–95.
[52] Okong'o NA, Bellan J. Consistent large-eddy simulation of a temporal mixing layer laden with evaporating drops. Part 1. Direct numerical simulation, formulation and a priori analysis. J Fluid Mech 2004;499:1–47.
[53] Apte SV, Mahesh K, Gorokhovski M, Moin P. Stochastic modeling of atomizing spray in a complex swirl injector using large eddy simulation. Proc Combus Inst 2009;32(2):2257–66.
[54] O'Rourke PJ, Zhao PP, Snider D. A model for collisional exchange in gas/liquid/solid fluidized beds. Chem Eng Sci 2009;64(8):1784–97.
[55] Allen MP, Tildesley DJ. Computer simulation of liquids. Oxford, United Kingdom: Oxford University Press; 1989.
[56] Matuttis HG, Luding S, Herrmann HJ. Discrete element simulations of dense packings and heaps made of spherical and non-spherical particles. Powder Technol 2000;109(1–3):278–92.
[57] Alam M, Luding S. Rheology of bidisperse granular mixtures via event-driven simulations. J Fluid Mech 2003;476:69–103.
[58] Cundall PA, Strack ODL. A discrete numerical model for granular assemblies. Geotechnique 1979;29:47–65.

[59] Sun J, Battaglia F, Subramaniam S. Hybrid two-fluid DEM simulation of gas–solid fluidized beds. J Fluids Eng – Trans ASME 2007;129(11):1394.
[60] Ishii M. Thermo-fluid dynamic theory of two-phase flow. Paris, France: Eyrolles; 1975.
[61] Pope SB. Turbulent flows. Port Chester, NY: Cambridge University Press; 2000.
[62] Monin AS, Yaglom AM. Statistical fluid mechanics II. MIT Press; 1975.
[63] Hopf E. Statistical hydromechanics and functional calculus. J Rational Mech Anal 1952;1:87–123.
[64] Edwards CF. Toward a comprehensive theory of dense spray flows. Atom Sprays 2000;10(3–5):335–53.
[65] Sundaram S, Collins LR. A numerical study of the modulation of isotropic turbulence by suspended particles. J Fluid Mech 1999;379:105–43.
[66] Subramaniam S. Statistical representation of a spray as a point process. Phys Fluids 2000;12(10):2413–31.
[67] Daley DJ, Vere-Jones D. An introduction to the theory of point processes. New York: Springer-Verlag; 1988.
[68] Panchev S. Random functions and turbulence. New York: Pergamon Press; 1971.
[69] Adler RJ. The geometry of random fields. Chichester, NY: SIAM; 1981.
[70] Brilliantov NV, Poschel T. Kinetic theory of granular gases. 1st ed. New York: Oxford University Press; 2004.
[71] Stoyan D, Kendall WS, Mecke J. Stochastic geometry and its applications. In: Wiley Series in Probability and Mathematical Statistics. 2nd ed. New York: John Wiley and Sons; 1995.
[72] Stoyan D, Stoyan H. Fractals, random shapes and point fields. In: Wiley Series in Probability and Mathematical Statistics. New York: John Wiley and Sons; 1995.
[73] Liboff RL. Kinetic theory: classical, quantum, and relativistic descriptions. 3rd ed. New York: Springer-Verlag; 2003.
[74] Subramaniam S. Statistical modeling of sprays using the droplet distribution function. Phys Fluids 2001;13(3):624–42.
[75] Chiu HH, Su SP. Theory of droplets (II): states, structures, and laws of interacting droplets. Atom Sprays 1997;7(1):1–32.
[76] Kirkpatrick T, Ernst M. Kinetic theory for lattice-gas cellular automata. Phys Rev A 1991;44:8051–61.
[77] Brito R, Ernst M. Ring kinetic theory for tagged-particle problems in lattice gases. Phys Rev A 1992;46(2):875–87.
[78] Subramaniam S, Pai MG. Second-Order Transport due to Fluctuations in Clustering Particle Systems. Presented at the 60th Annual Meeting of the Division of Fluid Dynamics; The American Physical Society: Salt Lake City, UT, November 2007; Paper FM.00008.
[79] Hill RJ, Koch DL, Ladd AJC. The first effects of fluid inertia on flows in ordered and random arrays of spheres. J Fluid Mech 2001;448:213–41.
[80] Hill RJ, Koch DL, Ladd AJC. Moderate-Reynolds-number flows in ordered and random arrays of spheres. J Fluid Mech 2001;448:243–78.
[81] van der Hoef MA, Beetstra R, Kuipers JAM. Lattice-Boltzmann simulations of low-Reynolds-number flow past mono- and bidisperse arrays of sphere: results for the permeability and drag force. J Fluid Mech 2005;528:233–54.
[82] Garg R, Tenneti S, Mohd-Yusof J, Subramaniam S. Direct numerical simulation of gas–solids flow based on the immersed boundary method. In: Pannala S, Syamlal M, O'Brien TJ, editors. Computational gas–solids flows and reacting systems: theory, methods and practice; 2011.
[83] Sundaram S, Collins L. Numerical considerations in simulating a turbulent suspension of finite-volume particles. J Comput Phys 1996;124:337–50.
[84] Moses B, Edwards C. Beyond the point particle: LES-style filtering of finite-sized particles. In: Proceedings of the twentieth annual conference on liquid atomization and spray systems. Intl. Liquid Atomization and Spray Systems Soc.; 2007.
[85] Apte SV, Martin M, Patankar NA. A numerical method for fully resolved simulation (FRS) of rigid particle-flow interactions in complex flows. J Comput Phys 2009;228(8):2712–38.
[86] Ferrante A, Elghobashi S. Reynolds number effect on drag reduction in a microbubble-laden spatially developing turbulent boundary layer. J Fluid Mech 2005;543:93–106.
[87] Ferrante A, Elghobashi S. On the physical mechanisms of drag reduction in a spatially developing turbulent boundary layer laden with microbubbles. J Fluid Mech 2004;503:345–55.
[88] Ning W, Reitz RD, Lippert AM, Diwakar R. Development of a next-generation spray and atomization model using an Eulerian–Lagrangian methodology. In: Proceedings of the 20th annual conference on liquid atomization and spray systems. Chicago, IL: Intl. Liquid Atomization and Spray Systems Soc.; 2007.
[89] Kim D, Desjardins O, Herrmann M, Moin P. Toward two-phase simulation of the primary breakup of a round liquid jet by a coaxial flow of gas. In: Annual res. briefs. Center for Turbulence Research; 2006. p. 185–95.
[90] Garzó V, Tenneti S, Subramaniam S, Hrenya CM. Enskog kinetic theory for monodisperse gas–solid flows. J Fluid Mech 2012;712:129–68.
[91] Shevyrin AA, Bondar YA, Ivanov MS. Analysis of repeated collisions in the DSMC method. In: AIP conference proceedings, vol. 762; 2005. p. 565–70.
[92] Kac MK. Foundations of kinetic theory. In: Third Berkeley symposium on Mathematical Statistics and Probability, 1954–1955. Berkeley: Univ. California Press; 1956. p. 171–97.
[93] Passalacqua A, Fox RO, Garg R, Subramaniam S. A fully coupled quadrature-based moment method for dilute to moderately dilute fluid-particle flows. Chem Eng Sci 2010;65(7):2267–83.
[94] Fox RO, Laurent F, Massot M. Numerical simulation of spray coalescence in an Eulerian framework: direct quadrature method of moments and multi-fluid method. J Comput Phys 2008;227(6):3058–88.
[95] van Wachem BGM, Schouten JC, van den Bleek CM, Krishna R. Comparative analysis of CFD models of dense gas–solid systems. AIChE J 2001;47(5): 1035–51.
[96] Clift R, Grace JR, Weber M. Bubbles, drops and particles. Academic Press; 1978.
[97] Schiller L, Naumann AZ. A drag coefficient correlation. Z. Ver. Deutsch Ing; 1933. 318–320.
[98] Durbin P. A Reynolds stress model for near-wall turbulence. J Fluid Mech 1993;249:465–98.
[99] Dreeben TD, Pope SB. Probability density function and Reynolds-stress modeling of near-wall turbulent flows. Phys Fluids 1997;9(1):154–63.
[100] Tenneti S. Momentum, energy and scalar transport in polydisperse gas-solid flows using particle-resolved direct numerical simulations. PhD thesis, Iowa State University. 2013.
[101] Squires KD, Eaton JK. Preferential concentration of particles by turbulence. Phys Fluids A 1991;3:1169–78.
[102] Eaton JK, Fessler JR. Preferential concentration of particles by turbulence. Int J Multiphase Flow 1994;20:169–209.
[103] Fessler JR, Kulick JD, Eaton JK. Preferential concentration of heavy-particles in a turbulent channel flow. Phys Fluids 1994;6:3742–9.
[104] Cocco R, Shaffer F, Hays R, Reddy Karri S, Knowlton T. Particle clusters in and above fluidized beds. Powder Technol 2010;203(1):3–11.
[105] Tsuji T, Ito A, Tanaka T. Multi-scale structure of clustering particles. Powder Technol 2008;179(3):115–25.
[106] Garg R, Narayanan C, Lakehal D, Subramaniam S. Accurate numerical estimation of interphase momentum transfer in Lagrangian–Eulerian simulations of dispersed two-phase flows. Int J Multiphase Flow 2007;33(12):1337–64.
[107] Garg R, Narayanan C, Lakehal D, Subramaniam S. A numerically convergent Lagrangian–Eulerian simulation method for dispersed two-phase flows. Int J Multiphase Flow 2009;35(4):376–88.
[108] Mckeen T, Pugsley T. Simulation and experimental validation of a freely bubbling bed of FCC catalyst. Powder Technol 2003;129(1–3):139–52.
[109] Ormancey A, Martinon J. Prediction of particle dispersion in turbulent flows. PhysChem Hydrodyn 1984;3/4(5):229–44.
[110] Brown DJ, Hutchinson P. The interaction of solid or liquid particles and turbulent fluid flow fields – a numerical simulation. J Fluids Eng – Trans ASME 1979;101:265–9.
[111] Gosman AD, Ioannides E. Aspects of computer simulation of liquid fueled combustors. J Engine Res 1983;6(7):482–90.
[112] Dwyer HA, Dandy DS. Some influences of particle shape on drag and heat transfer. Phys Fluids A 1990;2(12):2110–8.
[113] Dwyer HA. Calculations of droplet dynamics in high temperature environments. Prog Energy Combust Sci 1989;15:131–58.
[114] Warnica WD, Renksizbulut M, Strong AB. Drag coefficients of spherical liquid droplets, Part 2: Turbulent gaseous fields. Exp Fluids 1995;18(4):265–76.
[115] Warnica WD, Renksizbulut M, Strong AB. Drag coefficients of spherical liquid droplets, Part 1: Quiescent gaseous fields. Exp Fluids 1995;18(4):258–64.
[116] Helenbrook BT, Edwards CF. Quasi-steady deformation and drag of uncontaminated liquid drops. Int J Multiphase Flow 2002;28(10):1631–57.
[117] Maxey MR, Riley JJ. Equation of motion for a small rigid sphere in a nonuniform flow. Phys Fluids 1983;26(4):883–9.
[118] Gatignol D. The Faxen formulas for a rigid particle in an unsteady non-uniform Stokes flow. J Mech Theor Appl 1983;1:143–54.
[119] Michaelides EE, Feng Z-G. Analogies between the transient momentum and energy equations of particles. Prog Energy Combust Sci 1996;22(2):147–62.
[120] Crowe CT, Sommerfeld M, Tsuji Y. Multiphase flows with droplets and particles. Boca Raton, FL: CRC Press; 1999.
[121] Abbad M, Souhar M. Experimental investigation on the history force acting on oscillating fluid spheres at low Reynolds number. Phys Fluids 2004; 16(10):3808–17.
[122] Abbad M, Souhar M. Effects of the history force on an oscillating rigid sphere at low Reynolds number. Exp Fluids 2004;36(5):775–82.
[123] Weinstein JA, Kassoy DR, Bell MJ. Experimental study of oscillatory motion of particles and bubbles with applications to Coriolis flow meters. Phys Fluids 2008;20(10):103306.
[124] Michaelides EE. Hydrodynamic force and heat/mass transfer from particles, bubbles, and drops – the Freeman scholar lecture. J Fluids Eng 2003;125(2): 209–38.
[125] Boussinesq J. Applications L'etude des Potentiels, re-edition 1969 edition. Paris: Blanchard; 1885.
[126] Basset AB. Treatise on hydrodynamics. London: Bell; 1888.
[127] Basset AB. On the motion of a sphere in a viscous liquid. Philos Trans R Soc Lond 1888;179(Ser. A):43–63.
[128] Vojir DJ, Michaelides EE. The effect of the history term on the motion of rigid spheres in a viscous fluid. Int J Multiphase Flow 1994;20:547–56.
[129] Li L, Michaelides EE. The magnitude of Basset forces in unsteady multiphase flow computations. J Fluids Eng 1992;114(3):417–9.
[130] Elghobashi SE, Truesdell GC. On the two-way interaction between homogeneous turbulence and dispersed solid particles. I: turbulence modification. Phys Fluids A 1993;5:1790–801.
[131] Truesdell GC, Elghobashi S. On the two-way interaction between homogeneous turbulence and dispersed solid particles. II. Particle dispersion. Phys Fluids 1994;6(3):1405–7.

[132] Lumley JL. Two-phase and non-Newtonian flows. Topics Phys 1978;12:290–324.
[133] Coimbra CFM, Rangel RH. Spherical particle motion in harmonic Stokes flows. AIAA J 2001;39:1673–82.
[134] Coimbra CFM, Kobayashi MH. On the viscous motion of a small particle in a rotating cylinder. J Fluid Mech 2002;469:257–86.
[135] Lim EA, Coimbra CFM, Kobayashi MH. Dynamics of suspended particles in eccentrically rotating flows. J Fluid Mech 2005;535:101–10.
[136] Han Z, Reitz RD. Turbulence modeling of internal combustion engines using RNG k-epsilon models. Combust Sci Technol 1995;106(4–6):267–95.
[137] Peirano E, Leckner B. Fundamentals of turbulent gas–solid flows applied to circulating fluidized bed combustion. Prog Energy Combust Sci 1998;24:259–96.
[138] Simonin O, Deutsch E, Minier J-P. Eulerian prediction of the fluid/particle correlated motion in turbulent two-phase flows. Appl Sci Res 1993;51:275–83.
[139] Ying X, Subramaniam S. Consistent modeling of interphase turbulent kinetic energy transfer in particle-laden turbulent flows. Phys Fluids 2007;19(8):085101.
[141] Xu Y, Subramaniam S. A multiscale model for dilute turbulent gas-particle flows based on the equilibration of energy concept. Phys Fluids 2006;18:033301-1–033301-17.
[142] O'Rourke PJ. Statistical properties and numerical implementation of a model for droplet dispersion in a turbulent gas. J Comput Phys 1989;83(2):345–60.
[143] Gardiner CW. Handbook of stochastic methods. 2nd ed. Berlin: Springer; 1985.
[144] Dreeben TD, Pope SB. Probability density function Monte Carlo simulation of near-wall turbulent flows. J Fluid Mech 1998;357:141–66.
[145] Ermak DL, McCammon JA. Brownian dynamics with hydrodynamic interactions. J Chem Phys 1978;69(4):1352–60.
[146] Markutsya S, Subramaniam S, Vigil RD, Fox RO. On Brownian dynamics simulation of nanoparticle aggregation. Ind Eng Chem Res 2008;47(10):3338–45.
[147] Lu QQ. An approach to modeling particle motion in turbulent flows – I. Homogeneous, isotropic turbulence. Atmos Environ 1995;29(3):423–36.
[148] Csanady GT. Turbulent diffusion of heavy particles in the atmosphere. J Atmos Sci 1963;20:201–8.
[149] Snyder WH, Lumley JL. Some measurements of particle velocity autocorrelation function in turbulent flow. J Fluid Mech 1971;48:41–71.
[150] Mashayek F. Droplet-turbulence interaction in low-Mach-number homogeneous shear two-phase flows. J Fluid Mech 1998;367:163–203.
[151] Gao Z, Mashayek F. Stochastic modeling of evaporating droplets polydispered in turbulent flows. Int J Heat Mass Transf 2004;47(19–20):4339–48.
[152] Pozorski J, Minier J-P. On the Lagrangian turbulent dispersion models based on the Langevin equation. Int J Multiphase Flow 1998;24:913–45.
[153] Haworth DC, Pope SB. A generalized Langevin model for turbulent flows. Phys Fluids 1986;29:387–405.
[154] Chagras V, Oesterle B, Boulet P. On the heat transfer in gas–solid pipe flows: effects of collision induced alterations of the flow dynamics. Int J Heat Mass Transf 2005;48:1649–61.
[155] Chen X-Q, Pereira JCF. Efficient computation of particle dispersion in turbulent flows with a stochastic-probabilistic model. Int J Heat Mass Transf 1997;40(8):1727–41.
[156] Berlemont A, Desjonqueres P, Gouesbet G. Particle Lagrangian simulation in turbulent flows. Int J Multiphase Flow 1990;16:19–34.
[157] Kloeden P, Platen E. Numerical solution of stochastic differential equations. New York: Springer-Verlag; 1992.
[158] Pai MG, Subramaniam S. Modeling droplet dispersion and interphase turbulent kinetic energy transfer using a new dual-timescale Langevin model. Int J Multiphase Flow 2007;33(3):252–81.
[159] Kloeden P, Platen E, Schurz H. Numerical solution of SDE through computer experiments. New York: Springer; 2003.
[160] Pai GM, Subramaniam S. Accurate numerical solution of the spray equation using particle methods. Atom Sprays 2006;16(2):159–94.
[161] Pope SB. Particle method for turbulent flows: integration of stochastic model equations. J Comput Phys 1995;117(2):332–49.
[162] Lakehal D, Narayanan C. Numerical analysis of the continuum formulation for the initial evolution of mixing layers with particles. Int J Multiphase Flow 2003;29:927–41.
[163] Are S, Hou S, Schmidt DP. Second-order spatial accuracy in Lagrangian–Eulerian spray calculations. Numer Heat Transf, Part B: Fundamentals 2005;48(1):25–44.
[164] Squires KD, Eaton JK. Particle response and turbulence modification in isotropic turbulence. Phys Fluids A 1990;2:1191–203.
[165] Yeung PK, Pope SB. An algorithm for tracking fluid particles in numerical simulation of homogeneous turbulence. J Comput Phys 1988;79:373–416.
[166] Balachandar S, Maxey MR. Methods for evaluating fluid velocities in spectral simulations of turbulence. J Comput Phys 1989;83:96–125.
[167] Crowe CT. Review – numerical models for dilute gas–particle flows. J Fluids Eng – Trans ASME 1982;104:297–303.
[168] Evans M, Harlow FH. Hydrodynamic problems involving large fluid distortions. J Assoc Comput Mach 1957;4:137–42.
[169] Harlow FH. PIC and its progeny. Comp Phys Commun 1988;48:1–10.
[170] Narayanan C, Lakehal D, Yadigaroglu G. Linear stability analysis of particle-laden mixing layers using particle tracking. Powder Technol 2002;125:122–30.
[171] Dreeben TD, Pope SB. Nonparametric estimation of mean fields with application to particle methods for turbulent flows, Tech. rep. FDA 92-13, Sibley School of Mechanical and Aerospace Engineering, Cornell University, Ithaca, NY. Nov 1992. p. 14853.
[172] Subramaniam S, Haworth DC. A PDF method for turbulent mixing and combustion on three-dimensional unstructured deforming meshes. J Engine Res 2000;1(2):171–90.
[173] Haworth DC, Tahry SHE. Probability density function approach for multidimensional turbulent flow calculations in reciprocating engines. AIAA J 1991;29(2):208–18.
[174] Jaberi FA, Colucci PJ, James S, Givi P, Pope SB. Filtered mass density function for large-eddy simulation of turbulent reacting flows. J Fluid Mech 1999;401:85–121.
[175] Raman V, Pitsch H, Fox RO. Hybrid large-eddy simulation/Lagrangian filtered-density-function approach for simulating turbulent combustion. Combus Flame 2005;143:56–78.
[176] Ling Y, Haselbacher A, Balachandar S. A numerical source of small-scale number-density fluctuations in Eulerian Lagrangian simulations of multiphase flows. J Comput Phys 2010;229(5):1828–51.
[177] Desjardins O, Blanquart G, Balarac G, Pitsch H. High order conservative finite difference scheme for variable density low Mach number turbulent flows. J Comput Phys 2008;227:7125–59.
[178] Capecelatro J, Desjardins O. An Euler–Lagrange strategy for simulating particle-laden flows. J Comput Phys (in review).
[179] Capecelatro J, Desjardins O. Detailed investigation of clustering in riser flows using an Euler–Lagrange approach. In: 244th ACS national meeting & exposition, Philadelphia, PA, 2012.
[180] Ge HW, Gutheil E. Probability density function (PDF) simulation of turbulent spray flows. Atom Sprays 2006;16(5):531–42.
[181] Brady JF, Bossis G. Stokesian dynamics. Annu Rev Fluid Mech 1988;20:111–57.
[182] Krall NA, Trivelpiece AW. Principles of plasma physics. New York: McGraw-Hill; 1973.
[183] Markutsya S. Modeling and simulation of nanoparticle aggregation in colloidal systems, Ph.D thesis, Iowa State University. 2010.
[184] Pope SB. Self-conditioned fields for large-eddy simulations of turbulent flows. J Fluid Mech 2010;652:139–69.
[185] Montanero J, Santos A. Monte Carlo simulation method for the Enskog equation. Phys Rev E 1996;54(1):438–44.
[186] Montanero J, Santos A. Simulation of the Enskog equation á la Bird. Phys Fluids 1997;9(7):2057–60.
[187] Pai MG, Subramaniam S. Two-way coupled stochastic model for dispersion of inertial particles in turbulence. J Fluid Mech 2012;700:29–62.
[188] Chun J, Koch DL, Rani SL, Ahluwalia A, Collins LR. Clustering of aerosol particles in isotropic turbulence. J Fluid Mech 2005;536:219–51.
[189] Markutsya S, Fox RO, Subramaniam S. Coarse-graining approach to infer mesoscale interaction potentials from atomistic interactions for aggregating systems. Ind Eng Chem Res, in press.